GEOPHYSICAL DETECTION OF ON-SITE WASTEWATER PLUMES IN THE NORTH CAROLINA COASTAL PLAIN, USA

by

Matthew Smith

January, 2014

Directors of Thesis: Michael O'Driscoll and David Mallinson

Major Department: Geological Sciences

Nonpoint source pollution (NSP) continues to be the leading cause of water quality degradation in the United States. On-site wastewater systems (OWS) contribute to NSP; however, due to the range of system designs and complexity of the subsurface, OWS contributions to groundwater pollution are not well understood. As the population of coastal North Carolina continues to increase, better methods to locate and characterize wastewater impacted groundwater are needed. Previous studies have demonstrated the ability of non-intrusive geophysical methods to provide high resolution information on various contaminants in different geologic settings. The goals of this study were to evaluate the utility of ground penetrating radar (GPR) and capacitively coupled resistivity (CCR) for detecting OWS components, delineating associated wastewater plumes, and monitoring temporal variations in groundwater quality. Cross-sectional and three dimensional (3D) geophysical surveys were conducted periodically over a one year period (February 2011 – January 2012) at two schools utilizing OWS in the lower Neuse River Basin in the North Carolina Coastal Plain. Cores were collected at both study sites; as well as monthly groundwater depth, temperature, and specific conductivity measurements to better constrain the geophysical interpretations. Additionally,

dissolved inorganic nitrogen and chloride concentrations were monitored bi-monthly to assess nutrient transport at the sites.

The 3D GPR surveys effectively located the wastewater drainage trenches at both sites, in close agreement with locations described in as-built OWS blueprints. Regression analysis of resistivity versus groundwater specific conductivity revealed an inverse relationship, suggesting resistivity $\leq$ 250 ohm.m was indicative of wastewater impacted groundwater at both sites. The 3D resistivity models identified regions of low resistivity beneath the drainfields relative to background values. Regression analysis of GPR signal absolute peak amplitude (APA) versus groundwater specific conductivity revealed a decrease in APA indicative of radar signal attenuation at locations where groundwater specific conductivity was elevated. The 3D GPR models identified regions of attenuated radar signal beneath the drainfields relative to background locations. Comparisons of groundwater specific conductivity, GPR, and CCR lateral wastewater plume estimates indicated similar dimensions at both sites.

The sensitivity of resistivity measurements tended to decline with increased water-table depth; although, differences in resistivity associated with seasonal water-table depth changes were noticeable. Overall, results of this study suggest that GPR and CCR surveys combined with sediment, hydrologic, and water quality data may provide reliable information on the location of OWS components and extent of associated wastewater plumes. The GPR surveys successfully located the wastewater drainage trenches and helped image the uppermost surface of the wastewater plumes. The CCR surveys delineated the lateral wastewater plume dimensions and revealed temporal changes in groundwater quality associated with differences in groundwater recharge.

GEOPHYSICAL DETECTION OF ON-SITE WASTEWATER PLUMES IN THE NORTH CAROLINA COASTAL PLAIN, USA

A Thesis

Presented to the Faculty of the Department of Geological Sciences

East Carolina University

In Partial Fulfillment of the Requirements for the Degree

Master of Science

Geological Sciences

by

Matthew Smith

January, 2014

© Matthew Smith, 2014

GEOPHYSICAL DETECTION OF ON-SITE WASTEWATER PLUMES IN THE NORTH CAROLINA COASTAL PLAIN, USA

by

Matthew Smith

APPROVED BY:

CO-DIRECTOR OF THESIS:_____
Michael O'Driscoll, PhD

CO-DIRECTOR OF THESIS:_____
David Mallinson, PhD

COMMITTEE MEMBER:_____
Charles Humphrey, PhD

COMMITTEE MEMBER:_____
Richard Spruill, PhD

CHAIR OF THE DEPARTMENT
OF GEOLOGICAL SCIENCES:_____
Stephen Culver, PhD

DEAN OF THE
GRADUATE SCHOOL:_____
Paul Gemperline, PhD

ACKNOWLEDGMENTS

I'd like to use this opportunity to firstly thank my thesis advisors Dr. Mike O'Driscoll and Dr. Dave Mallinson for all of their help and guidance during this project. I couldn't have asked for better advisors and couldn't have done this without your help. I'm grateful for the opportunity to work with you. I've learned much from you both; I appreciate it. I'd also like to thank my thesis committee: Dr. Charlie Humphrey and Dr. Richard Spruill for their help and guidance throughout my graduate studies. I'm grateful to Jim Watson and John Woods who provided expert technical support both in the field and in the lab, which was a great contribution to the success of this project. I owe a special thanks to Sarah Hardison and Rob Howard who both helped with this project from the beginning, and also any other students who helped with field and lab work. I'd also like to thank the Craven County School System, specifically James W. Smith Elementary School and West Craven High School for allowing us to install 49 piezometers on their grounds, as well as conduct periodic monitoring. This study was funded by an East Carolina University (ECU) Research and Development Grant, as well as the North Carolina Water Resources Research Institute (NCWRRI). Thank you for supporting this work. The ECU Department of Geological Sciences, Environmental Health Sciences Program, and the Department of Biology provided a variety of resources and equipment in support of this project of which I'm grateful. Lastly, I thank my family for their love, encouragement, and support over the years; without which I couldn't have made it this far.

TABLE OF CONTENTS

LIST OF TABLES

LIST OF FIGURES

Chapter 1

Introduction

Nonpoint source pollution (NSP) is the predominant water quality problem in the United States (USEPA, 2012). The Clean Water Act (CWA) of 1972 regulates point source pollution; however, nonpoint sources have been more challenging to control. Nonpoint source pollution is not easily understood because pollutant loads and discharge locations are often unclear. Declining water quality trends can be linked to population increase and associated land-use changes (Ren et al., 2003). Coastal environments are particularly vulnerable to water pollution due to increasing stress from human activities (Vitousek et al., 1997; Epstein, 1998). The population of North Carolina's 20 coastal counties regulated under the Coastal Area Management Act (CAMA20) is projected to increase by approximately 31% from 2013 – 2033 (NCOSBM, 2013). Much of this growth will likely occur in rural areas where public utilities such as centralized sewage services are often unavailable.

Decentralized on-site wastewater treatment systems (OWS) are the primary means of wastewater treatment and disposal in many rural areas and are known contributors to NSP (USEPA, 2012). On-site wastewater treatment systems have three major components for the treatment of effluent: a septic tank, wastewater drainfield, and soil (Figure 1).

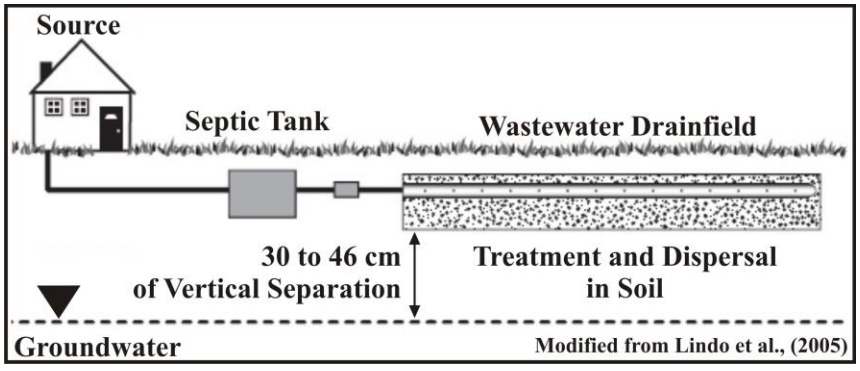

Figure 1. Generalized schematic of a decentralized OWS.

The septic tank retains solids and allows wastewater to exit the tank and flow through drainage trenches in the wastewater drainfield, where it then infiltrates the soil. The wastewater undergoes various physical, chemical and biological treatment processes in aerated soil beneath the drainage trenches (Humphrey et al., 2012). When installed and functioning properly, OWS effectively treat wastewater before contacting the surficial aquifer. However, inadequate treatment, excessive water use, and/or high system density can allow contaminants to impact shallow groundwater quality (Scandura and Sobsey, 1997; Borchardt et al., 2003). Depending on the fate and transport of specific wastewater related contaminants in the surficial aquifer, OWS can potentially affect surface water quality down gradient of the system.

Approximately 20% of homes in the U.S. use OWS, releasing approximately 4 billion gallons of wastewater to the subsurface per day (USEPA 2005, 2013). The distribution and density of systems varies significantly by state. More than a third of homes in the southeastern U.S. use OWS to treat and dispose of wastewater (USEPA, 2002). In 1990, approximately 1.4 million OWS were used in North Carolina, and each subsequent year 20,000 – 40,000 more have been installed (USEPA, 2002; NCCE, 2004). According to 1990 census data, approximately 60% of homes in North Carolina's CAMA20 relied on OWS for wastewater treatment and disposal compared to 50% of homes in the rest of the state; indicating that communities with the most direct link to coastal and estuarine waters have the greatest potential to negatively impact coastal water quality (NCNERR, 2001). While North Carolina has OWS design criteria that directly influences the area required for OWS drainfields and replacement systems, system density is not generally regulated. In a Report to Congress, the USEPA suggested that groundwater contamination becomes a risk when system densities exceed 40 systems per mi^2 (USEPA, 1977). OWS effluent contains elevated nutrient (nitrogen and phosphorous) and

chloride concentrations (Lee et al., 2006; Roy et al., 2008), as well as bacteria and viruses (Fetter, 2001). Studies linking waterborne disease outbreaks to wastewater impacted water supplies in the U.S. found that OWS density was the most significant factor (Yates, 1985; Borchardt et al., 2003). Based on 1990 census data, system densities exceeded 200/mi^2 at some communities within the Neuse River Basin (NRB) (Pradhan et al., 2008), posing a significant threat to water resources, public health, and aquatic ecosystems downstream. Due to excessive growth of aquatic microscopic and macroscopic vegetation in the NRB, the North Carolina Environmental Management Commission enacted the Neuse River Basin Nutrient Sensitive Waters Management Strategy in 1998 (amended in 2007) (15A NCAC 02B.0232-.0236) to reduce nitrogen loading to surface waters. Point and nonpoint sources were addressed in the plan; however, OWS inputs were not known, and are therefore unregulated under the nutrient management strategies (NCDENRDWQ, 2007). The population of the NRB is projected to increase by approximately 36% from 2010 – 2030 (NCDENROEE, 2007).

Other studies have shown that OWS effluent can affect water quality down gradient from a site. A study conducted in the sandy surficial aquifer on St. George Island, Florida found that in areas with a shallow water-table, wastewater originating from OWS may affect groundwater quality (Corbett et al., 2002). Wastewater is naturally attenuated when soil conditions and groundwater flow paths are sufficient for treatment to occur. However, studies (Robertson et al., 1991; Corbett et al., 2002) have shown that wastewater constituents can migrate distances > 90 m, potentially impacting surface waters.

Better methods are needed to detect and monitor the effects of wastewater discharges to the surficial aquifer. The knowledge gained from improved wastewater monitoring techniques

may help with the development of policies and regulations to guide watershed management in nutrient sensitive coastal settings.

Related work

Monitoring contaminants in the surficial aquifer can be resource intensive and typically requires the installation of groundwater monitoring wells or piezometers to locate and track contaminant plumes. Piezometers provide access to groundwater for characterization of physical, chemical, and biological properties at discrete points in the subsurface. However, the process of installing a piezometer network is resource intensive, often limiting the number installed. It is important that enough piezometers are installed to provide groundwater quality data that accurately delineates contaminant plumes and determines the orientation of flow paths to surface waters. Therefore, methods that can help reduce the number of piezometers installed and decrease site disturbance, labor, and costs while providing adequate groundwater quality data are needed.

Due to the increased concentration of dissolved ions in wastewater, wastewater impacted groundwater often has elevated specific electrical conductivity that may be detectable with geoelectrical methods (Urish, 1983; Roy et al., 2009). Geophysical methods such as ground penetrating radar (GPR) and electrical resistivity (ER) have been used previously to image various contaminant plumes in different geologic settings, including wastewater plumes. A study was conducted in New England, in a buried glacial valley composed of alternating fine to coarse-grained sand where the water-table was approximately 9 meters below the ground surface (mbgs) to locate a landfill leachate plume. It was found that electrical resistivity profiling can provide a relatively fast and inexpensive means of detecting regions with decreased resistivity and elevated groundwater specific conductivity associated with landfill leachate (Urish, 1983).

In a study conducted in Arizona, GPR was used to detect hydrocarbon contamination from a leaking underground storage tank in sandy-gravel and clay sediments where the water-table was approximately 4.5 mbgs. The GPR surveys were useful for outlining the boundaries of the hydrocarbon plume, which helped determine the placement of groundwater monitoring wells (Benson, 1995). Integration of the GPR and groundwater quality data, as well as the hydraulic gradient and groundwater flow direction were useful to understand the extent and magnitude of groundwater contamination at the site. In Sao Paulo, Brazil, in an area of mainly consolidated sand with clay lenses where the water-table was approximately 10 mbgs, GPR was useful in determining the lateral extent of a landfill leachate plume and ER surveys were able to determine the vertical dimensions of the plume (Porsani et al., 2004). In southwest Nigeria, an ER survey was conducted in clayey-sand sediments during the dry season when the water-table was >10 mbgs to evaluate the impact of a sewage disposal system (Amidu and Olayinka, 2006). The survey was conducted within and outside of the wastewater drainfield. Four soil/groundwater sampling pits were dug within and outside of the wastewater plume boundaries, as determined by the ER surveys to measure groundwater specific conductivity. The resistivity measurements correlated well with the location and distribution of groundwater specific conductivity measurements, suggesting that ER surveys can delineate wastewater plumes in clayey-sand sediments. A study was carried out using electromagnetic induction (EMI) surveys to detect malfunctioning septic systems in Indiana in an area of glacial-till derived soil where the water-table was approximately 1.2 mbgs (Lee et al., 2006). The study found that the EMI surveys could help identify the location of OWS components and their associated effluent plumes. The authors suggested more work should be done to investigate the usefulness of other geoelectrical methods for delineating wastewater impacted soil and groundwater in other geologic settings.

In 2008, EMI and capacitively coupled resistivity (CCR) surveys were conducted in an area of boulder/glacial-till sediments where the water-table was approximately 0.5 mbgs to map a wastewater plume discharging to Lake O'Hara in Yoho National Park, British Columbia (Roy et al., 2008). The EMI surveys were useful for initially locating areas of elevated specific conductivity, while the CCR surveys provided detailed cross-sections of low resistivity regions indicative of wastewater impacted groundwater. Insitu specific conductivity measurements of the lake water were used to confirm the groundwater flow direction and discharge to the lake. The authors concluded that combining non-intrusive geophysical methods with specific conductivity measurements of surface water at the lake shoreline was a promising approach for delineating wastewater plumes in a rocky alpine lake setting. This study provided encouraging evidence of the usefulness of CCR surveys to detect regions of decreased resistivity associated with wastewater inputs; however the resistivity measurements were not confirmed with groundwater quality measurements. More work is needed to understand how resistivity and groundwater quality measurements relate and to determine if the method is suitable for detecting wastewater plumes in surficial Coastal Plain settings. These previous studies are summarized in Table 1.

Location	Year	Method	Sediment	Contaminant	Author
U.S.	1983	ER	Fine-coarse Grained Sand	Landfill Leachate	Urish
U.S.	1995	GPR	Sand, Gravel, and Clay	Hydrocarbons	Benson
Brazil	2004	GPR ER	Consolidated Sand with Clay Lenses	Landfill Leachate	Porsani et al.
Nigeria	2006	ER	Unconsolidated Clayey-sand	Wastewater	Amidu and Olayinka
U.S.	2006	EMI	Glacial Till Derived Soil	Wastewater	Lee et al.
Canada	2008	EMI CCR	Glacial Boulder and Till	Wastewater	Roy et al.

Table 1. Previous geophysical contaminant plume studies.

These studies demonstrated the usefulness of geoelectrical methods for detecting various contaminant plumes in different geologic settings, and that water-table depth, groundwater quality, and lithological data can help ground truth geophysical interpretations in surficial aquifers. However, published studies combining GPR and CCR to delineate OWS derived wastewater plumes in surficial Coastal Plain aquifers have been limited. There is a gap in understanding as to how useful these methods are for delineating wastewater plumes in unconsolidated siliciclastic sediments typical of Coastal Plain settings. It was hypothesized that GPR and CCR can locate OWS components, delineate associated wastewater plumes, and detect temporal variations in groundwater quality in surficial Coastal Plain aquifers. The objectives of this study were to determine if 1) GPR and CCR can locate subsurface OWS components, 2) if GPR and CCR can delineate wastewater plumes in three dimensions (3D), and 3) if these geophysical methods are sensitive enough to detect temporal variations in groundwater quality associated with wastewater inputs to North Carolina Coastal Plain (NCCP) surficial aquifers.

Chapter 2

Study Area

Regional Hydrogeology

This study was conducted in the lower Neuse River Basin (NRB), in the NCCP. The geology of the NCCP may be characterized as a gently southeastward dipping and thickening wedge of sediments and sedimentary rock ranging in age from Cretaceous through Recent unconformably resting on an underlying basement complex of Paleozoic age rocks (Lautier, 2001). Deposition of the sediment wedge occurred sequentially through transgressions and regressions of the Atlantic Ocean. It is comprised of layers and lenses of sand, clay, silt, limestone, gravel, shell material and combinations thereof (Lautier, 2001). The hydrogeological system of the NCCP consists of 10 aquifers separated by 9 confining units; the confining units are typically composed of silt and clay. From basement rock to the land surface the system is composed of crystalline bedrock followed by the Lower Cretaceous aquifer, Lower Cape Fear aquifer, Upper Cape Fear aquifer, Black Creek aquifer, Peedee aquifer, Beaufort aquifer, Castle Hayne aquifer, Pungo aquifer, Yorktown aquifer and the Surficial aquifer (Winner and Coble, 1996). The surficial hydrogeological framework of the NCCP is sub-divided into seven subregions, primarily on the basis of physiography and the predominant texture of near surface sediments (Ator et al., 2005). The surficial aquifer in the study area is located in hydrogeological subregion 7, and is characterized as predominantly alluvial and estuarine valley fill material, ranging in age from Pliocene to Recent (Ator et al., 2005). It was estimated to be approximately 4 m thick by the North Carolina Department of Environment and Natural Resources Division of Water Quality (NCDENRDWQ) during installation of monitoring well

R23X5 located approximately 10 km southwest of the study area (35◦10'20", 77◦18'40"). Porosity of NCCP surficial sediments is variable. A study was conducted in Kinston, NC, located approximately 35 km west of the study area to evaluate the spatial variability of Coastal Plain soil physical properties. The study found that porosity of surficial sediments in the NCCP can range from 29% - 55% (Duffera et al., 2007). Additionally, approximately 25 km southwest of the study area Coes et al., (2007) estimated porosity of surficial sediments to be approximately 31%, and horizontal saturated hydraulic conductivity (K) 9 x 10^{-3} m/day. Mean annual recharge estimated at the same location using the Darcy-flux method from 1987-2004 was estimated to be 110 cm/year (Coes et al., 2007); however, the net loss to evapotranspiration and leakage to underlying aquifers were not included in this estimate, which could account for a large percentage of infiltrating groundwater.

Ground and surface water are not isolated components of the hydrologic system, but instead interact in a variety of physiographic and climatic landscapes creating the potential for exchange between the two components (Sophocleous, 2002). Most groundwater recharged to the NCCP surficial aquifer discharges to nearby surface water bodies (Ator et al., 2005). The potential for flooding is increased in the NCCP due to its predominantly sandy and flat low-elevation characteristics (Sweet and Geratz, 2003). Maximum flow of NCCP streams typically occurs during the winter and spring months, but may occur in the fall if tropical storms make landfall (Williams and Pinder, 1990). Due to the relatively high porosity of sediments, high frequency of flooding, and shallow water-table, the potential for groundwater-surface water exchange in the study area is likely. According to Ator et al., (2005), in areas with sandy, more permeable sediments, contaminants may be readily transported to groundwater.

Watershed Description and Climate

The NRB is the 3rd largest drainage basin in North Carolina covering an area of 9,756 km^2 with 5,486 km of streams (NCDENROEE, 2007). The study area consists of two locations, both located in the Middle Neuse Watershed (MNW) (USGS HUC 03020202) (USGS, 2013). The MNW is located in the lower NRB and occupies approximately 2,776 km^2 (USEPA, 2013). This watershed and study sites were chosen on the basis of their close proximity to the Neuse River, similar sediments, and contrasting water-table depths. Historical mean annual precipitation in the study area recorded from 1899 – 2012 at the Kinston 5 SE gauging station (ID# 314684) was 126 cm/year and the mean air temperature was 16.4º C (Southeast Regional Climate Center, 2013). Total precipitation during the study period (February 2011 – January 2012) recorded at the USGS gauging station Contentnea Creek (ID# 02091764) was 113 cm and the mean air temperature was 17.2º C (USGS, 2013; Southeast Regional Climate Center, 2013). The region was impacted by drought during the summer of 2011 followed by widespread flooding in late August 2011 due to Hurricane Irene.

Chapter 3

Methods

To test if GPR and CCR can locate subsurface OWS components, delineate wastewater impacted groundwater, and detect temporal variations in groundwater quality, geophysical and ground/surface water monitoring were conducted throughout the study period (February 2011 – January 2012) at two schools utilizing OWS located in the study area. The hydrogeology was characterized at both study sites to better constrain the geophysical interpretations. The geophysical measurements were compared to the geologic and hydrologic parameters to test for relationships, and to determine the accuracy of the geophysical methods.

James W. Smith Elementary School

James W. Smith Elementary School (JWSES) is located approximately 4 km south of the Neuse River in Craven County, North Carolina (35◦15'4.50", 77◦17'19.03") (Figure 2). Water is supplied to JWSES by the Craven County Water Department (CCWD) that is extracted from the Late Cretaceous age Black Creek and Peedee aquifers. JWSES uses a pump to gravity driven OWS for wastewater treatment and disposal. The OWS consists of 2 distribution boxes with 32, 0.9 m x 0.3 m x 30 m drainage trenches separated by approximately 2 m in a wastewater drainfield. Wastewater is pumped to the distribution boxes where it then gravity flows through the drainage trenches and eventually percolates through the soil for treatment. A 48 m x 70 m survey area was positioned directly above the drainfield for 3D geophysical measurements. A 180 m south to north trending transect was marked for cross-sectional surveys across the site from A to A'. Twenty one piezometers were installed across the site at varying depths depending on the intersection with the water-table. The piezometers were positioned within and

outside of the drainfield for collection of water-table depth and groundwater quality measurements. Those positioned outside and up gradient of the drainfield were used to determine background values. Relative ground surface elevations were surveyed at each piezometer using a rotating AUTOLASER 300 level. Relative piezometer elevations were subtracted from the North American Datum of 1983 (NAD83) to obtain accurate ground surface and hydraulic head elevations in meters above mean sea level (mamsl). Based on hydraulic head contours determined from mean monthly (n = 12) hydraulic head values at piezometers 1/GP1 – 15, groundwater generally flows in a northwesterly direction (Appendix A). Cores were collected at JWSES1/GP1, JWSES3/GP2 and JWSES12/GP3 to determine lithology and grain-size characteristics. A spring was identified approximately 25 m north of the drainfield and was included in the water quality monitoring plan. The spring discharge flowed approximately 15 m overland to converge with an unnamed tributary of Core Creek located approximately 40 m north of the drainfield.

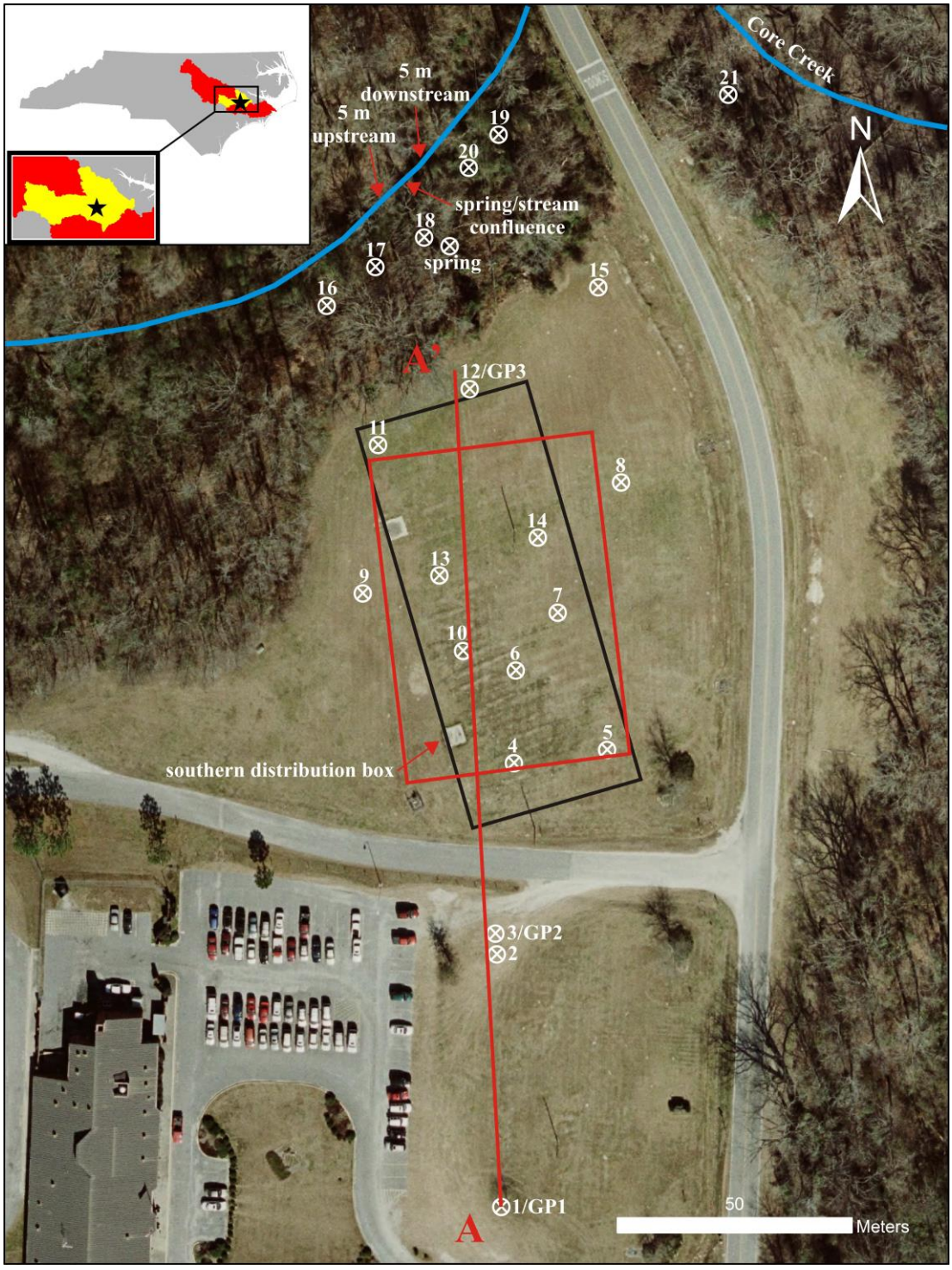

Figure 2. Site map of study area at JWSES. The wastewater drainfield is represented in black and the geophysical survey area and transect in red. Piezometer, surface water sampling points, and core locations are shown. Core locations are indicated by GP. Aerial photo is from Google Earth (2012).

West Craven High School

West Craven High School (WCHS) is located approximately 2 km north of the Neuse River in Craven County, North Carolina (35◦14'13.97", 77◦8'9.47") (Figure 3). Water is supplied to WCHS by the CCWD that is extracted from the Late Cretaceous age Black Creek and Peedee aquifers. WCHS uses a low pressure OWS for wastewater treatment and disposal. The OWS consists of 2 distribution manifolds each with 16, 0.6 m x 0.3 m x 38 m drainage trenches separated by approximately 2.1 m in two wastewater drainfields. Wastewater is pumped to the manifolds where under low pressure it flows through the drainage trenches and eventually percolates through the soil for treatment. An inactive drainfield with 16, 0.6 m x 0.3 m x 38 m drainage trenches separated by approximately 2.1 m was located immediately north of the two active fields. A 42 m X 125 m survey area was positioned directly above the drainfields for 3D geophysical measurements. A 300 m south to north trending transect was marked for cross-sectional surveys across the site from A to A'. Twenty eight piezometers were installed across the site at varying depths depending on the intersection with the water-table. The piezometers were positioned within and outside of the drainfields for collection of water-table depth and groundwater quality measurements. Those positioned outside of the active drainfields were used to determine background values. Relative ground surface elevations were surveyed at each piezometer using a rotating AUTOLASER 300 level. Relative piezometer elevations were subtracted from the NAD83 to obtain accurate ground surface and hydraulic head elevations in mamsl. Based on hydraulic head contours determined from mean monthly (n = 12) hydraulic head values at piezometers 1d/GP4 – 24, groundwater generally flows in a northerly to northwesterly direction (Appendix A). Cores were collected at WCHS1d/GP4, WCHS13d/GP5 and WCHS22d/GP6 to determine lithology and grain-size characteristics.

Figure 3. Site map of study area at WCHS. The active wastewater drainfields are represented in black along with the inactive drainfield to the north. The geophysical survey area and transect are represented in red. Piezometer, surface water sampling points, and core locations are shown. Core locations are indicated by GP. Aerial photo is from Google Earth (2012).

Lithology and Grain-size

Three cores were collected at each site at varying depths ranging from 4.6 – 5.6 mbgs using a truck-mounted Geoprobe coring rig. Cores were collected adjacent to the transects to help constrain the geophysical and water quality measurements (Figures 2 and 3). Cores were logged and sampled at 50 cm intervals or where a distinct lithological contrast was observed. Samples were sieved at 0.5 phi intervals in a Ro-Tap sieve shaker for 15 minutes per sample to separate the sediment into grain-size fractions ranging from 0.063 – 4 mm (4 φ to – 2 φ). Grain-size statistical analysis was carried out using GRADISTAT 4.0, according to the Folk and Ward graphical method (Blott, 2000). Grain-sizes were determined using to the Wentworth Grain-size scale.

Porosity

According to Vukovic and Soro (1992), porosity can be derived from the empirical relationship between porosity and the uniformity coefficient based on equation 1:

$$n = 0.255(1 + 0.83^{U}) \quad \text{(Eq. 1)}$$

Where n is porosity (voids/total volume) and U is the uniformity coefficient (d_{60}/d_{10}) in mm. Porosity was estimated for each sample to approximate median porosity across the sites.

Hydrology

Piezometers were initially installed near the corners and center of each drainfield at each site to approximate the direction of groundwater flow using the three point method (Heath, 1983). Once the groundwater flow direction was estimated, additional piezometers were installed up and down-gradient of the drainfields. After the networks of piezometers were installed and hydraulic head data was available for a broader area, these data were used to

contour hydraulic head elevations across the sites using mean monthly (n = 12) hydraulic head values at site piezometers. Additionally, piezometers were nested at locations across the sites to assess vertical groundwater flow in order to determine groundwater recharge and discharge areas.

Hydraulic head recovery was measured at the sites on March 13, 2013, and was evaluated using the Bouwer and Rice Slug-test Method (1976). K was calculated from the hydraulic head recovery data according to equation 2:

$$K = \frac{r_c^2 \ln(R_e/R)}{2L} \frac{1}{t} \ln \frac{H_0}{H_t} \quad \text{(Eq. 2)}$$

Where K is hydraulic conductivity in m/day, r_c is the radius of the piezometer casing, R_e is the effective radius, R is the radius of the sand pack, L is the length of the screened interval, t is total time of the test, H_0 is the hydraulic head at time 0 and H_t is the hydraulic head at time t during the test.

K was also approximated from sediment samples using the Hazen Method defined in equation 3 to help better constrain K across the sites (Hazen, 1911):

$$K = C(d_{10})^2 \quad \text{(Eq. 3)}$$

Where K is hydraulic conductivity in cm/second, C is a coefficient based on sorting and the median grain-size of the sample, and d_{10} is the effective grain-size in cm where 10% of the grains are finer by weight. C ranges from 40 (poorly sorted very fine-grained sand) to 150 (clean, well sorted coarse-grained sand) (Fetter, 2001). The lowest values of C appropriate for the degree of sorting and grain-size range of each sample were used for the calculations. K was converted to m/day.

Groundwater velocity was calculated using median K estimates, and a mean effective porosity estimate of 0.2 for similar sandy soils estimated by Humphrey, (2002) in order to approximate groundwater travel times using the groundwater velocity equation defined in equation 4 (Heath, 1983):

$$V = \frac{Kdh}{ndl} \quad \text{(Eq. 4)}$$

Where V is velocity in m/day, K is saturated horizontal hydraulic conductivity in m/day, n is effective porosity, and $\frac{dh}{dl}$ is the hydraulic gradient in m/m.

Ground and Surface Water Monitoring

Ground and surface water monitoring were conducted throughout the study period at the sites. The monitoring plan included all site piezometers, JWSESspring, the un-named tributary to Core Creek at JWSES, and the un-named intermittent tributary to Swift Creek at WCHS. Depth to groundwater (m), temperature (C), and specific conductivity (µS/cm) were measured monthly using a calibrated Solinst TLC meter. NO3, NH4, and Cl concentrations (mg/L) were measured bi-monthly using a calibrated YSI multimeter. Additionally, ground/surface water samples were collected at the sites on three dates (July 13, October 28, and December 21, 2011) into sterile 250 mL plastic sample bottles for analysis at the East Carolina University Central Environmental Laboratory (ECUCEL).

Capacitively Coupled Resistivity

Electrical resistance is a measure of a material's opposition to the flow of electrical current and is defined by Ohm's Law:

$$R = V/I \quad \text{(Eq. 5)}$$

Where R is resistance in ohms (Ω), V is volts, and I is amps. Electrical resistivity quantifies how strongly a material opposes the flow of electric current for a homogeneous volume of material and is quantified in units of ohm.m (Ω.m) according to equation 6:

$$\rho = {}^{RA}/_{l} \qquad \text{(Eq. 6)}$$

Where ρ is resistivity in Ω.m, R is resistance in Ωs, A is the cross-sectional area in m^2, and l is length in meters (Burger, 1992). Electrical resistivity can be determined using a wide range of geophysical techniques (Kuras et al., 2006). Methods of measuring electrical resistivity involve applying direct current or low frequency alternating current at the ground surface and measuring the potential difference between two points (Burger, 1992). This study used a capacitively coupled OhmMapper system operating at a frequency of approximately 16.5 kHz for resistivity measurements. CCR mapping involves applying alternating current into the ground and measuring the potential difference between two dipoles (Geometrics, 2013). The OhmMapper uses coaxial cables with transmitter and receiver sections arranged in a dipole-dipole array that are towed along the ground (Geometrics, 2013). Investigation depth increases with increased distance between the dipoles. Dipole spacings of 2.5, 5, 10 and 20 m were used for the resistivity surveys in order to target depths ranging from 0 – 9 mbgs. All surveys were conducted in variable off-set mode. 3D surveys were conducted within the geophysical survey areas in a south to north trending zigzag pattern adjacent to the drainage trenches using 4 m line spacing. Cross-sectional surveys were conducted from A to A'. Resistance varies with the distance between and orientation of the transmitter and receiver dipoles. It is normalized by adding a geometric factor appropriate for the antenna array that converts the measurement to apparent resistivity.

Apparent resistivity is not the true resistivity of the subsurface, but an "apparent" value that is the resistivity of a homogeneous ground that will give the same resistance value for the same electrode arrangement (Loke, 2004). Variations in resistance to current flow at depth cause distinctive variations in the potential difference measurements, providing information on the subsurface structure and materials (Burger, 1992). The resistivity of subsurface materials is related to various geologic parameters such as the mineral and fluid content, porosity, hydraulic conductivity, and degree of water saturation (Urish, 1981; Loke, 2000). To better understand these parameters an iterative inverse modeling process was necessary to estimate the true resistivity from apparent resistivity data.

Inverse modeling was carried out using RES2DINV (v. 3.55) and RES3DINV (v. 2.15) resistivity inversion software (Geotomo, 2010, 2011). True resistivity data was gridded with Delaunay two-dimensional (2D) and 3D filters for interpolation using an open graphics library (OpenGL) by means of Paraview.org open-source visualization application (v. 3.98.1).

Ground Penetrating Radar

GPR is a high resolution geophysical method widely used to study the shallow subsurface and identify various features that reflect or attenuate electromagnetic (EM) energy (Daniels, 2000). It has broad application in hydrogeological studies since EM reflections are dominated by the presence and quality of groundwater (Annan, 2005). GPR provides stratigraphic and soil water information by transmitting an EM signal into the subsurface at frequencies ranging from 1 MHz – 1 GHz and recording reflections in two-way travel time. Reflection and attenuation of the signal are generated within the stratigraphic column where a change in dielectric properties occurs across a stratigraphic contact or in water quality. Dielectric permittivity is expressed as $\varepsilon_r = (C/V)^2$, where ε_r is the dielectric constant, C = 0.3 m/ns which is the speed of light in a

vacuum, and V is velocity. GPR performs best in coarse-grained materials, such as resistive sands and gravels with relatively low dielectric constants (Annan, 2005). Dielectric permittivity controls radar signal velocity, while electrical conductivity has a large effect on attenuation (Knight, 2001). Attenuation of the EM signal is a function of the magnetic permeability and the electrical conductivity of sediments (Baker et al., 2007). The magnetic permeability for most nonferromagnetic rocks and soil is approximately equal to 1 (Reppert et al., 2000). Therefore, electrical conductivity is the dominant control on radar signal attenuation. Electrically conductive materials increase the dielectric permittivity of a material, decreasing radar signal velocity due to increased signal attenuation. Leucci, (2008) presented a method for measuring radar signal attenuation directly from individual EM radar traces. This study used a similar approach to interpret signal attenuation by evaluating the absolute peak amplitude (APA) of individual EM radar traces. The APA measured in this study is not a real measure of radar wave amplitude, but a relative measure of signal strength after various filters were consistently applied to the data. APA was used as a proxy to assess radar signal attenuation across the sites.

A Geophysical Survey Systems Incorporated (GSSI), SIR-2000 operating with a 200-MHz antenna was used for GPR data collection for increased resolution at depths ranging from 0 – 12 mbgs. All surveys were conducted in continuous monostatic mode using a calibrated survey wheel for spatial reference. Data were collected at a rate of 20 traces/m and 1023 samples/trace with a sampling window of 200 nanoseconds. 3D surveys were conducted within the geophysical survey areas in a south to north trending zigzag pattern adjacent to the drainage trenches using 2 m line spacing. Cross-sectional surveys were conducted from A to A'. The post-processing sequence consisted of correcting the surface delay to time-zero, band-pass filtering, a Kirchhoff constant velocity migration, and gain adjustments to aid in interpretation

(Radan v. 6.6). All data were post-processed using the same settings. APA values were measured before applying the constant velocity migration for dielectric consistency between data sets.

Laboratory Analysis

All water samples were vacuum filtered through ashed 1.5 micron carbon filters prior to analysis. Samples containing an excess of suspended solids were centrifuged before filtering. Samples were analyzed using a Westco Scientific Instruments Incorporated automated SmartChem 200 Discrete Wet Chemistry Analyzer in accordance with EPA approved methods. Analysis consisted of dissolved kjeldahl nitrogen (DKN), ammonium (NH4), nitrate (NO3+NO2), chloride (Cl) and phosphate (PO4). Analytical methods are summarized in Table 2 and ECUCEL reports are included in Appendix B.

Constituent	EPA Approved Analytical Method
DKN	390-200
NH4	210-201B
NO3+NO2	375-100E-1
Cl	231N-0406C
PO4	410-3651

Table 2. Water sample constituents and SmartChem 200 EPA approved analytical methods.

NO3+NO2 and NH4 concentrations were summed to quantify dissolved inorganic nitrogen (DIN) loading at the sites. Laboratory DIN and Cl concentrations were compared to the YSI multimeter measurements to create calibration curves in order to correct the field measurements on the three sampling dates. Corrected measurements were used to better

understand the DIN and Cl contribution to groundwater specific conductivity for a broader sampling area across the sites.

Statistical Analysis

To elucidate the controls on GPR and CCR variations in the study, geophysical measurements (Ω.m and APA) were compared to geologic and hydrologic parameters (porosity, hydraulic conductivity, water-table depth, and groundwater specific conductivity) using linear regressions. Nested shallow piezometers at WCHS were not included in the comparisons due to incomplete data sets resulting dry piezometers. Non-parametric Mann-Whitney tests were also used to compare data sets and test whether their median values were significantly different (Minitab v.16.1). P-values from Mann-Whitney tests are presented and considered significant when below 0.05.

Chapter 4

Results

Hydrogeological Characterization

Lithology and Porosity

Sediment samples (n = 31) from cores collected at 1/GP1 (5.1 mbgs), 3/GP2 (5.4 mbgs) and 12/GP3 (5.6 mbgs) (Figure 2) indicated that sediments at JWSES from 0 – 5.6 mbgs were composed of unconsolidated, predominantly siliciclastic grains. Median (d_{50}) grain-size ranged from fine (2.58 φ) to very coarse-grained (-0.003 φ) sand (Appendix C). Grain-size proportions were 2.2% gravel, 91% sand and 6.8% silt and clay (Folk, 1954) (Figure 4). Based on uniformity coefficients (d_{60}/d_{10}), median (n=31) porosity was estimated to be 41% across the site (Appendix D).

Sediment samples (n = 25) from cores collected at 1d/GP4 (4.7 mbgs), 13d/GP5 (4.75 mbgs) and 22d/GP6 (4.6 mbgs) (Figure 3) indicated that sediments at WCHS from 0 – 4.75 mbgs were composed of unconsolidated, predominantly siliciclastic grains. Median (d_{50}) grain-size ranged from fine (2.71 φ) to coarse-grained (0.68 φ) sand (Appendix C). Grain-size proportions were 2.6% gravel, 92.1% sand and 5.3% silt and clay (Folk, 1954) (Figure 4). Based on uniformity coefficients (d_{60}/d_{10}), median (n = 25) porosity was estimated to be 43% across the site (Appendix D). These data indicate that surficial sediments at both sites were comprised of similar sandy sediments with comparable porosities.

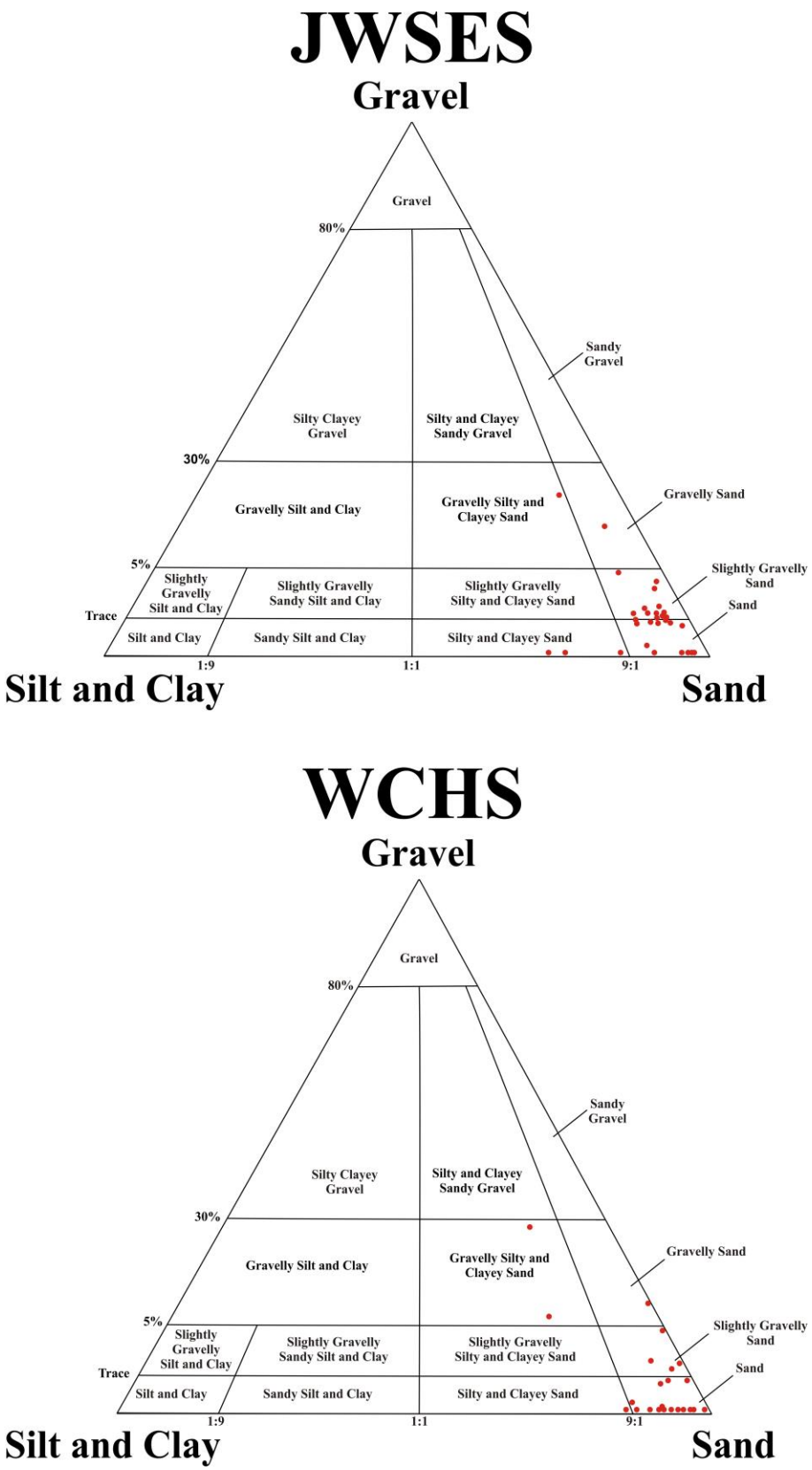

Figure 4. Grain-size proportions at JWSES (n = 31) and WCHS (n = 24).

Groundwater Hydrology

At JWSES, hydraulic head varied throughout the study. Mean monthly (n = 12) hydraulic head elevations at piezometers 5, 9, and 18 (Appendix E) indicated the hydraulic gradient was 3.7×10^{-2} m/m and that groundwater beneath the drainfield flowed in a northwesterly direction before discharging to a spring or unnamed tributary of Core Creek located approximately 40 m north of the drainfield (Figure 2). The spring discharge flowed in a northerly direction across the floodplain for approximately 15 m before converging with the tributary. The difference in mean monthly (n = 12) hydraulic head at piezometers 2 and 3/GP2 suggest this location to be an area of groundwater recharge at the site (Appendix F). Median K (n = 18) across the site determined from hydraulic head recovery data was 1.3×10^{-1} m/day (Appendix G). Based on Hazen approximations at the screened depth of piezometers 1/GP1, 3/GP2, and 12/GP3, median (n = 3) K at these locations was 5×10^{-1} m/day. Additionally, the Craven County Soil Survey (USDA, 1989) contained a permeability estimate from data obtained using the constant head permeameter method for samples of Autryville Loamy Sand, the dominant soil series at the site. This estimate was 1.2 m/day. According to the three methods of measuring K, K at the site was estimated to range from 1.3×10^{-1} – 1.2 m/day. Based on the median K value calculated from hydraulic head recovery data, the K value obtained from the constant head permeameter method, and the effective porosity estimate for the site, groundwater velocity was estimated to range from 2.4×10^{-2} – 2.2×10^{-1} m/day. At this rate it would take approximately 112 days to 2.8 years for groundwater at the northern edge of the drainfield to reach the spring located approximately 25 m north (Figure 2). An analysis of the groundwater quality across the site is included in Appendix H.

At WCHS, hydraulic head varied throughout the study. Mean monthly (n = 12) hydraulic head elevations at piezometers 9, 14, and 22 (Appendix E) indicated the hydraulic gradient was 6.0×10^{-4} m/m and that groundwater beneath the drainfields flowed in a northerly to northwesterly direction. The differences in mean monthly (n = 12) hydraulic head at piezometers 1s, 1d/GP4, 13s, 13d/GP5, 22s, and 22d/GP6 suggest that groundwater recharge/discharge was variable across the site. Groundwater tended to recharge at the locations of piezometers 1s/1d/GP4 and 13s/13d/GP5, and discharge at 22s/22d/GP6 (Appendix F). Median K (n = 23) across the site determined from hydraulic head recovery data was 1.1 m/day (Appendix G). Based on Hazen approximations at the screened depth of piezometers 1d/GP4, 13d/GP5, and 22d/GP/6, median (n = 3) K at these locations was 2.9 m/day. Additionally, the Craven County Soil Survey (USDA, 1989) contained a permeability estimate from data obtained using the constant head permeameter method for samples of Conetoe Loamy Sand, the dominant soil series at the site. This estimate was 12 m/day. According to the three methods of measuring K, K at the site was estimated to range from 1.1 to 12 m/day. Based on the median K value calculated from hydraulic head recovery data, the K value obtained using the constant head permeameter method, and the effective porosity estimate for the site, groundwater velocity was estimated to range from $3.3 \times 10^{-3} – 3.6 \times 10^{-2}$ m/day. The hydraulic gradient was approximately 2 orders of magnitude lower and groundwater velocity was approximately 1 order of magnitude lower, while hydraulic conductivity was approximately 1 order of magnitude higher relative to JWSES. An analysis of the groundwater quality across the site is included in Appendix H.

On-site Wastewater System Component Detection

The location of the wastewater drainfields at JWSES and WCHS (Figures 2 and 3) were determined from as-built OWS blueprints produced by Buffaloe, Morgan & Associates Incorporated and Matthews and Blizzard Registered Land Surveyors (Appendix I) and a field survey. Depths to the top of the drainage trenches were measured at both sites with a tile-drain probe. The average depth at JWSES was 0.6 mbgs and 0.7 mbgs at WCHS. To determine if GPR and CCR can detect subsurface OWS components, 3D surveys were conducted in the geophysical survey areas adjacent to the drainage trenches at JWSES on September 2, 2011 and WCHS on February 3, 2012.

At both sites, at approximately 1 mbgs, differences in resistivity were apparent in the drainfields (Figure 5). Generally, the CCR surveys indicated low resistivity in the shallow soils of the drainfields relative to surrounding soils, but did not distinguish individual drainage trenches at either site.

At 1 mbgs, high amplitude reflections defining linear features were observed at both sites, indicating the radar signal was not affected above the drainage trenches (Figure 5). These estimates were within 0.4 m of the measured depths. At JWSES, 32 drainage trenches existed; over the section of the drainfield surveyed, 25 trenches were detected consistent with the location and spacing described in the as-built OWS blueprint. At WCHS, over the section of the drainfields survey, all 32 active drainage trenches were identified, as well as 13 of the 16 inactive trenches, consistent with the location and spacing described in the as-built OWS blueprint. Based on these results, increasing the survey area boundaries may identify the remaining drainage trenches at the sites.

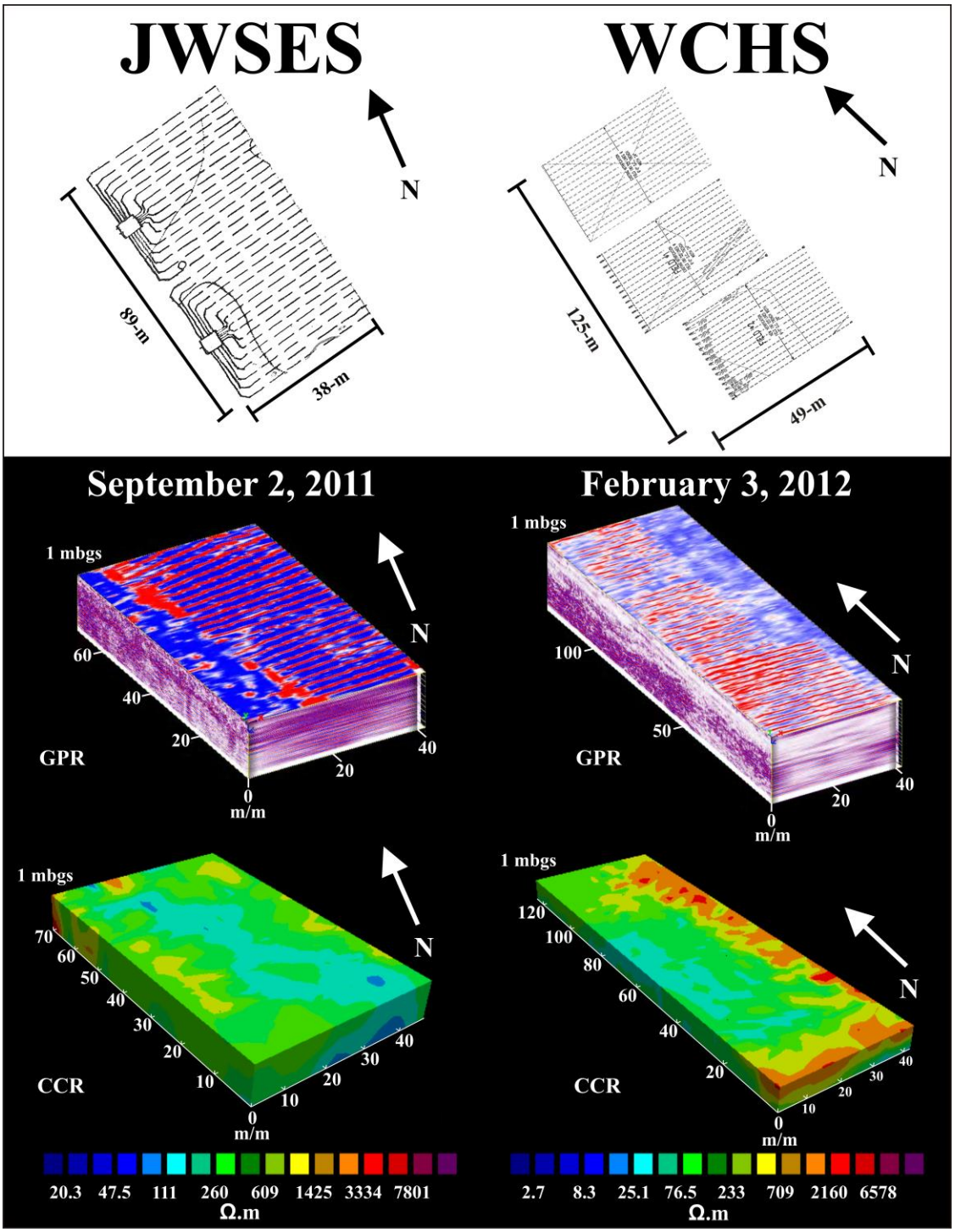

Figure 5. As-built OWS blueprints and 1 mbgs CCR and CPR models of the survey area at JWSES and WCHS. In the GPR models, blue indicates low amplitude reflections and red indicates high amplitude reflections.

Wastewater Plume Delineation

Hydrogeological and Water Quality Influences on Capacitively Coupled Resistivity

To characterize the dominant controls on resistivity at the sites, resistivity measurements at JWSES and WCHS transect piezometers were compared to variables that quantified porosity, hydraulic conductivity, saturation, and water quality.

To evaluate the influence of porosity on resistivity measurements, bi-monthly (n = 5) mean Log resistivity values (Appendix J) were compared to porosity values at JWSES1/GP1, JWSES3/GP2, JWSES12/GP3, WCHS1d/GP4, WCHS13d/GP5 and WCHS22d/GP6 (Appendix E) near the depths of sediment samples. At JWSES (n = 17), to a depth of approximately 5.5 mbgs, and at WCHS (n = 12), to a depth of approximately 3.2 mbgs, there were not strong relationships between porosity and resistivity. Although porosity may influence resistivity, differences in porosity were minimal at these locations; indicating porosity contrasts were not the likely cause of resistivity changes across the sites (Figure 6).

Since spatial variations in K can have an effect on resistivity; resistivity was compared to K values obtained from hydraulic head recovery data (Appendix G) at the sites. The highest K estimates at site piezometers were at JWSES20 (2.6 m/day) and WCHS9 (2.8 m/day). K calculated at transect piezometers ranged from 4.0×10^{-3} – 2.6 m/day at JWSES and 1.8×10^{-1} – 2.8 m/day at WCHS. Bi-monthly (n = 5) mean Log resistivity values (Appendix J) near the screened depth of transect piezometers versus K did not reveal a relationship at either site (Figure 6).

To evaluate whether changes in saturation had an effect on resistivity; resistivity was compared to water-table depths across the sites. Bi-monthly (n = 5) water-table depth

measurements at transect piezometers ranged from 3.6 – 7.2 mbgs at JWSES (n = 7) and 0.6 – 2.5 mbgs at WCHS (n =9) (Appendix E). Across sampling dates, the most extreme water-table depth fluctuations along the transects occurred at JWSES3/GP2 (1.2 m) between February 25 – July 13, 2011, and WCHS7 (1.4 m) between July 13, 2011 – September 2, 2011. To evaluate the influence of saturation on resistivity measurements, bi-monthly (n = 5) mean Log resistivity values (Appendix J) near the screened depth of transect piezometers were compared to bi-monthly (n = 5) mean water-table depths at the same locations. At JWSES, $R^2 = 0.02$ (n = 7) and $R^2 = 0.35$ at WCHS (n = 9) (Figure 6). Across sampling dates, resistivity tended to be lower in the drainfields relative to background values at both sites.

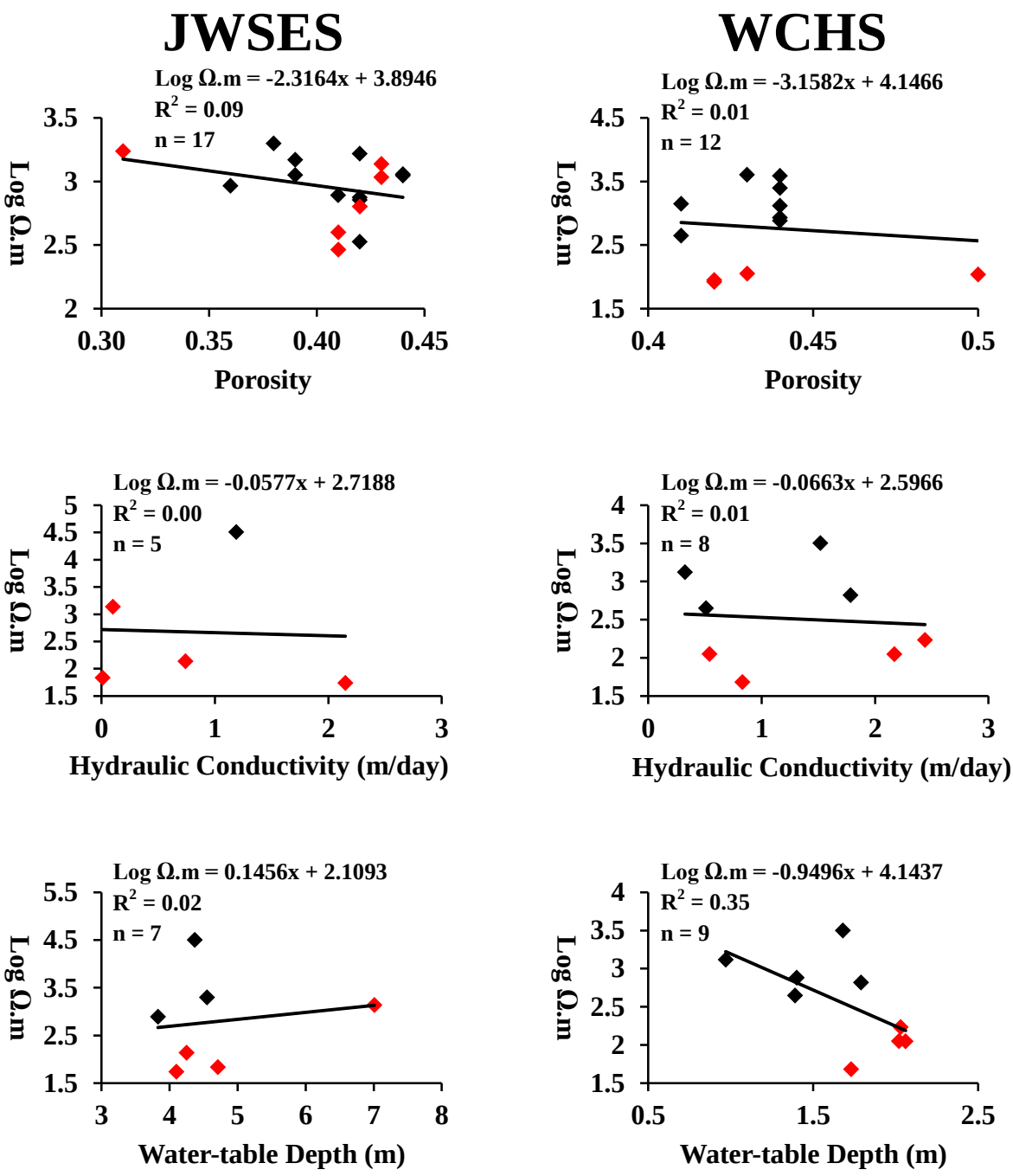

Figure 6. Scatterplots of Log resistivity versus porosity, hydraulic conductivity, and water-table depth at JWSES and WCHS. Drainfield piezometers are represented in red and background piezometers in black.

To evaluate the influence of water quality on resistivity at the sites, comparisons of bi-monthly (n = 5) Log resistivity values near the screened depth of transect piezometers (Appendix

J) versus groundwater specific conductivity (Appendix E) revealed an inverse relationship at both sites. At JWSES $R^2 = 0.69$ (n = 35); at WCHS $R^2 = 0.75$ (n = 45) (Figure 7).

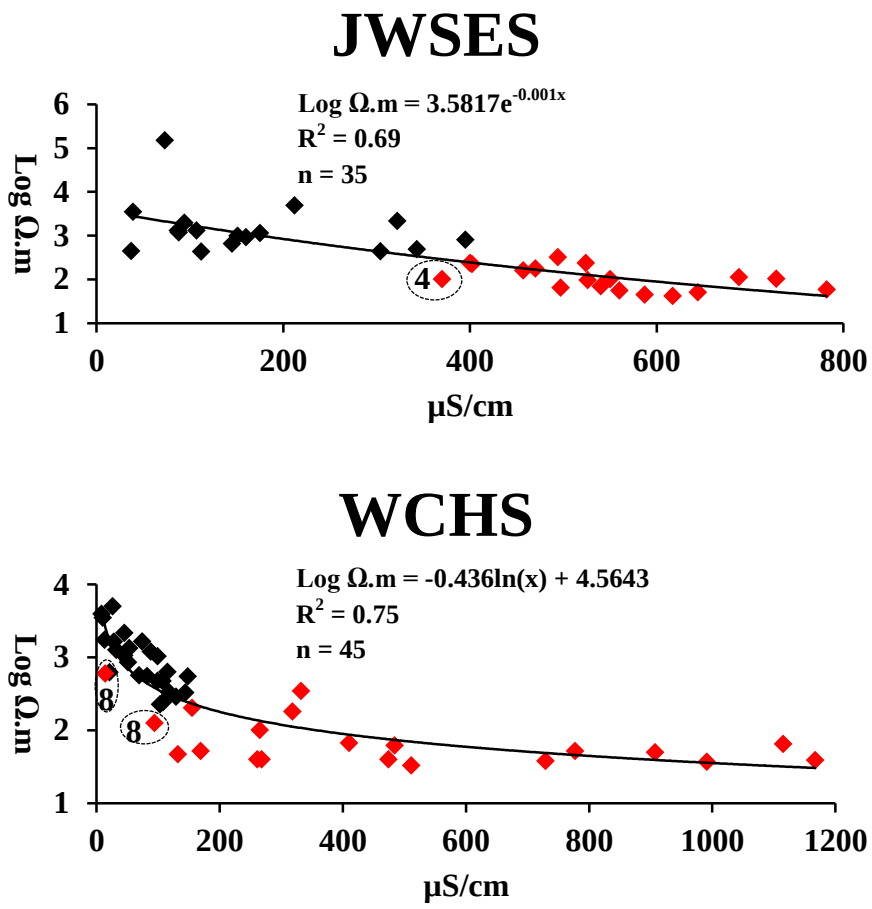

Figure 7. Scatterplots of Log resistivity versus groundwater specific conductivity at JWSES on 5/25, 7/13, 9/2, 11/11/2011, 1/31/2012 and WCHS on 5/25, 7/13, 9/2, 11/18/2011, and 2/3/2012. Drainfield piezometers are represented in red and background piezometers in black. JWSES4 and WCHS8 are circled to indicate outliers located at the up gradient edge of the drainfield.

At JWSES, with the exception of piezometer 4 on July 13, 2011 located at the up gradient edge of the drainfield, groundwater specific conductivity in the drainfield was consistently ≥ 400 µS/cm, corresponding to approximately ≤ 250 Ω.m. At WCHS, with the exception of piezometer 8 on September 2, 2011 and February 3, 2012, groundwater specific conductivity in the drainfield was consistently ≥ 130 µS/cm, corresponding to approximately ≤ 250 Ω.m. These

conductivity values contrasted with background values at the sites. At JWSES, mean monthly (n = 12) groundwater specific conductivity at background piezometers was 160 µS/cm (n = 3); and 53 µS/cm at WCHS (n = 7).

Contrasts in groundwater specific conductivity were apparent across the sites on all sampling dates. Specific conductivity was elevated in the drainfields relative to background piezometers (Appendix E). This is evident when viewing cross-sections of groundwater specific conductivity through the sites. For example, on July 13, 2011, notable differences in groundwater specific conductivity were apparent across both sites (Figure 8).

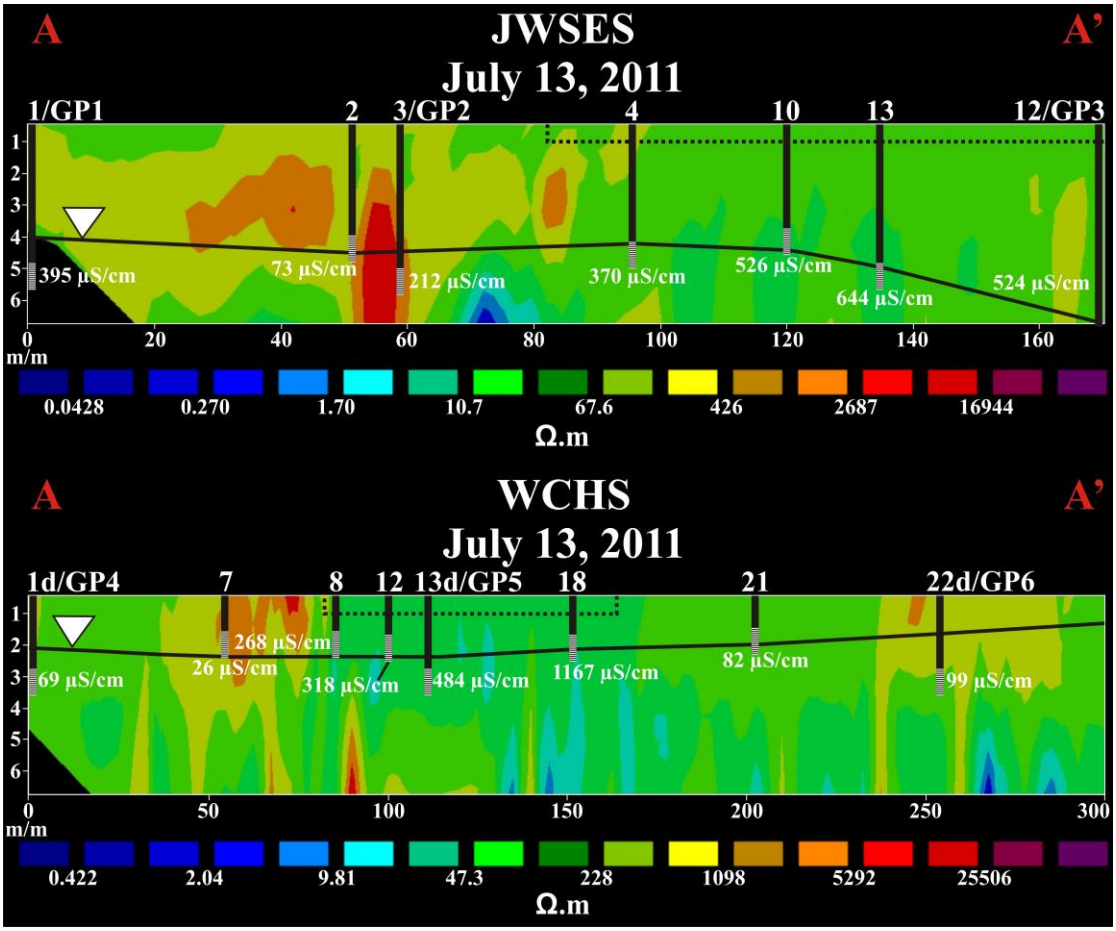

Figure 8. CCR cross-sections at JWSES and WCHS on July 13, 2011. The drainfields are represented with dashed lines and the water-table with solid lines. Transect piezometers are represented with corresponding groundwater specific conductivity values.

At JWSES on July 13, 2011, mean (n = 4) groundwater specific conductivity in the drainfield was 516 µS/cm and mean (n = 3) background was 227 µS/cm. At the same piezometers, mean resistivity in the drainfield was 146 Ω.m and mean background was 53306 Ω.m. At WCHS on July 13, 2011, mean (n = 4) groundwater specific conductivity in the drainfield was 559 µS/cm and mean (n = 4) background was 69 µS/cm. At the same piezometers, mean resistivity in the drainfield was 80 Ω.m and mean background was 901 Ω.m.

Bi-monthly (n = 5) groundwater specific conductivity values (Appendix E) and resistivity values (Appendix J) measured near the screened depth of transect piezometers located in the drainfields were compared to background values using Mann-Whitney tests (Figure 9).

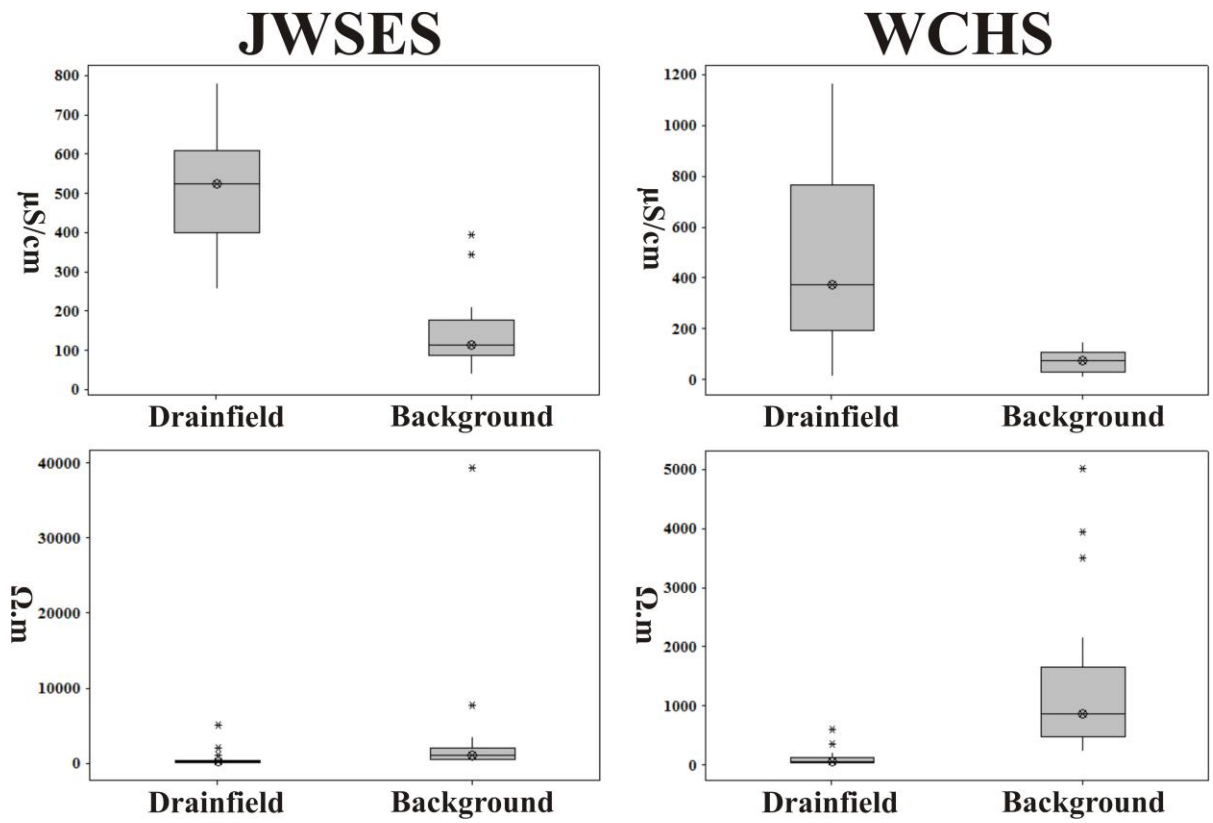

Figure 9. Boxplots of groundwater specific conductivity and resistivity values at transect piezometers located in the drainfields versus background values at JWSES on 5/25, 7/13, 9/2, 11/18/2011 and 1/31/2012 and WCHS on 5/25, 7/13, 9/2, 11/18/2011 and 2/3/2012.

At JWSES, median (n = 20) groundwater specific conductivity in the drainfield was 525 μS/cm and median (n = 15) background was 112 μS/cm (p = 0.0000). At the same piezometers, median resistivity was 104 Ω.m in the drainfield and 997 Ω.m at background piezometers (p = 0.0002). At WCHS, median (n=20) groundwater specific conductivity in the drainfield was 371 μS/cm and median (n = 20) background was74 μS/cm (p = 0.0000). At the same piezometers, median resistivity was 52 Ω.m in the drainfield and 857 Ω.m at background piezometers (p = 0.0000). P-values < 0.05 indicate that groundwater specific conductivity and resistivity values were significantly different in the drainfields relative to background values across all sampling dates.

To determine if the same resistivity patterns existed in the geophysical survey areas, Log resistivity values at the screened depth of survey area and transect piezometers (Appendix J and K) were compared to groundwater specific conductivity values at JWSES on January 31, 2012 and WCHS on February 3, 2012 (Appendix E). At JWSES, $R^2 = 0.57$ (n = 11); at WCHS $R^2 = 0.85$ (n = 14) (Figure 10).

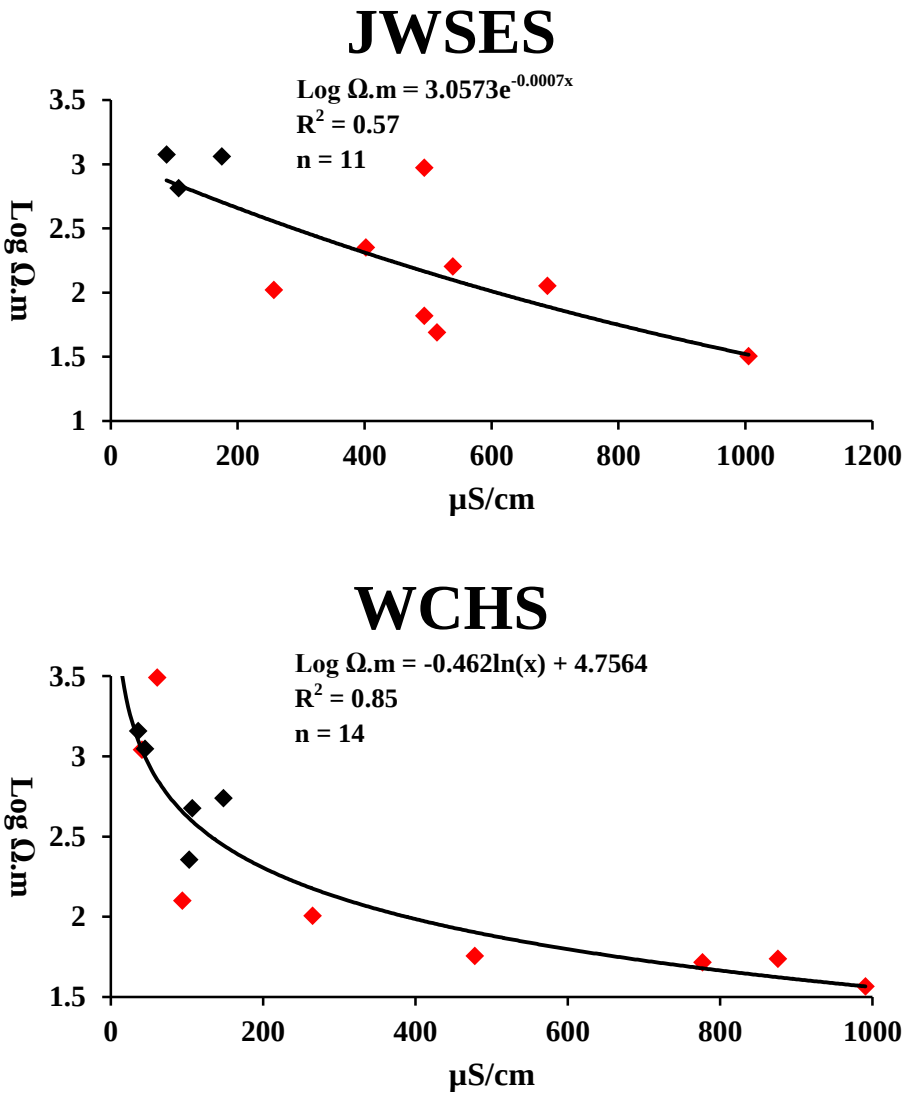

Figure 10. Scatterplots of Log resistivity values versus groundwater specific conductivity values at JWSES on January 31, 2012 and WCHS on February 3, 2012. Drainfield piezometers are represented in red and background piezometers in black.

At JWSES on January 31, 2012, mean (n = 8) groundwater specific conductivity in the drainfield was 549 µS/cm and mean (n = 3) background was 123 µS/cm. At the same piezometers, mean resistivity in the drainfield was 211 Ω.m and mean background was 999 Ω.m. At WCHS on February 3, 2012, mean (n = 8) groundwater specific conductivity in the drainfield was 448 µS/cm and mean (n = 8) background was 54 µS/cm. At the same piezometers, mean resistivity in the drainfield was 578 Ω.m and mean background was 1218 Ω.m. Overall, at both

sites, resistivity tended to decrease in the drainfields relative to background values on these dates.

To gauge the extent of wastewater impacted groundwater, regions of resistivity measuring ≤ 250 Ω.m beneath the drainfields were delineated to 9 mbgs at JWSES on January 31, 2012 and 5.5 mbgs at WCHS on February 3, 2012 (Figure 11).

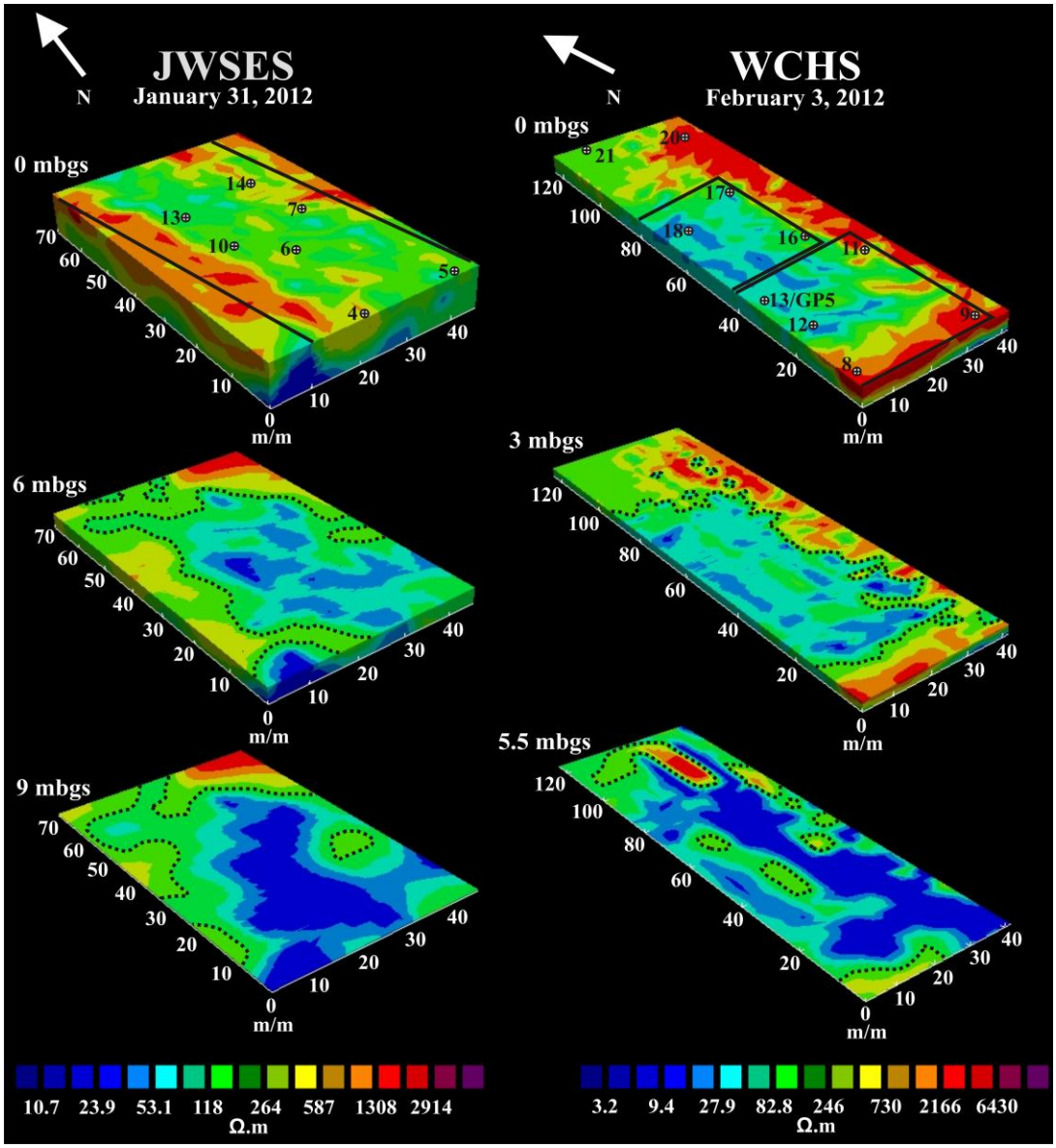

Figure 11. CCR models of the geophysical survey area at JWSES (46 m x 70 m x 9 m) and WCHS (42 m x 125 m x 5.5 m). The wastewater drainfields and piezometer locations are represented in the surface models. Areas of resistivity measuring ≤ 250 Ω.m are delineated with depth by dashed lines.

In the surface models (0 mbgs) at both sites, regions of low resistivity were identified in the drainfields relative to the surrounding soils. At JWSES on January 31, 2012, the mean (n = 7) water-table depth in the geophysical survey area was 5.3 mbgs (Appendix E). At 6 mbgs, a region of resistivity ≤ 250 Ω.m spanned approximately 40 m x 60 m. At 9 mbgs, the low

resistivity region increased laterally to approximately 46 m x 70 m. At WCHS on February 3, 2012, the mean (n = 10) water-table depth in the geophysical survey area was 1.9 mbgs (Appendix E). At 3 mbgs, a region of resistivity ≤ 250 Ω.m spanned approximately 35 m x 75 m. At 5.5 mbgs, the low resistivity region increased laterally to approximately 42 m x 120 m. In the deepest models, the low resistivity regions tended to extend in a northerly direction, in agreement with the approximated direction of groundwater flow beneath the drainfields at both sites. At JWSES, elevated specific conductivity, DIN, and Cl were measured at the spring. The spring discharge flowed approximately 15 m to the un-named tributary of Core Creek, which converges with the Neuse River approximately 4.5 km north of the site.

Hydrogeological and Water Quality Influences on Ground Penetrating Radar

To help understand the controls on radar signal attenuation at the sites, APA of individual radar traces near transect piezometers on July 13, September 2, November 18, 2011 and January 31, 2012 were compared to variables quantifying porosity, saturation, and water quality.

To evaluate the influence of porosity on APA measurements, bi-monthly mean (n = 4) Log APA values (Appendix L) were compared to porosity values near depths corresponding with sediment samples at JWSES1/GP1, JWSES3/GP2, JWSES12/GP3, WCHS1d/GP4, WCHS13d/GP5 and WCHS22d/GP6 (Appendix E). At JWSES (n = 26), to a depth of approximately 5.6 mbgs, and at WCHS (n = 22) to a depth of approximately 4.8 mbgs, there were no significant relationships between porosity and APA. While porosity can influence the radar signal, differences in porosity were minimal at these locations, indicating porosity contrasts did not likely cause radar signal attenuation across the sites (Figure 12).

To determine if the degree of saturation had an effect on radar signal attenuation, bi-monthly mean (n = 4) Log APA values near the screened depth of transect piezometers (Appendix L) were compared to water-table depths at the same locations (Appendix E). At JWSES, $R^2 = 0.02$ (n = 7), and $R^2 = 0.27$ at WCHS (n = 9) (Figure 12). Absolute peak amplitude values tended to decrease in the drainfields relative to background values at both sites.

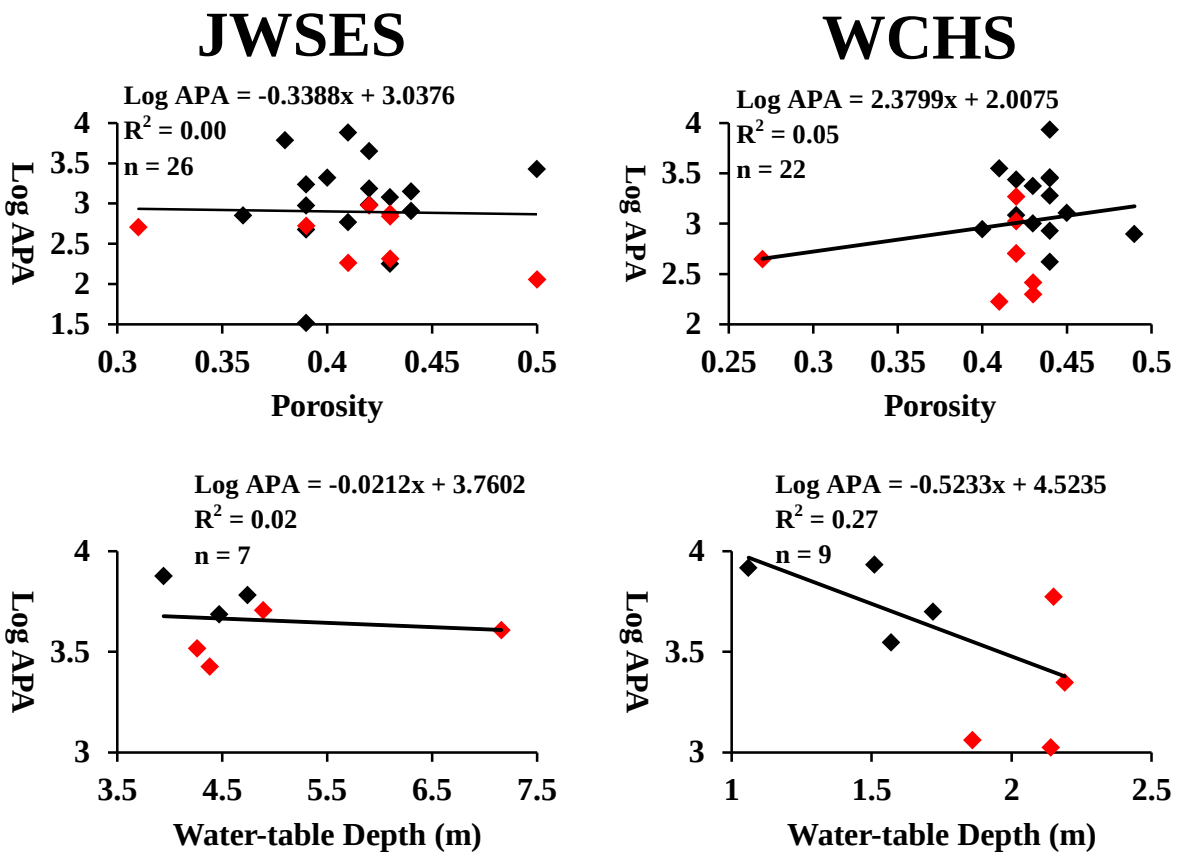

Figure 12. Scatterplots of Log APA versus porosity and water-table depths at JWSES and WCHS. Drainfield piezometers are represented in red and background piezometers in black.

To evaluate the influence of water quality on APA measurements at the sites, comparisons of bi-monthly (n =4) Log APA values near the screened depth of transect piezometers (Appendix L) versus groundwater specific conductivity values at the same locations

(Appendix E) revealed $R^2 = 0.02$ at JWSES (n = 28) and $R^2 = 0.37$ at WCHS (n = 36) (Figure 13).

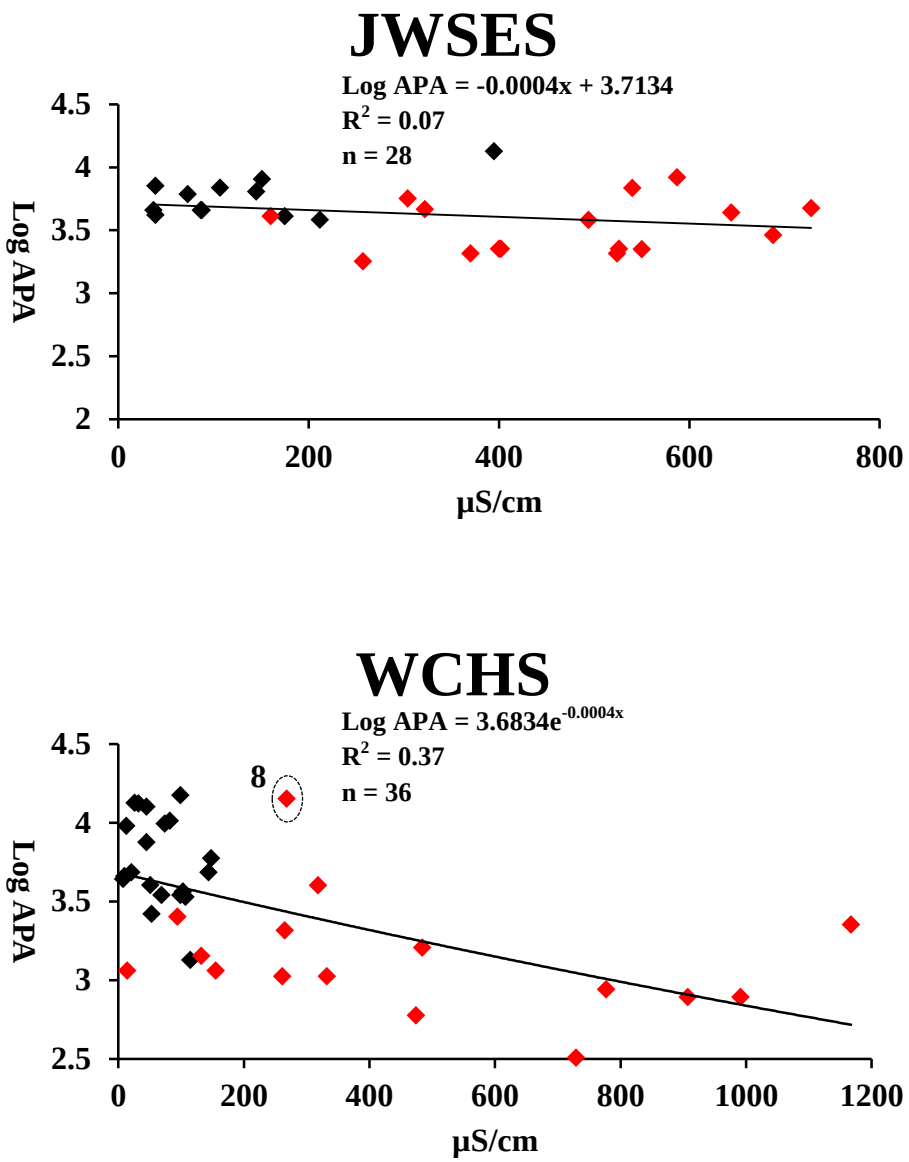

Figure 13. Scatterplots of Log APA versus groundwater specific conductivity at JWSES and WCHS on 7/13, 9/2, 11/18/2011 and 1/31/2012. Drainfield piezometers are represented in red and background piezometers in black. WCHS8 is circled to indicate an outlier located at the up gradient edge of the drainfield.

Across all sampling dates, APA tended to decrease in the drainfields relative to background values. Overall, APA tended to decrease in regions with elevated groundwater specific conductivity at the sites, with the exception of WCHS8 located at the up gradient edge of the drainfield.

Contrasts in APA associated with differences in groundwater specific conductivity were apparent across the sites on all sampling dates. Regions of decreased APA indicative of radar signal attenuation corresponded with regions of elevated groundwater specific conductivity at both sites. This is evident when viewing GPR cross-sections through the sites. For example, on July 13, 2011, notable differences in radar signal attenuation (indicated by whited out regions) were apparent across the sites (Figure 14).

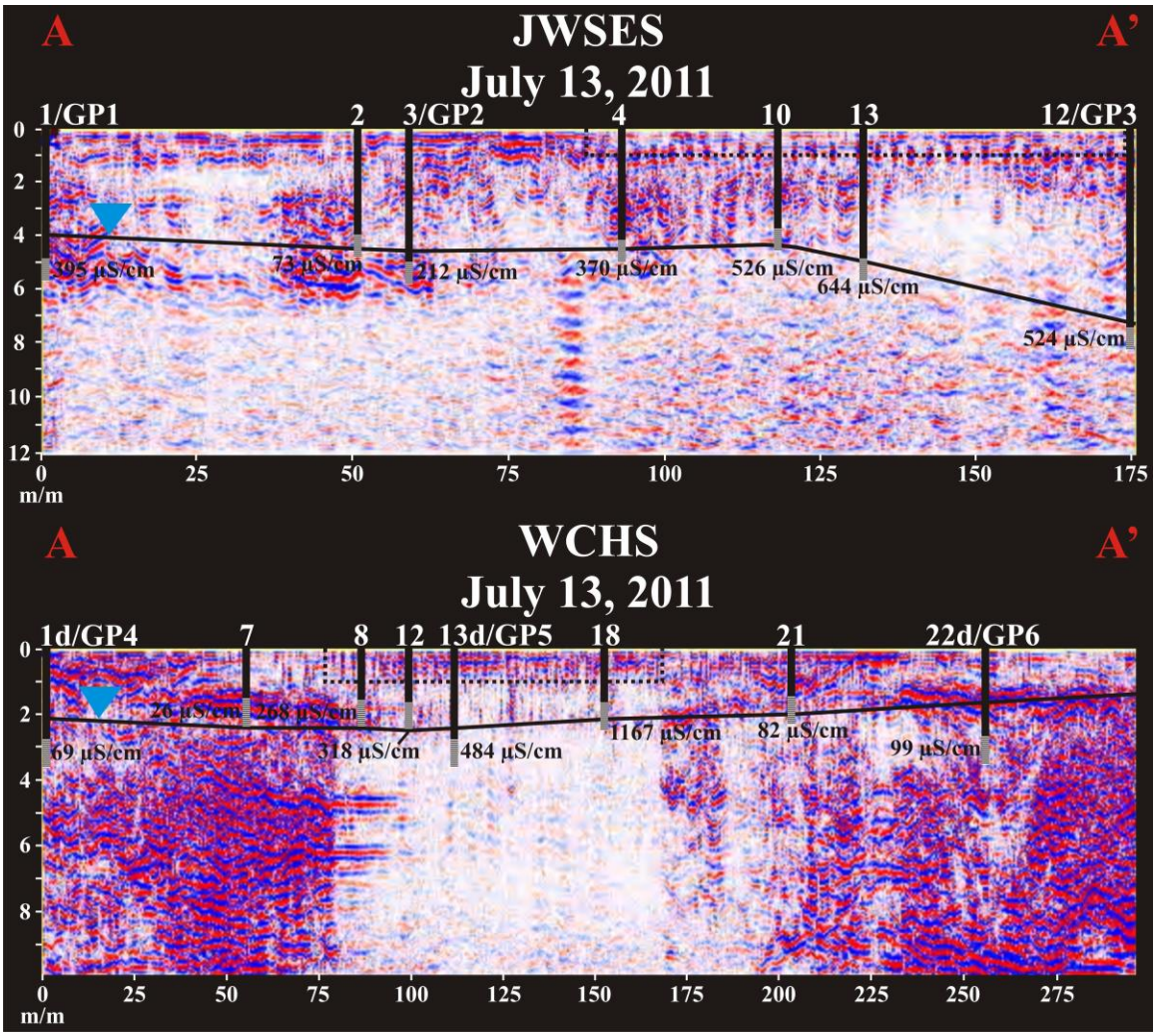

Figure 14. GPR cross-sections at JWSES and WCHS on July 13, 2011. The drainfields are represented by dashed lines and the water-table by solid lines. Transect piezometers are represented with corresponding groundwater specific conductivity values. Whited out regions indicate radar signal attenuation.

At JWSES, mean (n = 4) groundwater specific conductivity in the drainfield was 516 µS/cm and mean (n = 3) background was 227 µS/cm. Near the screened depth of the same piezometers, mean APA in the drainfield was 3133 and mean background was 7788. At WCHS, mean (n = 4) groundwater specific conductivity in the drainfield was 559 µS/cm and mean (n = 4) background was 69 µS/cm. Near the screened depth of the same piezometers, mean APA in the drainfield was 6835 and mean background was 11034. Whited out regions beneath the drainfields was indicative of wastewater impacted groundwater.

Bi-monthly (n = 4) groundwater specific conductivity (Appendix E) and APA values (Appendix L) measured near the screened depth of transect piezometers located in the drainfields were compared to background values using Mann-Whitney tests (Figure 15).

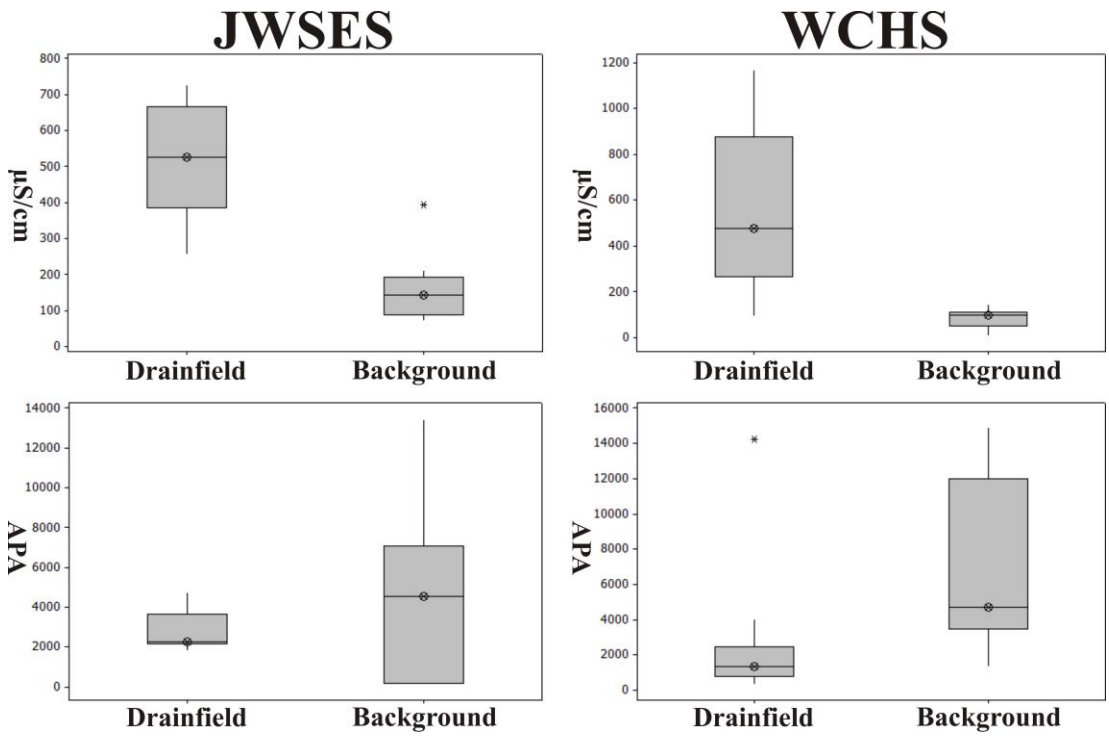

Figure 15. Boxplots of groundwater specific conductivity and APA values at transect piezometers located in the drainfields versus background values at JWSES and WCHS on 7/13/11, 9/2/11, 11/18/11 and 1/31/12.

At JWSES, median (n = 16) groundwater specific conductivity in the drainfield was 526 µS/cm and median (n = 12) background was 145 µS/cm (p = 0.0008). At the same piezometers, median APA was 2257 in the drainfield and 4562 at background piezometers (p = 0.4253). At WCHS, median (n = 16) groundwater specific conductivity in the drainfield was 479 µS/cm and median (n = 16) background was 99 µS/cm (p = 0.0002). At the same piezometers, median APA was 1336 in the drainfield and 4700 at background piezometers (p = 0.0029). Groundwater specific conductivity values were significantly different in the drainfields relative to background

values as indicated by p-values < 0.05. Absolute peak amplitude values were significantly different in the drainfield relative to background values at WCHS but not at JWSES.

Regions of attenuated radar signal beneath the drainfields were delineated to 7 mbgs at JWSES on January 31, 2012 and 12 mbgs at WCHS on February 3, 2012 (Figure 16).

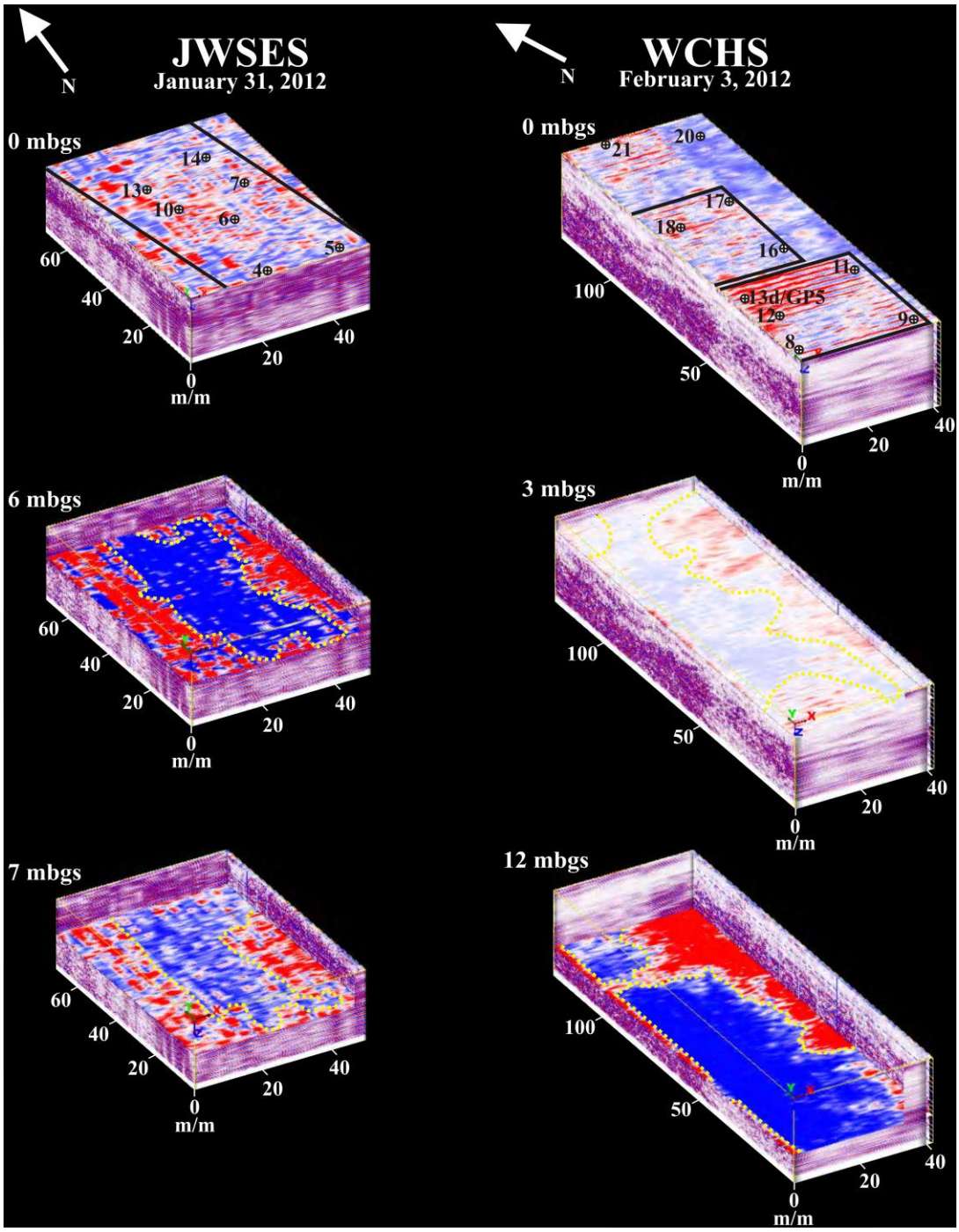

Figure 16. GPR models of the geophysical survey area at JWSES (46 m x 70 m x 7 m) and WCHS (42 m x 125 m x 12 m). The wastewater drainfields and piezometer locations are represented in the surface models. Areas of radar signal attenuation are represented in blue and delineated with depth by dashed yellow lines.

The radar signal was unaffected in the surface models (0 mbgs) at both sites. At depths beneath the drainage trenches, radar signal attenuation became apparent. At JWSES on January

31, 2012, mean (n = 7) water-table depth in the geophysical survey area was 5.3 mbgs (Appendix E). At 6 mbgs, a region of attenuation spanned approximately 30 m x 70 m. At 7 mbgs, the dimensions of the attenuated region remained relatively constant. Data collection below 7 m was not possible due to the weakened radar signal. At WCHS on February 3, 2012, mean (n = 10) water-table depth in the geophysical survey area was 1.9 mbgs (Appendix E). At 3 mbgs, a region of attenuation spanned approximately 25 m x 100 m. At 12 mbgs, the attenuated region increased laterally to approximately 35 m x 125 m. Data collection below 12 m was not possible due to the weakened radar signal.

Wastewater Plume Lateral Extent

To better constrain the wastewater plume dimensions and for comparison to the geophysical estimates, groundwater specific conductivity values at geophysical survey area piezometers were used to delineate the extent of wastewater impacted groundwater on the same dates as the 3D surveys. Based on the resistivity versus groundwater specific conductivity relationships (Figure 7), the lateral plume dimensions were estimated at the average screened depth of geophysical survey area piezometers at JWSES (6 mbgs) on January 31, 2012 and WCHS (3 mbgs) on February 3, 2012 (Figure 17).

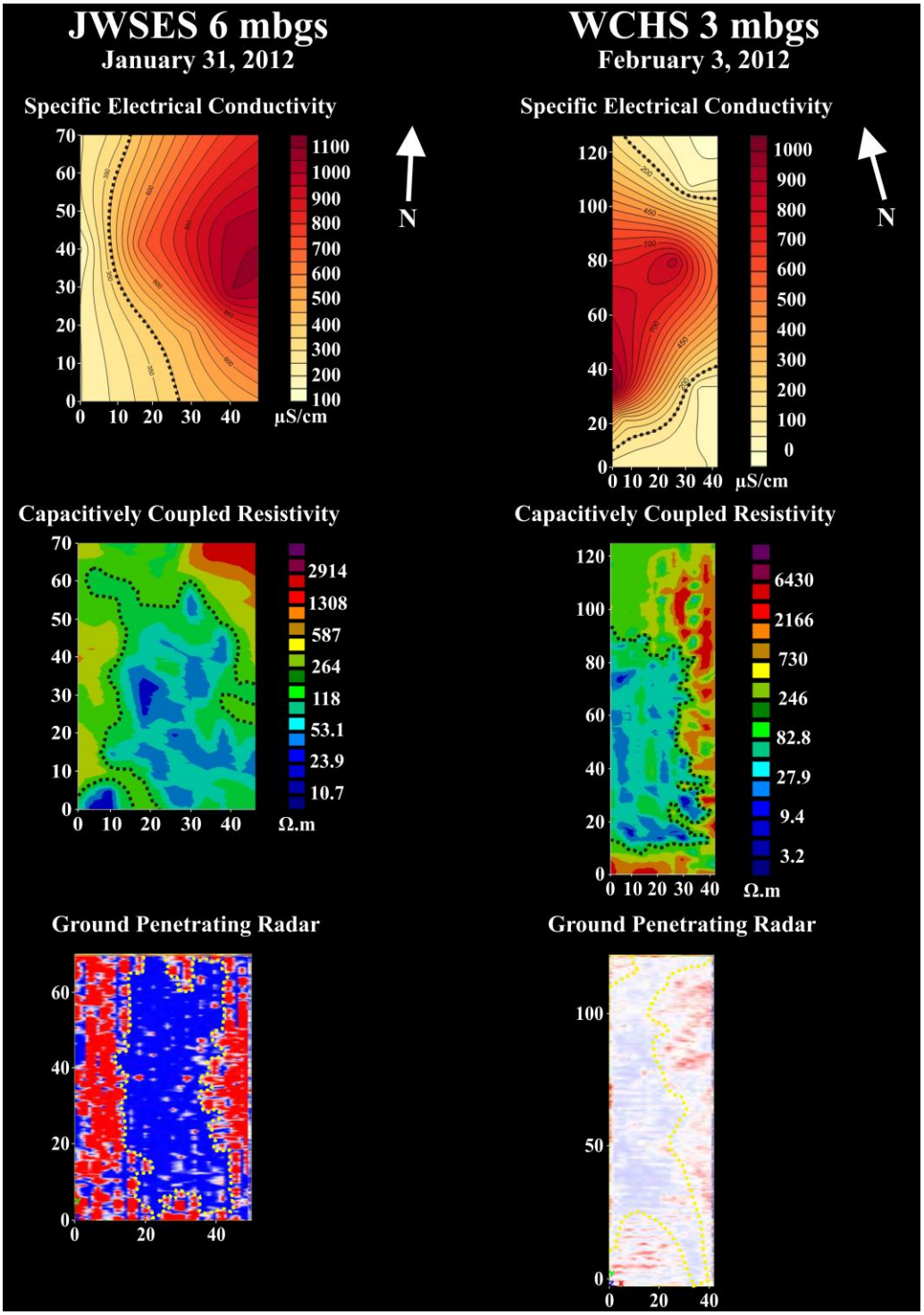

Figure 17. Planar view of groundwater specific conductivity, CCR, and GPR wastewater plume estimates at JWSES (6 mbgs) on January 31, 2012 and WCHS (3 mbgs) on February 3, 2012. In the GPR models, regions of radar signal attenuation are represented in blue and delineated with dashed yellow lines.

At JWSES, groundwater specific conductivity ≥ 400 μS/cm and resistivity ≤ 250 Ω.m was indicative of a wastewater plume. At WCHS, groundwater specific conductivity ≥ 130 μS/cm and resistivity ≤ 250 Ω.m indicated a wastewater plume. At both sites, increased radar signal attenuation was apparent beneath the drainfields suggesting a wastewater plume. Based on the three methods of assessing groundwater quality, the lateral dimensions of the wastewater plumes were approximated at both sites (Table 3).

Method	**JWSES**	**WCHS**
Groundwater Specific Conductivity	40 m x 70 m	42 m x 100 m
Capacitively Coupled Resistivity	45 m x 60 m	35 m x 90 m
Ground Penetrating Radar	20 m x 70 m	25 m x 125 m

Table 3. Groundwater specific conductivity, CCR, and GPR lateral wastewater plume lateral estimates at JWSES (6 mbgs) and WCHS (3 mbgs).

Wastewater Plume Spatial and Temporal Variability

To evaluate the sensitivity of GPR and CCR to monitor temporal variations in groundwater quality, geophysical and groundwater specific conductivity measurements collected at transect piezometers were compared over water-table depth changes at JWSES and WCHS.

Groundwater Levels and Specific Conductivity

Patterns in total monthly precipitation (Appendix M) and mean monthly (n = 12) water-table depths at transect piezometers (Appendix E) were apparent at the sites (Figure 18).

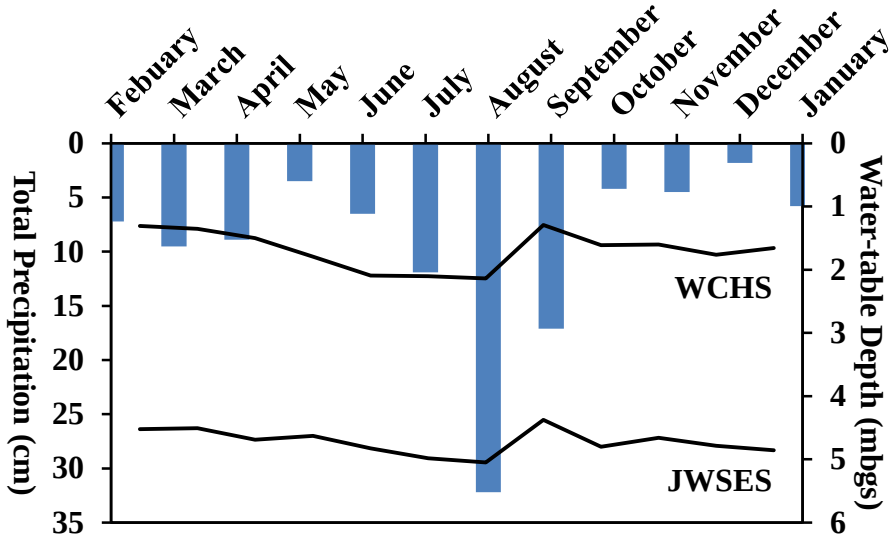

Figure 18. February 2011 – January 2012 total monthly precipitation (blue bars) and mean monthly (n = 12) water-table depths (black-lines) at JWSES and WCHS transect piezometers.

During the study period, total monthly precipitation recorded at the Craven County Airport (located approximately 25 km southeast of the study area) ranged from 1.8 – 32.2 cm. The lowest precipitation total was recorded in December, and the highest in August. At JWSES, the mean monthly (n = 12) water-table depth at transect piezometers (n = 7) ranged from 4.4 – 5.1 mbgs and 1.3 – 2.1 mbgs at WCHS (n = 9) (Appendix E). At both sites, the seasonal water-table low occurred in early August and the high in September. Increased precipitation increased

recharge to the surficial aquifer, causing water-table depths to decrease at both sites. The relationship was most apparent in September when water-table depths decreased sharply following significant precipitation across the region in late August due to Hurricane Irene.

Trends in groundwater specific conductivity associated with changes in water-table depth were apparent across the sites (Figure 19).

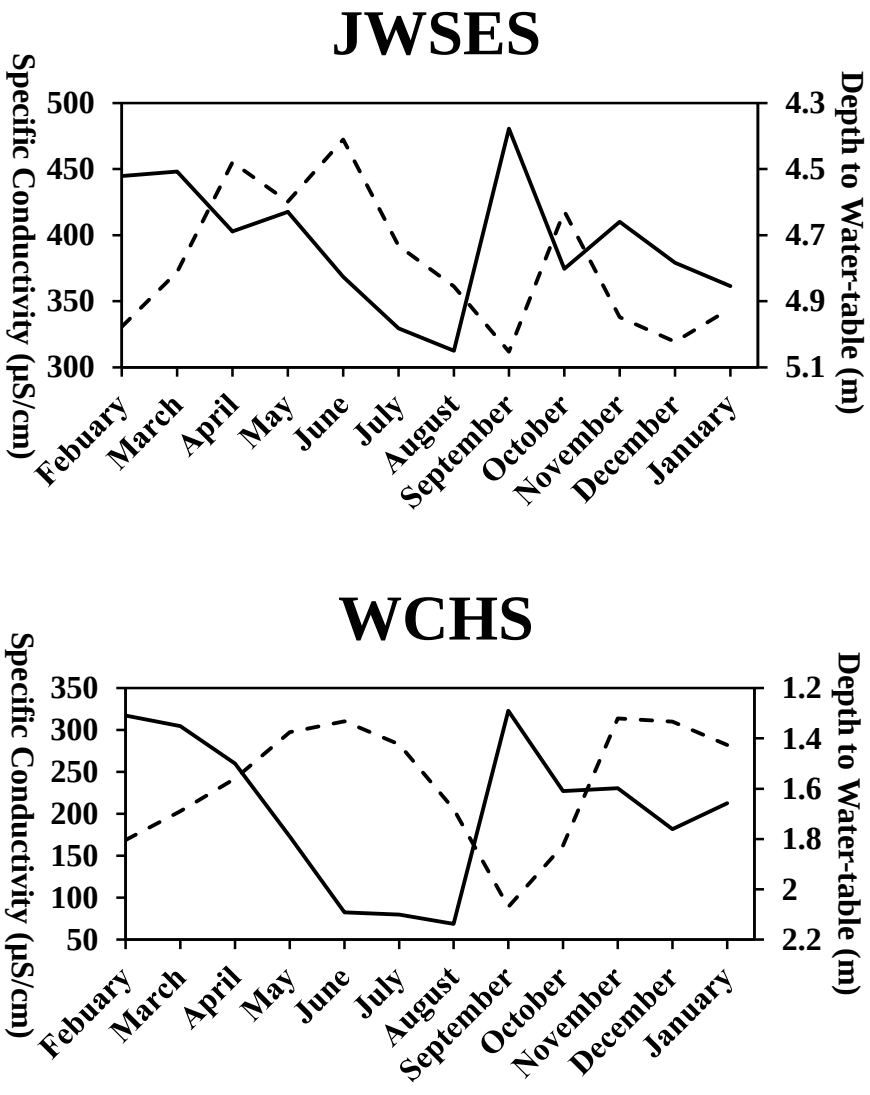

Figure 19. Mean monthly (n = 12) groundwater specific conductivity and water-table depths at JWSES (n = 7) and WCHS (n = 9) transect piezometers. The water-table is represented by solid lines and groundwater specific conductivity by dashed lines.

At JWSES transect piezometers (n = 7), mean monthly (n = 12) groundwater specific conductivity ranged from 312 – 472 μS/cm. At WCHS transect piezometers (n = 9), mean monthly groundwater specific conductivity ranged from 89 – 314 μS/cm. At both sites, as the water-table depth decreased, groundwater specific conductivity tended to decrease.

Water-table Depth Influences on Capacitively Coupled Resistivity

To evaluate the sensitivity of resistivity measurements to detect temporal changes in groundwater quality at the sites, Log resistivity values were compared to groundwater specific conductivity measurements at the screened depth of transect piezometers during a water-table low on July 13, 2011 and a water-table high on September 2, 2011. On both dates, groundwater specific conductivity increased and resistivity decreased in the drainfields relative to background values. Differences in resistivity were noticeable in the drainfields between sampling dates. Overall, $R^2 = 0.67$ at JWSES (n = 14); and $R^2 = 0.65$ at WCHS (n = 18) (Figure 20).

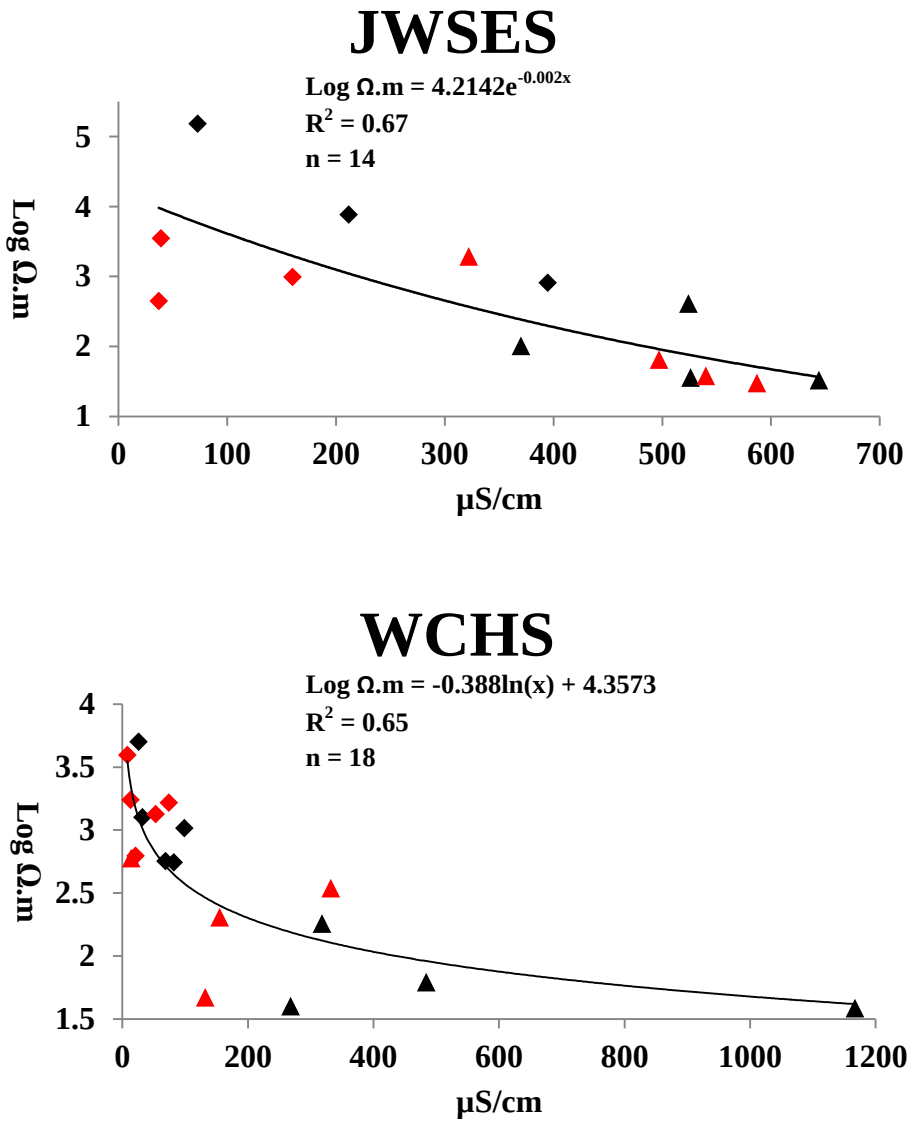

Figure 20. Scatterplots of Log resistivity values versus groundwater specific conductivity values at JWSES and WCHS transect piezometers on July 13 and September 2, 2011. July 13 data points are represented in black and September 2 data points in are represented in red. Drainfield piezometers are represented with triangles.

At JWSES, the mean (n = 4) water-table depth in the drainfield varied over approximately 0.4 m and approximately 1.0 m at WCHS (n = 4) between July 13 and September 2, 2011. At WCHS during the water-table high on September 2, 2011, groundwater specific conductivity tended to decrease and resistivity tended to increase relative to the water-table low on July 13, 2011.

In the drainfields, temporal variations in groundwater specific conductivity and resistivity associated with water-table depth changes were noticeable. At JWSES on July 13, 2011, at piezometers located in the drainfield (n = 4), the mean water-table depth was 5.2 mbgs, mean groundwater specific conductivity was 516 μS/cm, and mean resistivity was 146 Ω.m. At the same piezometers on September 2, 2011, the mean water-table depth was 4.8 mbgs, mean groundwater specific conductivity was 487 μS/cm, and mean resistivity was 517 Ω.m. At WCHS on July 13, 2011, at piezometers located in the drainfield (n = 4), the mean water-table depth was 2.4 mbgs, mean groundwater specific conductivity was 559 μS/cm, and mean resistivity was 81 Ω.m. At the same piezometers on September 2, 2011, the mean water-table depth was 1.4 mbgs, mean groundwater specific conductivity was 158 μS/cm, and mean resistivity was 299 Ω.m. At both sites, as the water-table depth decreased in the drainfield due to increased recharge from rainwater, groundwater specific conductivity tended to decrease, and resistivity tended to increase. This relationship was more straightforward at WCHS, where the mean water-table was significantly shallower.

Water-table Depth Influences on Ground Penetrating Radar

To evaluate radar signal attenuation over water-table depth changes, GPR cross-sections were compared on July 13 and September 2, 2011 at JWSES and WCHS (Figures 21 and 22).

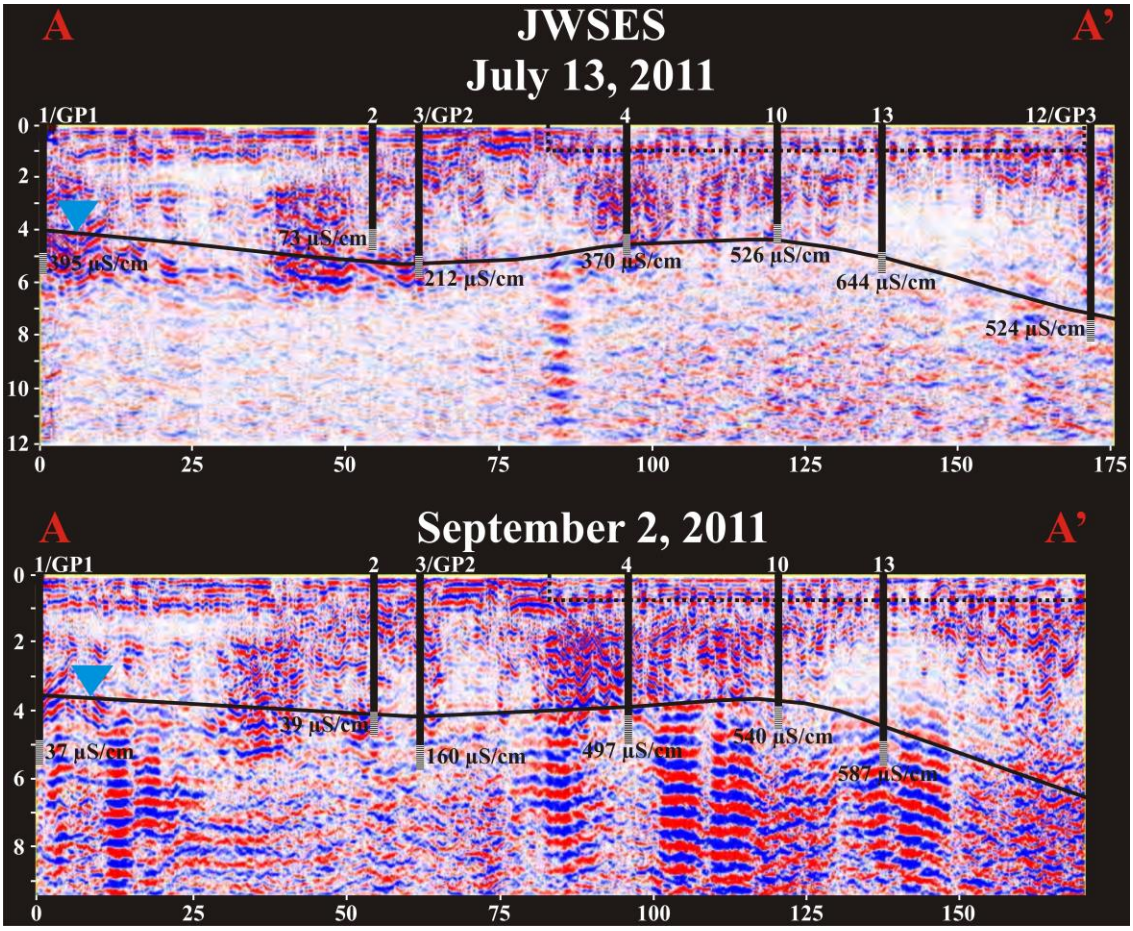

Figure 21. GPR cross-sections at JWSES on July 13 and September 2, 2011. The drainfields are represented by dashed lines and the water-table by solid lines. Transect piezometers are represented with corresponding groundwater specific conductivity values. Whited out regions indicate radar signal attenuation.

At JWSES on July 13, 2011, the radar signal was attenuated across the site below the depth of the water-table. On both survey dates, regions of attenuation were apparent at background locations along the transect, extending from approximately 0 – 45 m and 55 – 80 m. On both survey dates, a region of attenuation was apparent from approximately 130 m – 170 m at

locations where groundwater specific conductivity was elevated beneath the drainfield. The region extended vertically to the depth of the water-table on both dates.

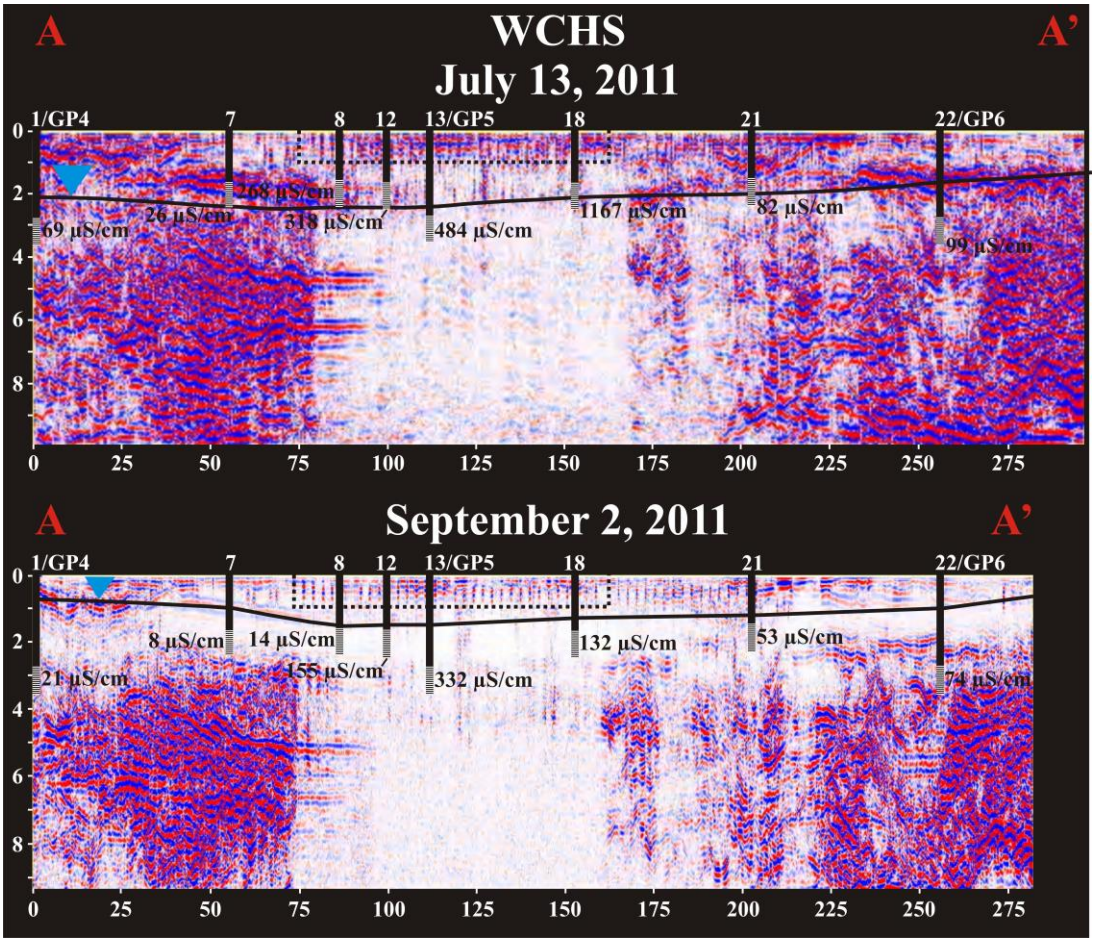

Figure 22. GPR cross-sections at WCHS on July 13 and September 2, 2011. The drainfields are represented by dashed lines and the water-table by solid lines. Transect piezometers are represented with corresponding groundwater specific conductivity values. Whited out regions indicate radar signal attenuation.

At WCHS on both survey dates, regions of attenuation were apparent at background locations along the transect, extending from approximately 180 – 230 m. On September 2, 2011, the radar signal was attenuated across the site at the approximate depth of the water-table. On both survey dates, at locations where groundwater specific conductivity was elevated, a region of attenuation was apparent from approximately 75 m – 170 m beneath the drainfields. The region extended to the vertical limit of the survey on both dates (approximately 9.5 mbgs). The

dimensions of the attenuated regions beneath the drainfields were relatively constant between surveys; however, differences in attenuation at the approximate depth of the water-table were noticeable across water-table depth changes at both sites.

Chapter 5

Discussion

On-site Wastewater System Component Detection

The usefulness of GPR to locate buried tanks and pipes has been documented (Omolaiye and Ayolabi, 2010; Allred, 2013). Omolaiye and Ayolabi, (2010) tested a 500 MHz and 250 MHz antenna to locate septic tanks in porous sandy sediments. The 500 MHz antenna did not provide interpretable information at depths of interest due to increased attenuation with depth associated with higher frequency antennas. Therefore, the 250 MHz antenna was used in the study to successfully locate five underground septic tanks. The length and width estimates from the radargrams agreed with the engineering design of underground utilities in the study area, suggesting higher frequency antennas may limit investigation depth in these sediments. Allred, (2013), evaluated the effect of antenna-to-pipe orientation to locate plastic agricultural drainage pipes at approximately 0.5 mbgs in clay-loam soils under saturated and unsaturated conditions using a 250 MHz antenna. The results of the study indicated that antenna orientation perpendicular to the drainage trenches provided the strongest reflections under moderately dry soil conditions with empty air-filled pipes; and antenna orientation parallel to the drainage trenches provided the strongest reflections under saturated conditions with water-filled or partially water-filled pipes. In the current study, the water-table depth was below the depth of the drainage trenches on all survey dates, and the drainlines were assumed to be partially filled. Soils were moderately dry and comprised of very-fine to coarse-grained sand. GPR survey lines were collected with a 200 MHz antenna over portions of the drainfields perpendicular to the drainage trenches. The surveys provided high amplitude linear reflections corresponding with

the locations of the drainage trenches in the as-built OWS blueprints. While not all of the drainage trenches were identified at either site; the trenches located in the survey areas were detected (Figures 2 & 3). These results suggest that GPR surveys conducted with lower frequency antennas perpendicular to wastewater drainfields may be a reliable method for locating OWS drainage trenches in sandy moderately saturated soils.

Wastewater Plume Delineation

Capacitively Coupled Resistivity

Traditional galvanic resistivity measurement has been used extensively to map groundwater contaminant plumes under different soil conditions with varying degrees of saturation, including wastewater plumes (Table 1). This method of resistivity measurement requires installation of electrodes into the ground using various electrode configurations for injection of direct current which can be cumbersome and sometimes impractical depending on site conditions. The current study used the non-intrusive CCR technique for collection of resistivity data using an OhmMapper (Geometrics Inc.). The OhmMapper measures resistivity using the dipole-dipole array to capacitively couple alternating current into the ground by towing transmitter and receiver sections along the ground surface. Roy et al. (2008) documented the usefulness of this technique for imaging wastewater impacted groundwater in boulder/glacial-till sediments where the water-table was approximately 0.5 mbgs. The authors found CCR to be a promising technique for producing detailed cross-sections of a wastewater plume under these hydrogeological conditions; however groundwater data was not collected to ground truth the accuracy of the resistivity interpretations.

The degree of saturation and quality of groundwater are known to influence resistivity measurements. According to Loke, (2000), the resistivity of quartz is relatively high, ranging from $10^2 – 2 \times 10^8$ Ω.m. Resistivity of groundwater is significantly lower than quartz on average, and varies from 10 – 100 Ω.m depending on the concentration of dissolved ions (Loke, 2000). These potentially large resistivity contrasts between quartz sediments and groundwater suggests that groundwater quality contrasts should be detectable by CCR in surficial Coastal Plain sediments and other similar geologic settings. Results of the current study suggest that resistivity at the sites was sensitive to groundwater quality changes associated with wastewater inputs. As expected, an inverse relationship was observed between resistivity and groundwater specific conductivity (Figure 7). As groundwater specific conductivity increased across the sites due to the presence of wastewater, resistivity tended to decrease and level off at approximately 30 – 100 Ω.m at locations where groundwater specific conductivity was elevated above 500 µS/cm. At both sites, resistivity measurements only fell under 100 Ω.m for groundwater beneath the drainfield that had elevated (> 400 µS/cm) specific conductivity. At the JWSES site, with the exception of piezometer 4, groundwater specific conductivity in the drainfield was consistently ≥ 400 µS/cm, corresponding with ≤ 250 Ω.m. These values contrasted with background measurements at the site. At JWSES2, located approximately 30 m up-gradient of the drainfield; mean (n = 10) groundwater specific conductivity throughout the study period was 80 µS/cm and mean (n = 5) resistivity was 31890 Ω.m. At the WCHS site, with the exception of piezometer 8, groundwater specific conductivity in the drainfield was consistently ≥ 130 µS/cm, corresponding to approximately ≤ 250 Ω.m. These values contrasted with background measurements at WCHS7, located approximately 25 m up gradient of the drainfield; mean (n = 12) groundwater specific conductivity throughout the study period at this location was 35 µS/cm and mean (n = 5)

resistivity was 3167 Ω.m. JWSES4 and WCHS8 were both located at the up-gradient edge of the drainfield which may have contributed to decreased groundwater specific conductivity and elevated resistivity at these locations. Overall, these relationships suggest that resistivity measuring ≤ 250 Ω.m at the sites may be indicative of a wastewater plume. This work demonstrates that a certain conductivity contrast between the drainfield and background is needed, which can help to quantify how much dilution or treatment is occurring beneath the drainfield at a site.

Frohlich et al. (1994) used resistivity measurements combined with groundwater specific conductivity measurements to detect a landfill leachate plume in well-sorted sands and glacial sediments near Provincetown, Cape Cod, Massachusetts. The authors found a good relationship between the data sets and concluded that resistivity measuring ≤ 230 Ω.m was indicative of a landfill leachate plume. This value is comparable to the resistivity range (≤ 250 Ω.m) found to be indicative of wastewater plumes in the current study. Based on the resistivity versus groundwater specific conductivity relationships at geophysical survey area and transect piezometers (Figure 10), the wastewater plumes were delineated in 3D to depths of approximately 9 mbgs at JWSES and approximately 5.5 mbgs at WCHS (Figure 11). Detection of the lower boundary of the plumes was limited by the investigation depth. Investigation depth is influenced by the geometry of the dipole-dipole array; however, for an alternating current the maximum transmitter-receiver separation that can be used in a conductive environment is a function of skin depth (Geometrics, 2001). Current amplitude is attenuated dramatically once it is beyond a certain skin depth; causing the signal to become essentially undetectable once dipole spacing exceeds skin depth. At large dipole spacings (40 m) there was not enough voltage to be accurately measured by the OhmMapper; therefore 20 m dipole spacings were used for the

deepest surveys, providing resistivity measurements to approximately 9.3 mbgs. A good approximation of skin depth in meters is $500*\sqrt{(\rho/f)}$ where ρ is resistivity and f is transmitter frequency in hertz (Geometric, 2001). At JWSES on January 31, 2012, skin depth in the geophysical survey area was estimated to be approximately 15.1m. At WCHS on February 3, 2012, skin depth in the geophysical survey area was estimated to be approximately 15.5 m. Dipole spacings of 40 m would have provided resistivity data to approximately 15 mbgs, which may have defined the lower plume boundaries; however, these data suggest that increased skin depth due to elevated groundwater specific conductivity in the drainfields may have limited the use of 40 m dipole spacing, and therefore investigation depth.

Groundwater specific conductivity measurements at drainfield piezometers helped provide information on the vertical extent of the wastewater plumes. At JWSES, the deepest groundwater specific conductivity measurement in the drainfield was at piezometer 11 (9.6 mbgs). Throughout the study period, mean groundwater specific conductivity at this location was 321 μS/cm, compared to 911 μS/cm at piezometer 14 (7.3 mbgs), the second deepest drainfield piezometer. The decrease in conductivity at piezometer11 may be indicative of the lower boundary of the plume. At the WCHS site, the deepest groundwater specific conductivity measurement in the drainfield was at piezometer 13 (3.6 mbgs). During the study period, mean groundwater specific conductivity at this location was 568 μS/cm compared to 353 μS/cm at piezometer 12 (2.5 mbgs), the second deepest piezometer in the drainfield. The increase in groundwater specific conductivity with depth provided no indication of the lower boundary of the plume. However, the resistivity data combined with groundwater specific conductivity data provided good information on the lateral extent of wastewater impacted groundwater at the sites, and suggests that installation of deeper piezometers in the drainfields or use of a different

resistivity technique may provide data to help better constraint the vertical extent of the wastewater plumes. In a follow up study at the WCHS site, in an effort to determine the lower plume boundary, additional piezometers were sited based on the resistivity and conductivity information provided in the current study. The deeper piezometers intersected the wastewater plume; indicating that CCR surveys can provide valuable information at sites where groundwater information may be limited. Some galvanically coupled systems can measure resistivity to deeper depths, which may provide better information on the vertical extent of a wastewater plume; however the installation of electrodes is necessary, which can significantly increase survey time.

Changes in water-table depth were found to influence groundwater specific conductivity and resistivity measurements in the drainfields. At both sites, recharge from rainwater caused the water-table to rise, resulting in decreased groundwater specific conductivity and increased resistivity. This relationship was expected from increased recharge, causing hydrodynamic dispersion and dilution of dissolved ions to increase. However, the relationship was more pronounced at the WCHS site where the water-table was significantly shallower and the contrast in groundwater specific conductivity between July 13 and September 2, 2012 greater relative to the JWSES site. These data suggest that at sites with deeper water-tables there may be a lag time associated with recharge, which may decrease the sensitivity of resistivity measurements to detect temporal variations in groundwater quality.

Ground Penetrating Radar

The use of GPR in groundwater contaminant studies has become increasingly common. This is mainly due to the presence and quality of soil water principally governing propagation of the radar signal (Lambot et al., 2008). Knight, (2001) noted that groundwater specific

conductivity has a large effect on radar signal attenuation. Previous studies (Benson, 1995; Porsani et al., 2004) have used this relationship to detect regions where groundwater specific conductivity was altered due to the presence of contaminants. Regions of attenuation in a radargram can provide qualitative information on the location and extent of regions with elevated groundwater specific conductivity. However, quantitative information is not as straight forward due to heterogeneity of the subsurface affecting the radar signal. A method was derived for this study to estimate the APA of individual radar traces based on Leucci, (2008); in order to help understand the controls on radar signal attenuation at the study sites. Leucci, (2008) stated that before studying the attenuation it is necessary to remove the gain applied during data collection and correct the radar trace amplitude for geometrical spreading. In the current study it was not possible to remove the gain, or therefore correct for geometrical spreading because these steps decreased the amplitude to below measureable values. Therefore, APA was measured after various filters used to aid in data interpretation were consistently applied to the data. Results found that APA tended to decrease in the drainfields at locations where groundwater specific conductivity was elevated, suggesting the radar signal was sensitive to groundwater quality changes associated with wastewater inputs. Elevated groundwater specific conductivity beneath the drainfields increased the dielectric permittivity in these regions causing increased attenuation of the radar signal, which resulted in decreased APA measurements. Increased radar signal attenuation also decreased the resolution of the radargrams and limited the investigation depth due to weakening of the signal. Based on the contrasts between radar signal attenuation beneath the drainfields and at background locations, the wastewater plumes were delineated in 3D to depths of approximately 7 mbgs at JWSES and approximately 12 mbgs WCHS (Figure 16). It was not possible to detect the lower plume boundaries at either site due to weakening of the radar

signal with depth. This was expected due to elevated conductivity limiting signal penetration and decreasing investigation depth. Overall, the GPR models provided good information on the surface and lateral extent of the wastewater plumes that was complimentary to the CCR models.

Changes in water-table depth did not influence radar signal attenuation beneath the drainfield at either site; however, differences in attenuation at the approximate water-table depth were noticeable across both sites. Across the JWSES site on July 13, 2011, the radar signal was attenuated below the water-table. On September 2, 2011, the opposite affect was observed, which provided no indication of the water-table depth. At the WCHS site on July 13, 2011, no attenuation was apparent at the depth of the water-table; however, on September 2, 2012 the radar signal was attenuated across the site at the approximate depth of the water-table. It has been documented that water content strongly controls radar signal propagation (Davis and Annan, 1989; Topp et al., 1980). These differences in radar signal attenuation near the depth of the water-table may be related to changes in dispersion and dilution of dissolved ions associated with changes in saturation at the sites.

Chapter 6

Synthesis and Conclusions

Due to ambiguities in data interpretation that can result from using a single geophysical method (Telford et al., 1990; Burger, 1992) it is desirable to acquire and integrate data from multiple methods to determine the best model of the subsurface (Benson and Mustoe, 1998). According to Olhoeft, (1986), resistivity and GPR techniques have limitations that restrict their sensitivity, and their limitations are nearly complimentary. Therefore, combining CCR and GPR data sets may provide interpretations of the subsurface with a relatively high degree of confidence.

In this study, the 200 MHz antenna used in the GPR surveys provided high resolution images of the drainage trenches at approximately 1 mbgs at both study sites. The CCR surveys distinguished areas of low resistivity at 1 mbgs relative to background measurements, but did not distinguish individual trenches at either site. The lack of resolution in the CCR models may be the result of the dipole spacing used, limiting small scale resistivity measurement. Iterative inverse modeling attempts to provide a best-fit of actual resistivity from the measured apparent resistivity values. The lack of small scale resistivity contrasts is in part associated with inverse modeling. The accuracy of the inverse model increases with increased number of dipole spacings used. However, increasing the number of dipole spacings in a survey increases the amount of data points collected, which increases the amount of time needed to complete the survey and to complete the inverse modeling process.

Resistivity and GPR data sets have been combined previously to estimate groundwater quality (Atekwana et al., 2000; Porsani et al., 2004). To detect hydro-carbon impacted

groundwater in sand-gravel sediments, Atekwana et al., (2000) found that regions of measured low resistivity coincided with regions of radar signal attenuation. The current study found a similar relationship in terms of wastewater impacted groundwater. Groundwater specific conductivity was elevated beneath the drainfields due to wastewater inputs which resulted in decreased resistivity and increased radar signal attenuation in these regions relative to background measurements. The resistivity surveys were effective at delineating the wastewater plumes, while the radargrams confirmed the locations and gave good indication of the plume surfaces in cross-section. Additionally, based on the relationships between DIN and groundwater specific conductivity at the sites ($R^2 = 0.10$ at JWSES; $R^2 = 0.82$ at WCHS), CCR surveys may have the potential to screen DIN concentrations of wastewater impacted groundwater in surficial sandy sediments, however increased water-table depths may decrease the reliability of the resistivity measurements (Appendix H).

Overall, combining GPR and CCR data sets provided a non-intrusive method for locating OWS drainage trenches and delineating the surface and lateral boundaries of associated wastewater plumes; although the lower plume boundaries were not determined at either site. These geophysical methods may be less effective in conductive regions where attenuation increases, limiting investigation depth. The strengths and limitations of each method are summarized in Table 4.

Geophysical Method	Strengths	Limitations
Ground Penetrating Radar	Drainage Trench Detection Plume Surface Delineation	Temporal Variability Detection Vertical Plume Delineation
Capacitively Coupled Resistivity	Lateral Plume Delineation Temporal Variability Detection	Plume Surface Delineation Vertical Plume Delineation

Table 4. Geophysical method strengths and limitations.

Future Work and Management Recommendations

The results of this study suggest that a combination of GPR and CCR surveys may be a reliable method for locating OWS components, delineating associated wastewater plume dimensions and detecting temporal groundwater quality changes associated with changes in recharge; and that sediment and hydrologic data can provide information to help ground truth the geophysical interpretations. It is expected that these results are not restricted to these sites, but similar results would be expected at other sites located in sandy settings; however lithology, sediment texture, and water-table depth may have an influence on the geophysical measurements.

The sites in this study were comprised of predominantly resistant quartz sand; however increased silt and clay content may affect resistivity and GPR data by increasing attenuation of the signal. Therefore, wastewater plume detection via geophysics is most easily interpreted in relatively homogeneous sandy surficial settings with shallow water-tables. Additionally, skin depth is increased in conductive regions beneath a drainfield, which limits CCR investigation depth. Other galvanically coupled resistivity techniques could overcome this obstacle and increase investigation depth, but with a tradeoff of more time needed to complete the survey.

Population growth is expected to increase in coastal North Carolina. Much of this growth is expected in rural areas where OWS is the only option for wastewater treatment and disposal. Based on the DIN and Cl concentrations measured at the spring at JWSES, the current NC OWS set-back regulations may not be adequately protecting surface waters from wastewater contamination in the NCCP. The spring is located approximately 25 m down gradient of the drainfield, 5 m short of the required 30 m setback distance from surface waters. As population and OWS density continue to increase in coastal North Carolina, OWS nutrient inputs to surface

waters can also be expected to increase. Furthermore, the locations of existing OWS drainfields are often unclear; which could be a significant impediment to future development in the region. Incorporating shallow geophysical surveys into existing best management practices and site assessment evaluations may provide a realistic improvement to overall watershed management, which could help sustain human and ecological health in the region.

Literature Cited

Allred, B. J. 2013. A GPR Agricultural Drainage Pipe Detection Case Study: Effects of Antenna Orientation Relative to Drainage Pipe Directional Trend. Journal of Environmental and Engineering Geophysics 18 (1): 55-69.

Amidu, S.A., and Olayinka, A.I. 2006. Environmental Assessment of Sewage Disposal Systems Using 2D Electrical-Resistivity Imaging and Geochemical Analysis: A Case Study from Ibadan, Southwestern Nigeria. Environmental & Engineering Geoscience XII (3): 261-272.

Annan, P.A. 2005. Hydrogeophysics: GPR Methods for Hydrogeological Studies. Water Science and Technology Library 50: 185-213.

Atekwana, E.A., Sauch, W,A., and Werkema, D.D. 2000. Investigations of Geoelectrical Signatures at a Hydrocarbon Contaminated Site. Journal of Applied Geophysics, 44 (2-3): 167-180.

Ator, S.W., Denver, J.M., Krantz, D.E., Newell, W.L., and Martucci, S.K. 2005. A Surficial Hydrogeologic Framework for the Mid-Atlantic Coastal Plain. U.S. Geological Survey Professional Paper 1680: 5, 19p.

Baker, G.S., and Jol, H.M. 2007. Stratigraphic Analysis using Ground Penetrating Radar. Geological Society of America Science Paper 432: 181p.

Benson, A.K., 1995. Applications of Ground Penetrating Radar in Assessing Some Geological Hazards: Examples of Groundwater Contamination, Faults, Cavities. Journal of Applied Geophysics 33: 177-193.

Benson, A.K., and Mustoe, N.B. 1998. Integration of Electrical Resistivity, Ground Penetrating Radar, and Very Low Frequency Electromagnetic Induction Surveys to Help Map Groundwater Contamination Produced by Hydrocarbons Leaking From Underground Storage Tanks. Environmental Geosciences 5 (2): 61-67.

Blott, S. 2000. Gradistat Version 4.0, A Grain-size Distribution and Statistics Package for the Analysis of Unconsolidated Sediments by Sieving or Laser Granulometer. Surface Processes and Modern Environments Research Group, Department of Geology, University of London.

Borchardt, M.A., Chyou, P., DeVries, E.O., and Belongia, E.A. 2003. Septic System Density and Infectious Diarrhea in a Defined Population of Children. Environmental Health Perspectives 111 (5): 742-748.

Bouwer, H., and Rice, R.C. 1976. A Slug Test for Determining Hydraulic Conductivity of Unconfined Aquifers with Completely or Partially Penetrating Wells. Water Resources Research 12 (3): 423-428.

Burger, R.H. 1992. Exploration Geophysics of the Shallow Subsurface (5): 241-316p.

Coes, A.L., Spruill, T.B., and Thomasson, M.J. 2007. Multiple-method Estimation of Recharge Rates at Diverse Locations in the North Carolina Coastal Plain, USA. Hydrogeology Journal 15: 733-788.

Corbett, D.R., Dillon, K., Burnett, W., and Schaefer, G. 2002. The Spatial Variability of Nitrogen and Phosphorus Concentrations in a Sand Aquifer Influenced by Onsite Sewage Treatment and Disposal Systems: A Case Study on St. George Island, Florida. Environmental Pollution 117: 337-345.

Daniels, J.J. 2000. Ground Penetrating Radar Fundamentals. Prepared as an Appendix to a report to the U.S.EPA, Region V: 21p.

Davis, J.L., and Annan , P.A. 1989. Ground Penetrating Radar for High-Resolution Mapping of Soil and Rock Stratigraphy. Geophysical Prospecting 37: 531-551.

Duffera, M., White, J.G., and Weisz, R. 2007. Spatial Variability of Southeastern U.S. Coastal Plain Soil Physical Properties: Implications for Site-specific Management. Geoderma 137: 327-339.

Epstein, P.R. 1998. Climate, Ecology, and Human Health. Infectious Diseases in Clinical Practice 7 (3): 100-116.

Fetter, C.W. 2001. Applied Hydrogeology, 4th ed: 416p.

Folk, R.L. 1956. The Role of Texture and Composition in Sandstone Classification. Journal of Sedimentary Research 26 (2): 166-171.

Frohlich, R.K., Urish, D.W., Fuller, J., and O'Reilly, M. 1994. Use of Geoelectrical Methods in Groundwater Pollution Surveys in a Coastal Environment. Journal of Applied Geophysics 32: 139-154.

Geometrics. 2001. OhmMapper TR1 Operation Manual: 147p.

Geometrics, 2013. OhmMapper Specifications. http://www.geometrics.com/geometrics-products/geometrics-electro-magnetic-products/ohm-mapper/. Accessed on January 11, 2014.

Geotomo Software. 2010. RES2DINV ver. 3.59: Rapid 2-D Resistivity & IP Inversion using the Least-squares Method: 148p.

Geotomo Software. 2011. RES3DINV ver. 2.23: Rapid 3-D Resistivity & IP Inversion using the Least-squares Method: 85p.

Hazen, A. 1911. Discussion: Dams on Sand Foundations. Transactions, American Society of Civil Engineers 73: 199.

Heath, R.C. 1983. Basic Groundwater Hydrology. United States Geological Survey Water-supply Paper 2220; 86p.

Hoover, M.T., and Konsler, T. 2004. Soil Facts: Septic Systems and their Maintenance. AG-439-13. North Carolina Cooperative Extension.

Humphrey, C.P. 2002. Hydrological Characterization of On-Site Wastewater and Groundwater Flow in Hoods Creek, North Carolina. A thesis submitted to the Graduate Faculty of North Carolina State University, Department of Soil Science.

Humphrey, C.P., O'Driscoll, M.A., and Armstrong, M.C. 2012. Onsite Wastewater System Nitrogen Loading to Groundwater in the Newport River Watershed, North Carolina. Environment and Natural Resources Research 2 (4): 70-79.

Knight, R. 2001. Ground Penetrating Radar for Environmental Applications. Earth and Planetary Sciences Annual Reviews 29: 229-255.

Kuras, O., Beamish, D., Meldrum, P.I., and Ogilvy, R.D. 2006. Fundamentals of the Capacitive Resistivity Technique 71 (3): 135-152.

Lambot, S., Binley, A., Slob, E., and Hubbard, S. 2008. Ground Penetrating Radar in Hydrogeophysics. Vadose Zone Journal 7 (1): 137-139.

Lautier, J.C. 2001. Hydrogeologic Framework and Ground-water Conditions in the North Carolina Central Coastal Plain. North Carolina Department of Environment and Natural Resources Division of Water Resources: 4p.

Lee, B.D., Jenkinson, B.J., Doolittle, J.A., Taylor, R.S., and Tuttle, J.W. 2006. Electrical Conductivity of a Failed Septic System Soil Absorption Field. Vadose Zone Journal 5: 757-763.

Leucci, G. 2008. Ground Penetrating Radar: The Electromagnetic Signal Attenuation and Maximum Penetration Depth. Scholarly Research Exchange (926091): 1-7.

Lindbo, D.L., Rashash, D., and Hoover, M.T. 2005. Why Do Septic Systems Fail? AG-439-44. North Carolina Cooperative Extension.

Loke, 2004. Tutorial: 2-D and 3-D Electrical Imaging Surveys: 128.

Loke, 2000. Electrical Imaging Surveys for Environmental and Engineering Studies, A Practical Guide to 2-D and 3-D Surveys: 59.

NCDENRDWQ. (2007). North Carolina Department of Environment and Natural Resources, Division of Water Quality. "Redbook", Surface Waters and Wetlands Standards: 54-71p.

NCDENROEE. (2007). North Carolina Department of Environment and Natural Resources, Office of Environmental Education. Neuse River Basin. http://www.eenorthcarolina.org/images/River%20Basin%20Images/final_web_neuse.pdf. Accessed on October 12, 1013.

NCNERR. (2001). North Carolina National Estuarine Research Reserve Technical Paper Series. Septic Systems in Coastal North Carolina: Basics for a Healthy Environment (4).

NCOSBM. (2013). North Carolina Office of State Budget and Management. County/State Population Projections. http://www.osbm.state.nc.us/ncosbm/facts_and_figures/socioeconomic_data/population_estimates/county_projections.shtm. Accessed on September 28, 2013.

Olhoeft, G.R. 1986. Direct Detection of Hydrocarbon and Organic Chemicals with Ground Penetrating Radar and Complex Resistivity. Proceedings of the NWWA/API Conference on Petroleum, Hydrocarbons and Organic Chemicals in Groundwater – Prevention, Detection, and Restoration: 284-305.

Omolaiye, G. E., and Ayolabi, E.A. 2010. Detection and Delineation of Underground Septic Tanks in Sandy Terrain using Ground Penetrating Radar. Exploration Geophysics 41: 219-223.

Pradhan, S., Hoover, M.T., and Austin, R. 2008. Enhanced GIS Procedure as a Screening Tool for Watershed-Scale Assessments of On-site System Nutrient Loading. Journal of Hydrologic Engineering 13: 744-751.

Porsani, J.L., Filho, W.M., Elis, V.R., Shimeles, F., Dourado, J.C., and Moura, H.P. 2004. The Use of GPR and VES in Delineating a Contamination Plume in a Landfill Site: A Case Study in SE Brazil. Journal of Applied Geophysics 55: 199-209.

Ren, W., Zhong, Y., Meligrana, J., Anderson, B., Watt, W.E., Chen, J., Leung, H. 2003. Urbanization, Land-use, and Water Quality in Shanghai 1947 – 1996. Environment International 29: 649-659.

Reppert, P.M., Morgan, D.F., and Toksoz, N.M. 2000. Dielectric Constant Determination using Ground Penetrating Radar Reflection Coefficients. Journal of Applied Geophysics 43: 189-197.

Robertson, W.D., Cherry, J.A., and Sudicky, E.A. 1991. Groundwater Contamination from 2 Small Septic Systems on Sand Aquifers. Groundwater 29 (1): 89-92.

Roy, J.W., Robillard, J.M., Watson, S.B., and Hayashi, M. 2008. Non-intrusive Characterization Methods for Wastewater-affected Groundwater Plumes Discharging to an Alpine Lake. Environmental Monitoring and Assessment 149: 201-211.

Scandura, J.E., and Sobsey, M.D. 1997. Viral and Bacterial Contamination of Groundwater from On-site Sewage Treatment Systems. Water Science and Technology 35 (11-12): 141-146.

Sophocleous, M. 2002. Interactions between Groundwater and Surface Water: The State of the Science. Hydrogeology Journal 10: 52-67.

Southeast Regional Climate Center. 2013. Historical Climate Summaries for North Carolina. http://www.sercc.com/cgi-bin/sercc/cliMAIN.pl?nc4684. Accessed on May 5, 2013.

Sweet, W.V., and Geratz, J.W. 2003. Bankfull Hydraulic Geometry Relationships and Recurrence Intervals for North Carolina's Coastal Plain. Journal of the American Water Resources Association 39 (4): 861-871.

Telford, W.M., Geldart, L.P., and Sheriff, R.E. 1990. Applied Geophysics, 2nd ed: 770p.

Topp, G.C., Davis, J.L., and Annan, A.P. 1980. Electromagnetic Determination of Soil Water Content: Measurements in Coaxial Transmission Lines. Water Resources Research 16 (3): 574-582.

USDA. (1989). United States Department of Agriculture, Soil Conservation Service. Soil Survey of Craven County, North Carolina: 157p.

USEPA. (1977). United States Environmental Protection Agency. The Report to Congress, Waste Disposal Practices and their Effects on Groundwater: 569p.

USEPA. (2002). United States Environmental Protection Agency. Onsite Wastewater Treatment Systems Manual: 369p.

USEPA. (2005). United States Environmental Protection Agency. Handbook for Managing Onsite and Clustered (Decentralized) Wastewater Treatment Systems: 59p.

USEPA. (2012). United States Environmental Protection Agency. What is Nonpoint Source Pollution. http://water.epa.gov/polwaste/nps/whatis.cfm. Accessed on January 11, 2014.

USEPA. (2013). United State Environmental Protection Agency. Middle Neuse Watershed. http://watersgeo.epa.gov/mwm/?layer=LEGACY_WBD&feature=03020202&extraLayers=null. Accessed on November 2, 2013.

USEPA. (2013). United States Environmental Protection Agency. Septic (Onsite/Decentralized) Systems. http://water.epa.gov/infrastructure/septic/. Accessed on November 15, 2013.

USGS. (2013). United States Geological Survey. Contentnea Creek Gauging Station. http://waterdata.usgs.gov/usa/nwis/uv?02091764. Accessed on September 17, 2013.

USGS. (2013). United States Geological Survey. Middle Neuse Watershed. http://water.usgs.gov/wsc/cat/03020202.html. Accessed on September 17, 2013.

Urish, D.W. 1981. Electrical Resistivity-Hydraulic Conductivity Relationships in Glacial Outwash Aquifers. Water Resources Research 17 (5): 1401-1408.

Urish, D.W. 1983. The Practical Application of Surface Electrical Resistivity to Detection of Ground-Water Pollution. Ground Water 21 (2): 144-152.

Vitousek, P.M., Mooney, H.A., Lubchenco, J., and Melillo, J.M. 1997. Human Domination of Earth's Ecosystems. Science 277 (5325): 494-499.

Vukovic, M., and Soro, A. 1992. Determination of Hydraulic Conductivity of Porous Media from Grain-size Composition. Water Resources Publications (Littleton, Colorado): 83p.

Williams, J.B., and Pinder, J.E. 1990. Groundwater Flow and Runoff in a Coastal Plain Stream. Water Resources Bulletin 26 (2): 343-352.

Winner, M.D. Jr., Coble, R.W. 1996. Hydrogeologic Framework of the North Carolina Coastal Plain. U.S. Geological Survey Professional paper 1404-I: 13p.

Yates, M.V. 1985. Septic Tank Density and Ground-Water Contamination. Ground Water 23 (5): 586-591.

Appendix A

Hydraulic Head

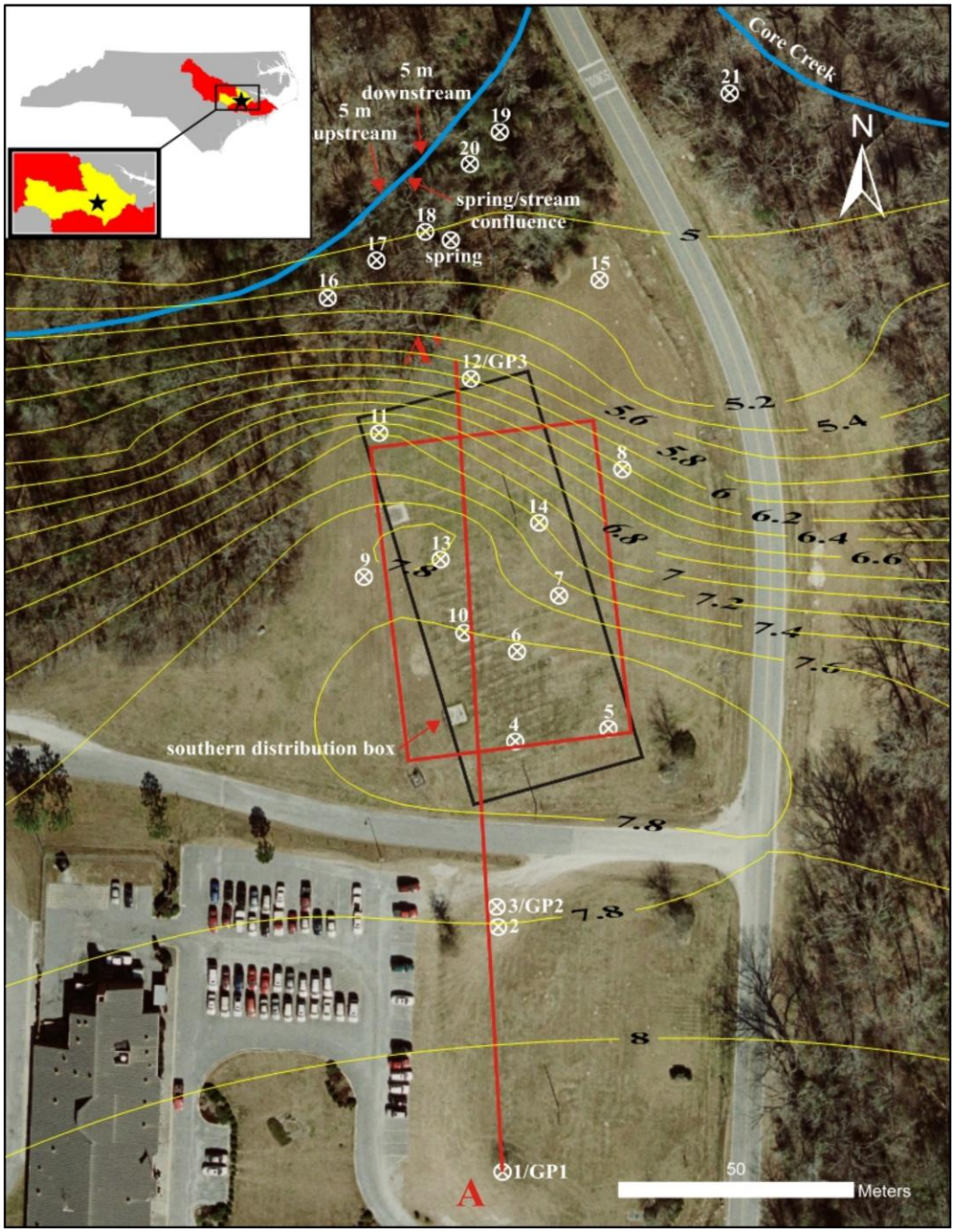

Figure 23. JWSES mean monthly (n = 12) hydraulic head map with 0.2 m contour intervals. Elevations are in mamsl. Aerial photo from Google Earth (2012).

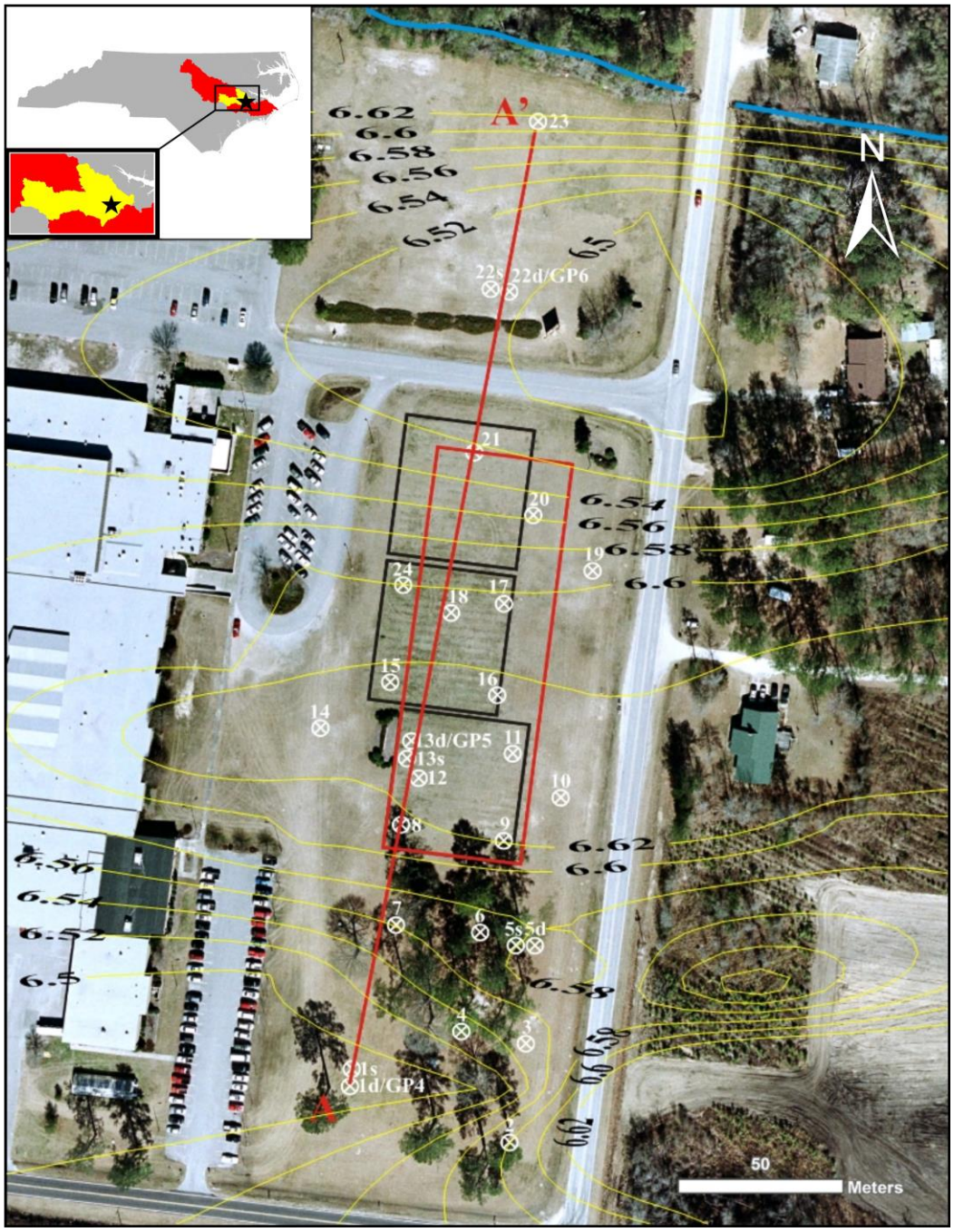

Figure 24. WCHS mean monthly (n = 12) hydraulic head map with 0.02 m contour intervals. Elevations are in mamsl. Aerial photo from Google Earth (2012).

Appendix B

ECUCEL Reports

Water Quality Data Summary Sheet (13-June-2011) Central Environmental Laboratory, Department of Biology, ECU					
Station or Sample	NH4 (mg N/L)	NO3+NO2 (mg N/L)	DKN (mg/L)	Cl (mg/L)	PO4 (mg P/L)
WC-1d	1.16	<0.008	2.05	30.94	<0.002
WC-5d	0.02	<0.008	0.38	3.60	<0.002
WC-9	0.18	20.71	0.54	39.72	<0.002
WC-12	0.14	7.89	4.10	29.66	<0.002
WC-13s	0.20	79.58	1.21	85.14	<0.002
WC-13d	0.07	66.68	0.54	63.40	<0.002
WC-14	0.11	0.43	0.23	2.99	<0.002
WC-15	0.12	94.68	0.64	96.04	0.24
WC-17	0.05	89.40	0.73	95.13	<0.002
WC-18	0.81	94.93	0.99	85.27	0.15
WC-20	0.26	0.89	0.96	10.44	0.34
WC-21	0.17	0.30	1.07	9.01	0.25
WC-22d	0.02	0.53	0.08	2.42	<0.002
WC-23	0.20	0.13	0.59	6.65	0.07
WC-24	0.02	no data	0.45	43.06	<0.002
JWS-1	0.04	0.09	0.40	28.71	0.19
JWS-3	0.55	0.01	1.25	8.69	0.12
JWS-4	0.11	28.62	0.33	54.39	0.06
JWS-7	0.23	20.29	1.09	88.44	0.31
JWS-9	0.07	0.56	0.12	3.55	0.37
JWS-10	0.07	45.48	0.30	80.66	0.12
JWS-12	0.02	0.19	0.57	37.28	1.43
JWS-13	0.27	36.77	0.69	74.37	0.54
JWS-14	0.14	35.17	0.56	73.57	<0.002
JWS-17	0.48	0.04	0.67	35.13	<0.002
JWS-spring	0.12	14.62	0.41	38.83	0.29
JWS-spring/stream	0.01	11.41	0.10	37.66	0.24
JWS-5m upstream	0.03	1.08	0.06	7.41	0.11
JWS-5m downstream	0.02	1.38	0.05	7.69	0.11
JWS-septic	57.15	0.19	54.67	86.52	4.05

Appendix B Continued

Water Quality Data Summary Sheet (28-October-2011) Central Environmental Laboratory, Department of Biology, ECU					
Station or Sample	NH4 (mg N/L)	NO3+NO2 (mg N/L)	DKN (mg/L)	Cl (mg/L)	PO4 (mg P/L)
WC-2d	1.14	0.14	1.60	10.51	0.01
WC-10	0.03	0.10	0.27	1.97	<0.015
WC-13d	0.11	34.01	0.78	32.92	0.01
JWS-Spring	0.07	6.59	0.33	30.10	0.19
JWS-4	26.49	3.86	27.76	91.50	0.03
JWS-9	0.12	0.31	0.30	3.14	0.08

Appendix B Continued

Water Quality Data Summary Sheet (21-December-2011) Central Environmental Laboratory, Department of Biology, ECU					
Station or Sample	NH4 (mg N/L)	NO3+NO2 (mg N/L)	DKN (mg/L)	Cl (mg/L)	PO4 (mg P/L)
WC-2d	0.26	0.01	0.53	48.26	<0.015
WC-10	<DL	<0.008	<0.59	1.04	<0.015
WC-13d	<DL	82.36	0.37	81.63	<0.015
JWS-Spring	<DL	9.53	0.25	31.73	0.13
JWS-4	6.49	12.89	6.45	47.89	0.01
JWS-9	<DL	0.03	0.10	2.16	0.08

Appendix C

Sediment Sample Descriptions and Grain-size

JWSES1d/GP1						
Sample (cmbgs)	Sediment Description	d_{60} (mm)	d_{50} (mm)	d_{10} (mm)	d_{50} (φ)	d_{10} (φ)
0-50	moderately sorted medium sand	0.37	0.28	0.14	1.82	0.70
50-100	poorly sorted medium sand	0.31	0.27	0.07	1.88	1.01
100-150	well sorted medium sand	0.48	0.44	0.28	1.20	0.57
150-200	slightly very fine gravelly very coarse sand	1.20	0.92	0.35	0.12	-0.52
200-210	slightly very fine gravelly medium sand	0.56	0.47	0.17	1.09	-0.25
210-250	slightly very fine gravelly medium sand	0.47	0.42	0.14	1.24	0.31
250-310	slightly very fine gravelly coarse sand	0.64	0.57	0.21	0.82	-0.31
310-350	slightly very fine gravelly coarse sand	0.68	0.58	0.19	0.79	-0.69
350-390	slightly very fine gravelly fine sand	0.25	0.20	0.10	2.32	0.66
390-410	slightly very fine gravelly fine sand	0.24	0.19	0.98	2.36	0.81
410-485	slightly very fine gravelly fine sand	0.25	0.20	0.10	2.32	0.65
485-510	slightly fine gravelly fine sand	0.30	0.22	0.11	2.19	0.20

Appendix C Continued

JWSES3/GP2						
Sample (cmbgs)	Sediment Description	d_{60} (mm)	d_{50} (mm)	d_{10} (mm)	d_{50} (φ)	d_{10} (φ)
0-60	moderately sorted medium sand	0.36	0.31	0.15	1.69	0.53
60-80	slightly very fine gravelly medium sand	0.47	0.40	0.12	1.31	0.19
80-110	slightly very fine gravelly medium sand	0.61	0.51	0.29	0.98	-0.27
110-185	slightly very fine gravelly coarse sand	0.67	0.58	0.28	0.78	-0.22
185-220	very fine gravelly very coarse sand	1.50	1.00	0.32	-0.003	-1.45
220-290	slightly very fine gravelly fine sand	0.43	0.33	0.16	1.58	0.12
290-325	moderately well sorted fine sand	0.24	0.21	0.14	2.23	1.50
325-415	slightly very fine gravelly fine sand	0.37	0.29	0.18	1.78	0.53
415-460	very fine gravelly fine sand	0.29	0.28	0.13	1.83	-0.22
460-540	slightly very fine gravelly fine sand	0.44	0.33	0.11	1.60	0.23

Appendix C Continued

JWSES12/GP3						
Sample (cmbgs)	Sediment Description	d_{60} (mm)	d_{50} (mm)	d_{10} (mm)	d_{50} (φ)	d_{10} (φ)
0-90	moderately sorted medium sand	0.33	0.28	0.13	1.85	0.62
90-170	slightly very fine gravelly coarse sand	0.70	0.58	0.26	0.79	-0.33
170-220	slightly very fine gravelly coarse sand	0.73	0.62	0.31	0.69	-0.44
220-310	moderately sorted coarse sand	0.70	0.62	0.35	0.69	0.002
310-340	very fine gravelly fine sand	1.20	0.63	0.14	0.67	-1.50
340-360	slightly very fine gravelly coarse sand	0.58	0.50	0.17	0.99	-0.11
360-450	moderately sorted fine sand	0.20	0.17	0.10	2.50	1.00
450-485	slightly very fine gravelly fine sand	0.20	0.19	0.95	2.58	0.62
485-560	poorly sorted fine sand	0.23	0.18	0.11	2.49	0.59

Appendix C Continued

WCHS1d/GP4						
Sample (cmbgs)	Sediment Description	d_{60} (mm)	d_{50} (mm)	d_{10} (mm)	d_{50} (φ)	d_{10} (φ)
0-50	moderately sorted medium sand	0.28	0.24	0.10	2.03	1.10
50-105	poorly sorted fine sand	0.23	0.20	0.65	2.35	1.37
105-160	very fine gravelly coarse silty fine sand	0.26	0.20	0.14	2.33	-0.93
160-175	moderately sorted fine sand	0.29	0.25	0.14	2.02	0.81
175-230	moderately well sorted medium sand	0.39	0.35	0.21	1.53	0.70
230-300	well sorted medium sand	0.28	0.25	0.15	2.00	1.50
300-350	slightly very fine gravelly medium sand	0.44	0.37	0.17	1.45	0.15
350-430	very fine gravelly coarse sand	0.74	0.60	0.24	0.74	-0.85
430-470	slightly very fine gravelly coarse sand	0.70	0.62	0.32	0.68	-0.47

Appendix C Continued

WCHS13d/GP5						
Sample (cmbgs)	Sediment Description	d_{60} (mm)	d_{50} (mm)	d_{10} (mm)	d_{50} (φ)	d_{10} (φ)
0-50	poorly sorted fine sand	0.24	0.21	0.97	2.26	1.37
50-70	slightly very fine gravelly fine sand	0.25	0.22	0.11	2.20	1.38
70-110	moderately sorted fine sand	0.27	0.23	0.12	2.10	1.01
110-230	slightly very fine gravelly fine sand	0.22	0.19	0.09	2.41	1.45
230-320	slightly very fine gravelly fine sand	0.18	0.15	0.09	2.71	1.43
320-350	slightly very fine gravelly medium sand	0.55	0.46	0.23	1.11	-0.06
350-400	slightly very fine gravelly medium sand	0.37	0.32	0.19	1.64	0.28
400-450	slightly very fine gravelly medium sand	0.49	0.39	0.19	1.34	-0.66
450-475	very coarse silty sand fine gravel	0.59	0.32	0.04	1.65	-2.29

Appendix C Continued

WCHS22d/GP6						
Sample (cmbgs)	Sediment Description	d_{60} (mm)	d_{50} (mm)	d_{10} (mm)	d_{50} (φ)	d_{10} (φ)
0-50	moderately well sorted fine sand	0.27	0.24	0.13	2.06	1.28
50-110	moderately well sorted fine sand	0.22	0.19	0.10	2.36	1.65
110-170	moderately well sorted fine sand	0.22	0.20	0.12	2.31	1.63
170-215	well sorted medium sand	0.29	0.27	0.19	1.89	1.36
215-315	moderately well sorted medium sand	0.43	0.39	0.25	1.37	0.69
315-350	slightly very fine gravelly medium sand	0.46	0.42	0.26	1.26	0.50
350-460	moderately well sorted medium sand	0.37	0.33	0.19	1.59	0.70

Appendix D

Uniformity Coefficients and Estimated Porosity

JWSES1/GP1		
Sample (cmbgs)	Uniformity Coefficient	Porosity
0-50	2.64	0.41
50-100	4.43	0.37
100-150	1.71	0.44
150-200	3.43	0.39
200-210	3.29	0.39
210-250	3.36	0.39
250-310	3.05	0.40
310-350	3.58	0.39
350-390	2.50	0.42
390-410	0.24	0.50
410-485	2.50	0.42
485-510	2.73	0.41

Previous porosity estimates in the NCCP

[a] Duffera et al., (2007): 29% -55%

[b] Coes et al., (2007): 31%

Appendix D Continued

JWSES3/GP2		
Sample (cmbgs)	Uniformity Coefficient	Porosity
0-60	2.40	0.42
60-80	3.92	0.38
80-110	2.10	0.43
110-185	2.39	0.42
185-220	4.69	0.36
220-290	2.69	0.41
290-325	1.71	0.44
325-415	2.06	0.43
415-460	2.23	0.42
460-540	4.00	0.38

Appendix D Continued

JWSES12/GP3		
Sample (cmbgs)	Uniformity Coefficient	Porosity
0-90	2.54	0.41
90-170	2.69	0.41
170-220	2.35	0.42
220-310	2.00	0.43
310-340	8.57	0.31
340-360	3.41	0.39
360-450	2.00	0.43
450-485	0.21	0.50
485-560	2.09	0.43

Appendix D Continued

WCHS1d/GP4		
Sample (cmbgs)	Uniformity Coefficient	Porosity
0-50	2.80	0.41
50-105	0.35	0.49
105-160	1.86	0.44
160-175	2.07	0.43
175-230	1.86	0.44
230-300	1.87	0.44
300-350	2.59	0.41
350-430	3.08	0.40
430-470	2.19	0.42

Appendix D Continued

WCHS13d/GP5		
Sample (cmbgs)	Uniformity Coefficient	Porosity
0-50	0.25	0.50
50-70	2.27	0.42
70-110	2.25	0.42
110-230	2.44	0.42
230-320	2.00	0.43
320-350	2.39	0.42
350-400	1.95	0.43
400-450	2.58	0.41
450-475	14.75	0.27

Appendix D Continued

WCHS22d/GP6		
Sample (cmbgs)	Uniformity Coefficient	Porosity
0-50	2.08	0.43
50-110	2.20	0.42
110-170	1.83	0.44
170-215	1.53	0.45
215-315	1.72	0.44
315-350	1.77	0.44
350-460	1.95	0.43

Appendix E

Piezometer Elevations, Depth, Hydraulic Parameters, and Water Quality Measurements

JWSES1/GP1 (12.2 mamsl)								
Depth (5.7 m)	Date Measured	Depth to Groundwater (m)	Hydraulic Head (mamsl)	Temperature (°C)	Specific Conductivity (uS/cm)	NH4-N (mg/L)	NO3-N (mg/L)	Cl (mg/L)
	2/25/2011	3.6	8.5	16.5	300	0.8	0.4	
	3/25/2011	3.6	8.6	17.6	355			
	4/15/2011	3.7	8.5	16.6	315	0.7	0.2	12
	5/25/2011	3.8	8.4	18	343			
	6/13/2011	3.8	8.3	19.1	502	0.7	0.6	54
	7/13/2011	4	8.2	20.1	395			
	8/12/2011	4.2	8	20.5	360	0.5	0.51	3.6
	9/2/2011	3.6	8.6	21.6	37			
	10/28/2011	3.8	8.3	22.2	176	23.7	2.7	4.9
	11/18/2011	3.8	8.3	20.7	151			
	12/21/2011	4	8.2	20.2	158	5.7	0.3	3
	1/31/2012	4	8.2	18.1	175			

Appendix E Continued

JWSES2 (12.1 mamsl)								
Depth (4.8 m)	Date Measured	Depth to Groundwater (m)	Hydraulic Head (mamsl)	Temperature (°C)	Specific Conductivity (uS/cm)	NH4-N (mg/L)	NO3-N (mg/L)	Cl (mg/L)
	2/25/2011	4.2	7.9	16.6	68	0.8	0.4	0.4
	3/25/2011	4.2	7.9	16.2	73			
	4/15/2011							
	5/25/2011	4.3	7.8	17.9	94			
	6/13/2011	4.5	7.6	20.5	75	0.5	0.2	9
	7/13/2011	4.6	7.5	20.1	73			
	8/12/2011							
	9/2/2011	4.1	8	22.4	39			
	10/28/2011	4.3	7.8	21.6	99	0.5	2.8	2.6
	11/18/2011	4.3	7.8	21	87			
	12/21/2011	4.4	7.7	20.2	99	0.1	1.8	5.4
	1/31/2012	4.5	7.6	18.6	88			

Appendix E Continued

JWSES3/GP2 (12.1 mamsl)								
Depth (5.8 m)	Date Measured	Depth to Groundwater (m)	Hydraulic Head (mamsl)	Temperature (°C)	Specific Conductivity (uS/cm)	NH4-N (mg/L)	NO3-N (mg/L)	Cl (mg/L)
	2/25/2011	4.2	7.9	17.6	150	0.2	0.2	6
	3/25/2011	4.2	7.9	16.9	113			
	4/15/2011	4.4	7.8	16.6	166	0.3	0.1	9
	5/25/2011	4.4	7.8	17.9	112			
	6/13/2011	4.9	7.3	19	73	0.1	1.2	6
	7/13/2011	5.3	6.8	19.4	212			
	8/12/2011	4.7	7.4	21.1	96	0.5	0.6	4.8
	9/2/2011	4.2	7.9	21.1	160			
	10/28/2011	4.3	7.8	22.2	86	1	3.9	14.3
	11/18/2011	4.3	7.8	21.7	145			
	12/21/2011	4.4	7.7	20.4	124	0.2	0.4	7.5
	1/31/2012	4.5	7.6	19.1	107			

Appendix E Continued

JWSES4 (12.1 mamsl)								
Depth (5.02 m)	Date Measured	Depth to Groundwater (m)	Hydraulic Head (mamsl)	Temperature (°C)	Specific Conductivity (uS/cm)	NH4-N (mg/L)	NO3-N (mg/L)	Cl (mg/L)
	2/25/2011	4.1	8	16.2	430	0.8	9.1	13
	3/25/2011	4	8.1	16.2	660			
	4/15/2011	4.2	7.9	16.2	396	0.1	3.2	115
	5/25/2011	4.2	7.9	17.2	560			
	6/13/2011	4.4	7.8	18.7	587	0.4	19.5	66
	7/13/2011	4.5	7.7	19.2	370			
	8/12/2011	4.6	7.5	20.5	345	1.5	1.5	5.7
	9/2/2011	3.9	8.2	21.6	497			
	10/28/2011	4.3	7.9	21.1	994	131.9	34.3	174.3
	11/18/2011	4.3	7.9	20.6	400			
	12/21/2011	4.3	7.9	20.1	206	275.6	2	225.82
	1/31/2012	4.4	7.7	18.2	402			

Appendix E Continued

JWSES5 (11.8 mamsl)								
Depth (5.2 m)	Date Measured	Depth to Groundwater (m)	Hydraulic Head (mamsl)	Temperature (°C)	Specific Conductivity (uS/cm)	NH4-N (mg/L)	NO3-N (mg/L)	Cl (mg/L)
	2/25/2011	4	7.8	16	500	0.4	9.9	18
	3/25/2011	3.9	7.9	15.9	379			
	4/15/2011	4.2	7.6	15.7	492	0.1	3.2	115
	5/25/2011	4.1	7.7	16.6	465			
	6/13/2011	4.3	7.5	18.2	240	0.3	7.4	38
	7/13/2011	4.8	7.1	18.5	333			
	8/12/2011							
	9/2/2011	3.8	8	20.6	200			
	10/28/2011	4.3	7.5	20.9	559	1.2	82.6	99.1
	11/18/2011	5.1	6.7	20.6	549			
	12/21/2011	4.5	7.3	19.9	609	0.2	8.2	143.3
	1/31/2012	4.5	7.3	18.1	539			

Appendix E Continued

JWSES6 (12 mamsl)								
Depth (6.4 m)	Date Measured	Depth to Groundwater (m)	Hydraulic Head (mamsl)	Temperature (°C)	Specific Conductivity (uS/cm)	NH4-N (mg/L)	NO3-N (mg/L)	Cl (mg/L)
	2/25/2011	4.8	7.2	17.9	580	0.3	23	14
	3/25/2011	4.9	7.1	17.4	457			
	4/15/2011	5	7	16.7	653	0.1	22.9	147
	5/25/2011	5	7	17.2	625			
	6/13/2011	5.2	6.8	17.7	718	0.2	47	77
	7/13/2011	5.3	6.7	18.4	640			
	8/12/2011	5.5	6.5	19	660	0.2	28.1	11.2
	9/2/2011	4.6	7.4	19.9	494			
	10/28/2011	5.2	6.8	20.2	641	0.8	242	56
	11/18/2011	5.5	6.5	20.7	507			
	12/21/2011	5.1	6.9	20.4	477	0.1	9.5	88.3
	1/31/2012	5.2	6.8	19.1	514			

Appendix E Continued

JWSES7 (12 mamsl)								
Depth (6.8 m)	Date Measured	Depth to Groundwater (m)	Hydraulic Head (mamsl)	Temperature (°C)	Specific Conductivity (uS/cm)	NH4-N (mg/L)	NO3-N (mg/L)	Cl (mg/L)
	2/25/2011	6.3	5.6	18.2	910	0.5	9	20
	3/25/2011	6.1	5.9	17.6	880			
	4/15/2011	6.1	5.8	17.1	933	0.1	6.7	150
	5/25/2011	6.1	5.8	17.9	844			
	6/13/2011	6.2	5.8	18	1002	0.2	12.1	108
	7/13/2011	6.2	5.8	18.2	1023			
	8/12/2011	6.2	5.8	18.9	1026	0.2	5.6	9.3
	9/2/2011	6	6	19.2	780			
	10/28/2011	6.2	5.8	19.9	1109	0.3	27.8	120.7
	11/18/2011	6.1	5.8	20.4	106			
	12/21/2011	6.2	5.8	19.9	1217	0.3	1.2	219.5
	1/31/2012	6.2	5.8	18.9	1050			

Appendix E Continued

JWSES8 (11.6 mamsl)								
Depth (8.1 m)	Date Measured	Depth to Groundwater (m)	Hydraulic Head (mamsl)	Temperature (°C)	Specific Conductivity (uS/cm)	NH4-N (mg/L)	NO3-N (mg/L)	Cl (mg/L)
	2/25/2011	6.1	5.5	18.6	780	0.7	0.3	13
	3/25/2011	6.1	5.4	18.4	730			
	4/15/2011	6.2	5.4	18	812	0.1	1	106
	5/25/2011	6.2	5.4	18.1	733			
	6/13/2011	6.2	5.3	18	851	0.1	6.4	42
	7/13/2011	6.7	4.8	17.6	740			
	8/12/2011	6.3	5.3	18.2	765	0.1	1.6	1.5
	9/2/2011	5.6	6	18.4	583			
	10/28/2011	6.3	5.3	19	756	0.2	12.4	28.6
	11/18/2011	6.2	5.3	19.1	582			
	12/21/2011	6.3	5.3	20	729	0.1	2.2	83.5
	1/31/2012	6.4	5.2	19.1	797			

Appendix E Continued

JWSES9 (11.8 mamsl)								
Depth (6.9 m)	Date Measured	Depth to Groundwater (m)	Hydraulic Head (mamsl)	Temperature (°C)	Specific Conductivity (uS/cm)	NH4-N (mg/L)	NO3-N (mg/L)	Cl (mg/L)
	2/25/2011	5.4	6.4	18.5	110	0.1	0.3	2
	3/25/2011	5.5	6.3	17.7	146			
	4/15/2011	5.5	6.3	17.1	153	0.1	0.2	11
	5/25/2011	5.6	6.2	17.5	134			
	6/13/2011	5.9	6	18.2	116	0.1	0.3	7
	7/13/2011	5.7	6.1	18.5	80			
	8/12/2011	5.8	6	18.7	122	0.4	0.8	1.7
	9/2/2011	4.9	6.9	19.5	30			
	10/28/2011	6	5.8	19.7	180	0.1	3.2	4.5
	11/18/2011	5.5	6.3	19.9	1105			
	12/21/2011	5.6	6.2	20.1	122	0.1	0.4	3.1
	1/31/2012	5.7	6.1	19	140			

Appendix E Continued

JWSES10 (12 mamsl)								
Depth (4.6 m)	Date Measured	Depth to Groundwater (m)	Hydraulic Head (mamsl)	Temperature (°C)	Specific Conductivity (uS/cm)	NH4-N (mg/L)	NO3-N (mg/L)	Cl (mg/L)
	2/25/2011	3.9	8.1	19.2	377	0.9	23.1	14
	3/25/2011	4	8	15.9	610			
	4/15/2011	4.1	7.9	16.6	735	0.5	15.2	122
	5/25/2011	4.1	8	17.5	782			
	6/13/2011	4.2	7.8	18.6	862	0.5	35.4	116
	7/13/2011	4.3	7.7	19.2	526			
	8/12/2011	4.5	7.5	21.2	524			
	9/2/2011	3.7	8.3	21.9	540			
	10/28/2011	4.2	7.8	21.4	497	1	23.4	64.4
	11/18/2011	4.1	7.9	20.9	550			
	12/21/2011	4.2	7.8	20.1	458	0.1	8.3	71
	1/31/2012	4.3	7.7	18.2	257			

Appendix E Continued

JWSES11 (12 mamsl)								
Depth (9.6 m)	Date Measured	Depth to Groundwater (m)	Hydraulic Head (mamsl)	Temperature (°C)	Specific Conductivity (uS/cm)	NH4-N (mg/L)	NO3-N (mg/L)	Cl (mg/L)
	2/25/2011	6.9	5.1	19.2	365	0.3	0.1	7
	3/25/2011	6.9	5.1	18.9	379			
	4/15/2011	7.1	4.9	18.4	383	0.1	0.1	9
	5/25/2011	7	5	18.2	364			
	6/13/2011	7.1	5	18.6	388	0.2	0.3	5
	7/13/2011	8.1	3.9	18	284			
	8/12/2011	7.1	4.9	18.2	238	0.4	0.7	1
	9/2/2011	6.9	5.1	18.4	220			
	10/28/2011	7.1	4.9	18.9	298	0.4	64.5	8.3
	11/18/2011	7	5	19.6	304			
	12/21/2011	7.1	4.9	19.8	315	0.1	0.6	10.8
	1/31/2012	7.1	5	19.1	319			

Appendix E Continued

JWSES12 (12.1 mamsl)								
Depth (8.3 m)	Date Measured	Depth to Groundwater (m)	Hydraulic Head (mamsl)	Temperature (°C)	Specific Conductivity (uS/cm)	NH4-N (mg/L)	NO3-N (mg/L)	Cl (mg/L)
	2/25/2011	7.1	5	19.1	455	0.3	0.2	7
	3/25/2011	7.1	5	19	414			
	4/15/2011	7.2	4.9	18.9	539	0.1	0.1	52
	5/25/2011	7.1	5	18.5	470			
	6/13/2011	7.2	4.9	18.6	550	0.1	0.2	37
	7/13/2011	7.2	4.9	18	524			
	8/12/2011	7.3	4.9	18.2	481	0.1	0.7	2.7
	9/2/2011	6.8	5.3	18.6	322			
	10/28/2011	7.3	4.8	18.7	487	0.2	294	29.7
	11/18/2011	7	5.1	19.6	304			
	12/21/2011	7.2	4.9	19.7	484	0.1	0.6	67.9
	1/31/2012	7.2	4.9	19.2	494			

Appendix E Continued

JWSES13 (12 mamsl)								
Depth (5.7 m)	Date Measured	Depth to Groundwater (m)	Hydraulic Head (mamsl)	Temperature (°C)	Specific Conductivity (uS/cm)	NH4-N (mg/L)	NO3-N (mg/L)	Cl (mg/L)
	2/25/2011	4.5	7.5	16.6	535	0.9	0.5	13
	3/25/2011	4.5	7.5	16.5	379			
	4/15/2011	4.5	7.5	16.2	580	0.3	12	84
	5/25/2011	4.5	7.5	17.2	617			
	6/13/2011	4.7	7.3	18.2	658	0.5	25.5	94
	7/13/2011	5	7.1	18.7	644			
	8/12/2011							
	9/2/2011	4.4	7.7	20.6	587			
	10/28/2011	5.4	6.7	20.2	588			
	11/18/2011	4.8	7.3	20.6	728			
	12/21/2011	5	7	20.2	706	0.5	13.2	128.31
	1/31/2012	4.9	7.1	18.6	688			

Appendix E Continued

JWSES14 (11.9 mamsl)								
Depth (7.3 m)	Date Measured	Depth to Groundwater (m)	Hydraulic Head (mamsl)	Temperature (°C)	Specific Conductivity (uS/cm)	NH4-N (mg/L)	NO3-N (mg/L)	Cl (mg/L)
	2/25/2011	7.1	5	19.1	455	0.4	0.8	13
	3/25/2011	7.1	5	19	414			
	4/15/2011	7.2	4.9	18.9	539	0.4	1.1	102
	5/25/2011	7.1	5	18.5	470			
	6/13/2011	7.2	4.9	18.6	550	0.2	20.3	84
	7/13/2011	7.2	4.9	18	524			
	8/12/2011	7.3	4.9	18.2	481	0.2	23.1	9.8
	9/2/2011	6.8	5.3	18.6	322			
	10/28/2011	7.3	4.8	18.7	487	0.4	173.2	74.8
	11/18/2011	7	5.1	19.6	304			
	12/21/2011	7.2	4.9	19.7	484	0.1	9.9	157.17
	1/31/2012	7.2	4.9	19.2	494			

Appendix E Continued

JWSES15 (12 mamsl)								
Depth (8.3 m)	Date Measured	Depth to Groundwater (m)	Hydraulic Head (mamsl)	Temperature (°C)	Specific Conductivity (uS/cm)	NH4-N (mg/L)	NO3-N (mg/L)	Cl (mg/L)
	2/25/2011	7.2	4.8	18.7	249	0.2	0.1	4
	3/25/2011	7.2	4.8	18.6	278			
	4/15/2011	7.2	4.8	18.2	368	1.3	0.1	5
	5/25/2011	7.2	4.8	18.2	279			
	6/13/2011	7.3	4.7	18.6	285	0.1	0.6	3
	7/13/2011	7.6	4.5	17.7	290			
	8/12/2011	7.3	4.7	18.2	228	0.1	0.9	0.6
	9/2/2011	6.8	5.2	18.5	160			
	10/28/2011	7.4	4.6	18.7	265	0.4	0.6	3.1
	11/18/2011	7.3	4.8	19.2	139			
	12/21/2011	7.6	4.4	19.7	169	1	0.6	4.5
	1/31/2012	7.3	4.7	19	94			

Appendix E Continued

JWSES16 (5.4 mamsl)								
Depth (1.5 m)	Date Measured	Depth to Groundwater (m)	Hydraulic Head (mamsl)	Temperature (°C)	Specific Conductivity (uS/cm)	NH4-N (mg/L)	NO3-N (mg/L)	Cl (mg/L)
	2/25/2011	1	4.5	13.7	344	0.1	1	7.5
	3/25/2011	1	4.5	14.6	383			
	4/15/2011	1	4.5	14.7	376	0.1	0.1	18
	5/25/2011	1.1	4.4	17.2	553			
	6/13/2011	1.1	4.4	17.6	470	0.1	0.3	9
	7/13/2011	1	4.4	18.4	370			
	8/12/2011	1.1	4.3	19.4	370	0.1	0.9	1.3
	9/2/2011	0.9	4.5	19.4	303			
	10/28/2011	1	4.4	18	399	0.1	0.1	8.8
	11/18/2011	1	4.5	17	395			
	12/21/2011	1	4.4	16.2	382	1	0.5	15.9
	1/31/2012	1	4.4	15	359			

Appendix E Continued

JWSES17 (5.3 mamsl)								
Depth (1.2 m)	Date Measured	Depth to Groundwater (m)	Hydraulic Head (mamsl)	Temperature (°C)	Specific Conductivity (uS/cm)	NH4-N (mg/L)	NO3-N (mg/L)	Cl (mg/L)
	2/25/2011	0.9	4.4	12.4	335	0.2	2	11.6
	3/25/2011	0.9	4.4	13.9	371			
	4/15/2011	0.9	4.4	15	328	0.1	0.4	42
	5/25/2011	1.1	4.2	17.4	489			
	6/13/2011	1.1	4.2	18.6	592	0.4	0.4	51
	7/13/2011	1.1	4.2	19.6	615			
	8/12/2011	1.1	4.1	21.1	628	0.3	2.5	4.1
	9/2/2011	0.8	4.4	20.6	460			
	10/28/2011	1	4.3	18.6	789	1.5	0.1	52.8
	11/18/2011	1	4.3	16.9	488			
	12/21/2011	1	4.3	15.7	488	0.1	0.5	37.7
	1/31/2012	1	4.3	13.9	421			

Appendix E Continued

JWSES18 (5.8 mamsl)								
Depth (1.3 m)	Date Measured	Depth to Groundwater (m)	Hydraulic Head (mamsl)	Temperature (°C)	Specific Conductivity (uS/cm)	NH4-N (mg/L)	NO3-N (mg/L)	Cl (mg/L)
	2/25/2011	1.2	4.6	14.4	593	0.2	2	8.1
	3/25/2011	1.2	4.6	15.5	668			
	4/15/2011	1.2	4.6	16	578	0.1	1	29
	5/25/2011	1.3	4.5	17.4	598			
	6/13/2011	1.3	4.5	19	642	0.1	7.2	36
	7/13/2011	1.2	4.6	19.7	870			
	8/12/2011	1.3	4.5	21.4	571	0.1	1.9	3.6
	9/2/2011	1.2	4.6	19.6	604			
	10/28/2011	1.3	4.5	17.2	790	0.2	0.2	18.4
	11/18/2011	1.2	4.6	16.4	693			
	12/21/2011	1.3	4.5	15.7	556	0.1	2.5	42
	1/31/2012	1.3	4.5	13.7	712			

Appendix E Continued

JWSES19							
Depth (1.5 m)	Date Measured	Depth to Groundwater (m)	Temperature (°C)	Specific Conductivity (uS/cm)	NH4-N (mg/L)	NO3-N (mg/L)	Cl (mg/L)
	2/25/2011	1	11.6	240	1.4	0.1	20
	3/25/2011	1.1	13.8	355			
	4/15/2011	1	13.5	301	0.7	0.1	11
	5/25/2011	1.1	16.4	341			
	6/13/2011	1.1	375	642	1.4	0.3	5
	7/13/2011	0.8	19.5	326			
	8/12/2011	1	20.9	344	1.6	1.2	1.8
	9/2/2011	0.5	20.7	302			
	10/28/2011	0.9	17.9	360	3.3	0.1	13.4
	11/18/2011	0.9	15.7	317			
	12/21/2011	1	14.4	427	0.3	0.5	13
	1/31/2012	1	12.9	327			

Appendix E Continued

JWSES20							
Depth (1.1 m)	Date Measured	Depth to Groundwater (m)	Temperature (°C)	Specific Conductivity (uS/cm)	NH4-N (mg/L)	NO3-N (mg/L)	Cl (mg/L)
	2/25/2011	0.3	11.6	370	0.2	0.4	6
	3/25/2011	0.4	13.6	448			
	4/15/2011	0.4	14.5	381	0.1	0.6	33
	5/25/2011	0.4	17.4	397			
	6/13/2011	0.4	20.4	412	0.2	0.9	20
	7/13/2011	0.4	19.4	476			
	8/12/2011	0.5	21.5	461	0.6	1.2	2.2
	9/2/2011	0.5	20.6	360			
	10/28/2011	0.4	17.2	497	0.6	0.2	7.9
	11/18/2011	0.4	15	437			
	12/21/2011	0.4	13.7	325	0.1	0.6	40
	1/31/2012	0.4	12.7	441			

Appendix E Continued

JWSES21							
Depth (1.6 m)	Date Measured	Depth to Groundwater (m)	Temperature (°C)	Specific Conductivity (uS/cm)	NH4-N (mg/L)	NO3-N (mg/L)	Cl (mg/L)
	2/25/2011	0.1	14.3	310	0.2	0.6	6
	3/25/2011	0.1	14.6	359			
	4/15/2011	0.2	15.2	337	0.1	0.1	15
	5/25/2011	0.2	18.1	476			
	6/13/2011	0.2	20.5	545	0.1	8.2	31
	7/13/2011	0.1	20.4	423			
	8/12/2011	0.2	22.9	384	0.1	4.6	2.6
	9/2/2011	0	21.9	279			
	10/28/2011	0.1	17.9	419	0.2	0.7	7.7
	11/18/2011	0.1	16.4	416			
	12/21/2011	0.2	14.9	396	0.1	1.8	24
	1/31/2012	0.5	13.7	440			

Appendix E Continued

JWSESspring					
Date Measured	Temperature (°C)	Specific Conductivity (uS/cm)	NH4-N (mg/L)	NO3-N (mg/L)	Cl (mg/L)
2/25/2011	18.1	424	0.2	3.2	6
3/25/2011	16.9	485			
4/15/2011	17.2	464	0.1	2.9	34
5/25/2011	18.2	494			
6/13/2011	18.2	577	0.2	6.8	46
7/13/2011	17.7	445			
8/12/2011	19.5	497	0.2	7.7	4.1
9/2/2011	19.2	273			
10/28/2011	18.6	431	0.1	0.3	24.2
11/18/2011	18.6	504			
12/21/2011	14.7	159	0.1	3.8	40
1/31/2012	17.9	466			

Appendix E Continued

JWSESspring/stream confluence					
Date Measured	Temperature (°C)	Specific Conductivity (uS/cm)	NH4-N (mg/L)	NO3-N (mg/L)	Cl (mg/L)
2/25/2011	17.4	43	0.2	5.1	6
3/25/2011	16.5	304			
4/15/2011	17.6	380	0.1	3.2	52
5/25/2011	18.9	438			
6/13/2011	20	530	0.2	5.9	42
7/13/2011	19.2	446			
8/12/2011	22.1	492			
9/2/2011	20.7	105			
10/28/2011	15.5	156	0.1	0.4	4.8
11/18/2011	15	437			
12/21/2011	14.7	159	0.1	1.4	9
1/31/2012	15	399			

Appendix E Continued

JWSES5m upstream					
Date Measured	Temperature (°C)	Specific Conductivity (uS/cm)	NH4-N (mg/L)	NO3-N (mg/L)	Cl (mg/L)
2/25/2011	14.5	116	0.2	0.6	2
3/25/2011	12.7	31			
4/15/2011	16.2	139	0.1	0.5	13
5/25/2011	19.6	145			
6/13/2011	20.9	142	0.1	0.54	13
7/13/2011	22.5	149			
8/12/2011	22.7	145	0.04	1.38	0.8
9/2/2011	20.2	243			
10/28/2011	15.6	155	0.1	0	4.3
11/18/2011	12.6	112			
12/21/2011	15	158	0.1	1.4	4
1/31/2012	12.9	141			

Appendix E Continued

JWSES5m downstream					
Date Measured	Temperature (°C)	Specific Conductivity (uS/cm)	NH4-N (mg/L)	NO3-N (mg/L)	Cl (mg/L)
2/25/2011	14.8		0.2	1.3	2
3/25/2011	13.4	133			
4/15/2011	16.4	191	0.1	0.3	9.5
5/25/2011	19.9	116			
6/13/2011	20.7	75	0.1	0.7	10
7/13/2011	22.4	151			
8/12/2011	22.5	147	0.1	2.0	2.0
9/2/2011					
10/28/2011	15.1	149	0.1	0.1	6.8
11/18/2011	12.2	131			
12/21/2011	15	178	0.1	1.4	7
1/31/2012	11.1	162			

Appendix E Continued

WCHS1s (7.9 mamsl)								
Depth (2 m)	Date Measured	Depth to Groundwater (m)	Hydraulic Head (mamsl)	Temperature (°C)	Specific Conductivity (uS/cm)	NH4-N (mg/L)	NO3-N (mg/L)	Cl (mg/L)
	2/25/2011	1	6.9	14.4	46	0.2	2.1	21
	3/25/2011	1	6.9	13.1	114			
	4/15/2011	1.2	6.7	14.7	124	0.1	0.1	9
	5/25/2011	1.5	6.4	17.6	104			
	6/13/2011	1.7	6.2	19.2	87	0.1	0.6	16
	7/13/2011	1.9	6.0	21	88			
	8/12/2011							
	9/2/2011	0.7	7.1	23.6	47			
	10/28/2011	1.2	6.7	20.1	79	0.1	0	18.9
	11/18/2011	1.2	6.6	18.2	72			
	12/21/2011	1.4	6.5	16.4	75	0.1	0.3	23
	2/3/2012	1.3	6.6	14.6	80			

Appendix E Continued

WCHS1d (7.9 mamsl)								
Depth (3.6 m)	Date Measured	Depth to Groundwater (m)	Hydraulic Head (mamsl)	Temperature (°C)	Specific Conductivity (uS/cm)	NH4-N (mg/L)	NO3-N (mg/L)	Cl (mg/L)
	2/25/2011	1	6.9	14.9	141	0.6	5	14
	3/25/2011	1	6.9	14.4	211			
	4/15/2011	1.2	6.7	15.9	197	0.2	0.1	29
	5/25/2011	1.5	6.4	17.5	118			
	6/13/2011	1.8	6.1	19.4	123	0.4	0.3	20
	7/13/2011	2.1	5.8	20	69			
	8/12/2011	1.9	6	21.7	9	0.2	0.2	0.7
	9/2/2011	0.8	7.1	21.5	21			
	10/28/2011	1.3	6.6	20.6	157	0.3	0.1	7.8
	11/18/2011	1.3	6.6	17.9	99			
	12/21/2011	1.4	6.5	17.4	90	0.5	0.4	21
	2/3/2012	1.3	6.6	15.1	103			

Appendix E Continued

WCHS2 (7.7 mamsl)								
Depth (2.3 m)	Date Measured	Depth to Groundwater (m)	Hydraulic Head (mamsl)	Temperature (°C)	Specific Conductivity (uS/cm)	NH4-N (mg/L)	NO3-N (mg/L)	Cl (mg/L)
	2/25/2011	0.9	6.9	13.4	45	0.2	1	7
	3/25/2011	0.9	6.8	13.5	49			
	4/15/2011	1	6.7	15.7	91	0.1	0.1	14
	5/25/2011	1.3	6.4	18.1	47			
	6/13/2011	1.6	6.1	21.4	50	0.1	0.2	10
	7/13/2011	1.6	6.2	22.2	83			
	8/12/2011	1.7	6	22.7	54	0.1	0.3	0.9
	9/2/2011	0.6	7.1	23	54			
	10/28/2011	1.1	6.7	20.2	142	1.9	0.1	13.3
	11/18/2011	1.1	6.6	18.4	138			
	12/21/2011	1.2	6.5	17.2	203	0.1	0.6	13
	2/3/2012	1.1	6.6	15.4	155			

Appendix E Continued

WCHS3 (8 mamsl)								
Depth (2 m)	Date Measured	Depth to Groundwater (m)	Hydraulic Head (mamsl)	Temperature (°C)	Specific Conductivity (uS/cm)	NH4-N (mg/L)	NO3-N (mg/L)	Cl (mg/L)
	2/25/2011	1	7.1	4.6	36	0.1	0.1	2
	3/25/2011	1	7.1	4.1	2			
	4/15/2011	1.2	6.9	4.4	1	0.1	0.1	5
	5/25/2011	1.5	6.6	5.4	4			
	6/13/2011	1.7	6.3	7.2	16	0.1	0.3	6
	7/13/2011	1.9	6.2	6.2	18			
	8/12/2011					0.1	0.5	1.2
	9/2/2011	0.7	7.3	3	60			
	10/28/2011	1.2	6.8	4.6	130	24.2	0.1	14.6
	11/18/2011	1.2	6.8	4.7	53			
	12/21/2011	1.4	6.7	5.1	16	0.1	0.3	3
	2/3/2012	1.3	6.8	5	14			

Appendix E Continued

WCHS4 (7.9 mamsl)								
Depth (2.6 m)	Date Measured	Depth to Groundwater (m)	Hydraulic Head (mamsl)	Temperature (°C)	Specific Conductivity (uS/cm)	NH4-N (mg/L)	NO3-N (mg/L)	Cl (mg/L)
	2/25/2011	1	6.8	13		0.1	0.3	2
	3/25/2011	1.1	6.8	12.7				
	4/15/2011	1.1	6.7	15.1	5	0	0.1	1.8
	5/25/2011	1.4	6.4	17.5				
	6/13/2011	1.7	6.1	20		0.1	0.2	3
	7/13/2011	1.7	6.2	21.4				
	8/12/2011	1.9	5.9	22.5	5	0.2	0.2	0.5
	9/2/2011	0.7	7.1	22.5	4			
	10/28/2011	1.2	6.7	19.9	6	0.9	0.1	2.6
	11/18/2011	1.2	6.6	18.1				
	12/21/2011	1.3	6.5	16.9	5	0.1	0.3	4
	2/3/2012	1.3	6.5	15.1	29			

Appendix E Continued

WCHS5s (8 mamsl)								
Depth (2.4 m)	Date Measured	Depth to Groundwater (m)	Hydraulic Head (mamsl)	Temperature (°C)	Specific Conductivity (uS/cm)	NH4-N (mg/L)	NO3-N (mg/L)	Cl (mg/L)
	2/25/2011	1	7	13	30	0.1	0.2	1
	3/25/2011	1.2	6.8	12.7	12			
	4/15/2011							
	5/25/2011	2	6	17.2	27			
	6/13/2011							
	7/13/2011							
	8/12/2011					0.1	0.3	2.0
	9/2/2011	0.8	7.2	23.7	14			
	10/28/2011	1.4	6.7	20	38	0.1	0.1	9.1
	11/18/2011	1.4	6.6	18.1	24			
	12/21/2011	1.5	6.5	16.9	24	0	0.4	5
	2/3/2012	1.4	6.6	14.6	39			

Appendix E Continued

WCHS5d (8 mamsl)								
Depth (2.4 m)	Date Measured	Depth to Groundwater (m)	Hydraulic Head (mamsl)	Temperature (°C)	Specific Conductivity (uS/cm)	NH4-N (mg/L)	NO3-N (mg/L)	Cl (mg/L)
	2/25/2011	1	7	12.7	34	0.1	0.2	1
	3/25/2011	1.2	6.8	12.6	10			
	4/15/2011	1.3	6.7	14.5	49	0	0.2	5
	5/25/2011	2	6	16.7	88			
	6/13/2011	1.9	6.1	19.6	70	0.1	0.6	5
	7/13/2011	1.8	6.2	20.9	16			
	8/12/2011	2	6	22.5	60			
	9/2/2011	0.8	7.2	22.1	42			
	10/28/2011	1.3	6.7	20	65	0.1	0.1	4.1
	11/18/2011							
	12/21/2011	1.5	6.5	16.6	44	0	0.3	5
	2/3/2012	1.4	6.6	14.6	42			

Appendix E Continued

WCHS6 (8.1 mamsl)								
Depth (2.3 m)	Date Measured	Depth to Groundwater (m)	Hydraulic Head (mamsl)	Temperature (°C)	Specific Conductivity (uS/cm)	NH4-N (mg/L)	NO3-N (mg/L)	Cl (mg/L)
	2/25/2011	1.2	6.9	13	0	0.1	0.2	2
	3/25/2011	1.2	6.8	13	14			
	4/15/2011	1.3	6.7	14.1	40	0.1	0.1	5
	5/25/2011	1.6	6.4	17.2	27			
	6/13/2011	1.9	6.1	18.5	25	0.1	0.2	11
	7/13/2011	1.9	6.2	20	21			
	8/12/2011	2.1	6	22	77	2.0	0.1	0.7
	9/2/2011	0.9	7.2	21.6	25			
	10/28/2011	1.4	6.7	19.4	68	0.2	0	3.2
	11/18/2011	1.4	6.6	18.1	56			
	12/21/2011	1.5	6.5	17	63	0	0.3	5
	2/3/2012	1.5	6.5	15	60			

Appendix E Continued

WCHS7 (8.2 mamsl)								
Depth (2.4 m)	Date Measured	Depth to Groundwater (m)	Hydraulic Head (mamsl)	Temperature (°C)	Specific Conductivity (uS/cm)	NH4-N (mg/L)	NO3-N (mg/L)	Cl (mg/L)
	2/25/2011	1.3	6.9	12.4	74	0.1	1.9	1
	3/25/2011	1.4	6.8	12.1	31			
	4/15/2011	1.5	6.7	14	58	0	0.1	1.7
	5/25/2011	1.8	6.4	17.2	88			
	6/13/2011	2.4	5.8	18.9	20	0.1	0.2	3
	7/13/2011	2.4	5.8	20.4	26			
	8/12/2011	2.2	6	22.2	10	0.1	0.3	0.6
	9/2/2011	1	7.2	23	8			
	10/28/2011	1.5	6.7	19.5	43	0.1	0.1	1.7
	11/18/2011	1.6	6.6	17.5	45			
	12/21/2011	1.7	6.5	16.4	12	0	0.9	2
	2/3/2012	1.6	6.6	14.1	10			

Appendix E Continued

WCHS8 (8.6 mamsl)								
Depth (2.4 m)	Date Measured	Depth to Groundwater (m)	Hydraulic Head (mamsl)	Temperature (°C)	Specific Conductivity (uS/cm)	NH4-N (mg/L)	NO3-N (mg/L)	Cl (mg/L)
	2/25/2011	1.7	6.9	11.6	132	0.4	3.2	6
	3/25/2011	1.7	6.9	12	144			
	4/15/2011	1.9	6.7	14.1	186	0.1	2.5	18.7
	5/25/2011	2.2	6.4	17.7	169			
	6/13/2011	2.4	6.2	21.2	110			
	7/13/2011	2.4	6.2	22.2	268			
	8/12/2011							
	9/2/2011	1.5	7.2	24.2	14			
	10/28/2011	2.4	6.2	21.4	67	0.8	0.1	5.8
	11/18/2011	2	6.6	19.1	261			
	12/21/2011	2.1	6.5	17.6	197	0.1	5.6	23
	2/3/2012	2.1	6.6	14.7	94			

Appendix E Continued

WCHS9 (8.6 mamsl)								
Depth (2.5 m)	Date Measured	Depth to Groundwater (m)	Hydraulic Head (mamsl)	Temperature (°C)	Specific Conductivity (uS/cm)	NH4-N (mg/L)	NO3-N (mg/L)	Cl (mg/L)
	2/25/2011	1.5	7.1	12.7	97	0.1	1.9	2
	3/25/2011	1.7	7	12.7	133			
	4/15/2011	1.9	6.8	14.2	62	0.1	1.8	17
	5/25/2011	2.1	6.5	18.1	306			
	6/13/2011	2.4	6.2	19.7	329	0.2	14.6	56
	7/13/2011	2.4	6.2	22.1	414			
	8/12/2011	2.6	6.1	23.9	1867			
	9/2/2011	1.4	7.2	24	59			
	10/28/2011	1.9	6.7	20.6	188	1.4	0.1	1.8
	11/18/2011	2	6.6	18.6	36			
	12/21/2011	2.1	6.5	17.1	48	0.3	0.8	2
	2/3/2012	2	6.6	14.6	61			

Appendix E Continued

WCHS10 (8.3 mamsl)								
Depth (2.5 m)	Date Measured	Depth to Groundwater (m)	Hydraulic Head (mamsl)	Temperature (°C)	Specific Conductivity (uS/cm)	NH4-N (mg/L)	NO3-N (mg/L)	Cl (mg/L)
	2/25/2011	1.4	6.9	13.7	1	0.1	0.4	1
	3/25/2011	1.5	6.8	13.9	0			
	4/15/2011	1.6	6.7	15.2	22	0.1	0.1	0.9
	5/25/2011	1.9	6.4	18.9	15			
	6/13/2011							
	7/13/2011	2.2	6.1	22.7	2			
	8/12/2011	2.3	6	24.4	14	0.1	0.1	0.5
	9/2/2011	1.1	7.2	24.9	8			
	10/28/2011	1.6	6.7	21.5	55	0.1	0.1	1.3
	11/18/2011	1.6	6.7	19.1	36			
	12/21/2011	1.8	6.5	17.6	11	0.1	0.3	1
	2/3/2012	1.7	6.6	15	11			

Appendix E Continued

WCHS11 (8.6 mamsl)								
Depth (2.3 m)	Date Measured	Depth to Groundwater (m)	Hydraulic Head (mamsl)	Temperature (°C)	Specific Conductivity (uS/cm)	NH4-N (mg/L)	NO3-N (mg/L)	Cl (mg/L)
	2/25/2011	1.7	7	12.9	17	0.1	2.2	1
	3/25/2011	1.7	6.9	13.2	39			
	4/15/2011	1.9	6.7	14.9	111	0.1	1.7	9
	5/25/2011	2.2	6.5	18.6	91			
	6/13/2011							
	7/13/2011							
	8/12/2011							
	9/2/2011	1.4	7.2	24	21			
	10/28/2011	1.8	6.8	21.4	173	1.5	0.1	2.4
	11/18/2011	2	6.6	19.2	36			
	12/21/2011	2.1	6.5	17.7	58	0.1	1.5	11
	2/3/2012	2.1	6.6	15.1	41			

Appendix E Continued

WCHS12 (7.9 mamsl)								
Depth (2.5 m)	Date Measured	Depth to Groundwater (m)	Hydraulic Head (mamsl)	Temperature (°C)	Specific Conductivity (uS/cm)	NH4-N (mg/L)	NO3-N (mg/L)	Cl (mg/L)
	2/25/2011	1.8	6.9	12.5	315	0.5	3.9	5
	3/25/2011	1.8	6.9	12.9	353			
	4/15/2011	1.9	6.7	15	490	0.1	7.0	31
	5/25/2011	2.2	6.5	18.1	511			
	6/13/2011	2.6	6.1	20.9	371	0.2	4.6	29
	7/13/2011	2.5	6.2	22	318			
	8/12/2011	2.6	6.1	22.7	247			
	9/2/2011	1.5	7.2	23	155			
	10/28/2011	2	6.7	21.4	339	0.9	0.3	6.7
	11/18/2011	2	6.6	19.5	474			
	12/21/2011	2.1	6.5	18.4	398	0.3	7.8	21
	2/3/2012	2.1	6.6	15.7	265			

Appendix E Continued

WCHS13s (8.6 mamsl)								
Depth (2.5 m)	Date Measured	Depth to Groundwater (m)	Hydraulic Head (mamsl)	Temperature (°C)	Specific Conductivity (uS/cm)	NH4-N (mg/L)	NO3-N (mg/L)	Cl (mg/L)
	2/25/2011	1.6	7	12.4	214	0.3	4.4	5
	3/25/2011	1.7	6.9	12.7	276			
	4/15/2011	1.8	6.8	15.2	350	0.1	5	23
	5/25/2011	2.1	6.5	17.6	588			
	6/13/2011	2.4	6.2	20.6	775	0.4	61	112
	7/13/2011	2.4	6.2	20.9	1120			
	8/12/2011	2.6	6	22.1	1045	0.6	77.8	12.22
	9/2/2011	1.4	7.2	23.2	376			
	10/28/2011	1.9	6.7	21.4	567	154.6	0.1	51.5
	11/18/2011	2	6.7	18.4	603			
	12/21/2011	2.1	6.5	18	802	3.6	11.7	98
	2/3/2012	2	6.6	15.7	888			

Appendix E Continued

WCHS13d/GP5 (8.6 mamsl)								
Depth (3.6 m)	Date Measured	Depth to Groundwater (m)	Hydraulic Head (mamsl)	Temperature (°C)	Specific Conductivity (uS/cm)	NH4-N (mg/L)	NO3-N (mg/L)	Cl (mg/L)
	2/25/2011	1.6	7	13.9	358	0.8	8.6	7
	3/25/2011	1.7	7	13.5	509			
	4/15/2011	1.9	6.8	14.9	380	0.1	1	24
	5/25/2011	2.2	6.5	18.1	410			
	6/13/2011	2.4	6.3	19.6	764	0.6	39.8	69
	7/13/2011	2.4	6.2	21.6	484			
	8/12/2011	2.6	6.1	21	413	0.4	23.5	2
	9/2/2011	1.5	7.2	21.7	332			
	10/28/2011	1.9	6.8	21.4	225	2.6	0.2	12.5
	11/18/2011	2	6.7	20.2	907			
	12/21/2011	2.1	6.6	18.4	1044	0.6	12.5	55
	2/3/2012	2	6.6	16	991			

Appendix E Continued

WCHS14 (8.2 mamsl)								
Depth (2.2 m)	Date Measured	Depth to Groundwater (m)	Hydraulic Head (mamsl)	Temperature (°C)	Specific Conductivity (uS/cm)	NH4-N (mg/L)	NO3-N (mg/L)	Cl (mg/L)
	2/25/2011	1.2	7	13.2	26	0.1	0.1	1
	3/25/2011	1.3	6.9	13.5	0			
	4/15/2011	1.4	6.7	15.2	31	0.1	0.1	2
	5/25/2011	1.7	6.5	19.7	11			
	6/13/2011	2	6.2	21.6	1	0.1	0.1	7
	7/13/2011	2.1	6.1	23.1	0			
	8/12/2011	2.1	6.1	24.7	5	0.1	1.4	2
	9/2/2011	1	7.2	26	50			
	10/28/2011	1.4	6.7	21.4	22	0.2	0.1	4.3
	11/18/2011	1.5	6.7	19.1	16			
	12/21/2011	1.6	6.6	17.1	34	0.1	0.3	0.8
	2/3/2012	1.6	6.6	14.9	17			

Appendix E Continued

WCHS15 (8.4 mamsl)								
Depth (2.5 m)	Date Measured	Depth to Groundwater (m)	Hydraulic Head (mamsl)	Temperature (°C)	Specific Conductivity (uS/cm)	NH4-N (mg/L)	NO3-N (mg/L)	Cl (mg/L)
	2/25/2011	1.4	7	12.6	326	0.4	9.5	5
	3/25/2011	1.5	6.9	12.7	444			
	4/15/2011	1.7	6.7	16.1	424	0.1	4.5	31
	5/25/2011	1.9	6.5	18.7	529			
	6/13/2011	2.2	6.2	20.6	777	1	63	98
	7/13/2011	2.2	6.2	22.1	101			
	8/12/2011	2.4	6	22.9	730	0.5	51.3	7
	9/2/2011	1.3	7.1	23.4	120			
	10/28/2011	1.7	6.7	21.2	302	1.1	0.2	6.4
	11/18/2011	1.8	6.6	19.4	421			
	12/21/2011	1.9	6.5	17.6	874	0.5	16.7	113
	2/3/2012	1.8	6.6	15.5	830			

Appendix E Continued

WCHS16 (8.5 mamsl)								
Depth (2.4 m)	Date Measured	Depth to Groundwater (m)	Hydraulic Head (mamsl)	Temperature (°C)	Specific Conductivity (uS/cm)	NH4-N (mg/L)	NO3-N (mg/L)	Cl (mg/L)
	2/25/2011	1.5	7	12.7	90	0.1	3.2	5
	3/25/2011	1.5	6.9	13.4	92			
	4/15/2011	1.7	6.8	15.2	161	0.1	1.4	28
	5/25/2011	2	6.5	17.7	256			
	6/13/2011	2.3	6.2	20.7	226	0.1	8.1	28
	7/13/2011	2.3	6.2	22	243			
	8/12/2011	2.4	6.1	22.5	368	294	13.7	9
	9/2/2011	1.3	7.2	23.2	55			
	10/28/2011	1.8	6.7	20.7	319	18.6	0.1	14.6
	11/18/2011	1.9	6.6	19.2	260			
	12/21/2011	2	6.5	17.7	527	0.3	12.2	81
	2/3/2012	1.9	6.6	15.5	478			

Appendix E Continued

WCHS17 (8.4 mamsl)								
Depth (2.4m)	Date Measured	Depth to Groundwater (m)	Hydraulic Head (mamsl)	Temperature (°C)	Specific Conductivity (uS/cm)	NH4-N (mg/L)	NO3-N (mg/L)	Cl (mg/L)
	2/25/2011	1.4	7	12.5	359	0.4	6.6	4
	3/25/2011	1.5	6.9	13	353			
	4/15/2011	1.7	6.8	15.2	1100	0.2	40	150
	5/25/2011	1.9	6.5	18.1	1076			
	6/13/2011	2.2	6.2	19.9	799	0.5	69	143
	7/13/2011	2.2	6.2	22	1160			
	8/12/2011	2.4	6	23	1043	142	5.9	5
	9/2/2011	1.2	7.2	24.4	150			
	10/28/2011	1.7	6.7	21.2	316	46.4	0.1	10
	11/18/2011	1.8	6.6	19.4	572			
	12/21/2011	1.9	6.5	17.4	785	2.6	18	152
	2/3/2012	1.8	6.6	15.4	876			

Appendix E Continued

WCHS18 (8.3 mamsl)								
Depth (2.5 m)	Date Measured	Depth to Groundwater (m)	Hydraulic Head (mamsl)	Temperature (°C)	Specific Conductivity (uS/cm)	NH4-N (mg/L)	NO3-N (mg/L)	Cl (mg/L)
	2/25/2011	1.4	7	11.9	293	0.2	6.6	4
	3/25/2011	1.4	6.9	12.1	306			
	4/15/2011	1.6	6.7	15	557	0.1	10	33
	5/25/2011	1.9	6.5	18	1115			
	6/13/2011	2.1	6.2	20.4	1189	1	81.3	119
	7/13/2011	2.1	6.2	22.9	1167			
	8/12/2011	2.3	6	23.6	655	0.5	60.5	8
	9/2/2011	1.2	7.2	23.9	132			
	10/28/2011	1.6	6.7	21.4	383	0.8	0.2	18
	11/18/2011	1.7	6.6	19.6	729			
	12/21/2011	2.1	6.2	17.3	902	0.5	20	150
	2/3/2012	1.8	6.6	15.1	777			

Appendix E Continued

WCHS19 (8.2 mamsl)								
Depth (2.2 m)	Date Measured	Depth to Groundwater (m)	Hydraulic Head (mamsl)	Temperature (°C)	Specific Conductivity (uS/cm)	NH4-N (mg/L)	NO3-N (mg/L)	Cl (mg/L)
	2/25/2011	1.2	7	13.5	84	0.1	0.7	1
	3/25/2011	1.3	6.9	13.5	224			
	4/15/2011	1.4	6.7	15.2	188	0.1	0.1	2.5
	5/25/2011	2.1	6.1	19.9	102			
	6/13/2011	2	6.2	22.6	67	0.1	0.2	3
	7/13/2011	2	6.2	23.4	10			
	8/12/2011	2.1	6	24.7	39	0.1	0.6	1.2
	9/2/2011	1	7.2	25	33			
	10/28/2011	1.5	6.7	20.7	87	0.1	0.2	0.8
	11/18/2011	1.5	6.6	19.1	72			
	12/21/2011	1.7	6.5	16.9	43	0	0.1	2
	2/3/2012	1.6	6.6	14.9	36			

Appendix E Continued

WCHS20 (8.2 mamsl)								
Depth (2.3 m)	Date Measured	Depth to Groundwater (m)	Hydraulic Head (mamsl)	Temperature (°C)	Specific Conductivity (uS/cm)	NH4-N (mg/L)	NO3-N (mg/L)	Cl (mg/L)
	2/25/2011	1.2	7	12.9	40	0.1	0.2	1
	3/25/2011	1.3	6.9	13.4	65			
	4/15/2011	1.5	6.7	15.1	50	0.1	0.1	1.6
	5/25/2011	2.2	6	18.6	110			
	6/13/2011	2.3	5.9	21.4	86	0.1	0.8	9
	7/13/2011	2	6.2	23.6	36			
	8/12/2011	2.2	6.1	24.4	29	0.2	0.5	2
	9/2/2011	1.1	7.2	25.9	13			
	10/28/2011	1.5	6.7	21.4	51	0.2	0.1	2.2
	11/18/2011	1.6	6.7	19.2	43			
	12/21/2011	1.7	6.5	17.2	40	0.1	0.8	1.5
	2/3/2012	1.6	6.6	15	36			

Appendix E Continued

WCHS21 (8.2 mamsl)								
Depth (2.3 m)	Date Measured	Depth to Groundwater (m)	Hydraulic Head (mamsl)	Temperature (°C)	Specific Conductivity (uS/cm)	NH4-N (mg/L)	NO3-N (mg/L)	Cl (mg/L)
	2/25/2011	1.3	6.9	13.7	124	0.2	8	1
	3/25/2011	1.3	6.8	13.6	157			
	4/15/2011	1.5	6.7	15.2	150	0.1	0.4	2.3
	5/25/2011	1.8	6.4	18.6	129			
	6/13/2011	2	6.2	19.6	101	0.1	1.2	7
	7/13/2011	2	6.2	22.9	82			
	8/12/2011	2.2	6	23.2	81	0.1	0.4	0.7
	9/2/2011	1.2	6.2	23.4	53			
	10/28/2011	1.5	6.7	20.6	124	0.3	0.1	2.0
	11/18/2011	1.6	6.6	18.7	115			
	12/21/2011	1.7	6.5	17.2	102	0.1	1.5	2.9
	2/3/2012	1.6	6.6	15	107			

Appendix E Continued

WCHS22s (7.9 mamsl)								
Depth (1.9 m)	Date Measured	Depth to Groundwater (m)	Hydraulic Head (mamsl)	Temperature (°C)	Specific Conductivity (uS/cm)	NH4-N (mg/L)	NO3-N (mg/L)	Cl (mg/L)
	2/25/2011	1	6.6	12.9	21	0.1	1.1	1
	3/25/2011	1.1	6.9	13.5	17			
	4/15/2011	1.3	6.7	16.6	113	0	0.2	1.2
	5/25/2011	1.8	6.2	20.2	2			
	6/13/2011	1.8	6.2	23	32	0.1	0.2	2
	7/13/2011							
	8/12/2011	1.9	6	25.2	30	0.5	0.6	1
	9/2/2011	1	7	25.4	50			
	10/28/2011	1.3	6.6	21.4	46	2.1	0.1	3.2
	11/18/2011	1.4	6.6	19.1	32			
	12/21/2011	1.5	6.5	17.2	159	0	1.4	3.2
	2/3/2012	1.4	6.5	14.6	2			

Appendix E Continued

WCHS22d (8 mamsl)								
Depth (3.6 m)	Date Measured	Depth to Groundwater (m)	Hydraulic Head (mamsl)	Temperature (°C)	Specific Conductivity (uS/cm)	NH4-N (mg/L)	NO3-N (mg/L)	Cl (mg/L)
	2/25/2011	1	6.9	15.2	82	0.1	1.1	1
	3/25/2011	1.1	6.9	14.7	97			
	4/15/2011	1.3	6.7	16.6	113	0	0.1	1.4
	5/25/2011	1.5	6.5	21.4	108			
	6/13/2011	1.8	6.2	22	102	0.1	0.3	2
	7/13/2011	1.7	6.2	24.5	99			
	8/12/2011	1.9	6	25.4	124	2.1	1.5	1.8
	9/2/2011	1	7	23.1	74			
	10/28/2011	1.3	6.7	21.5	78	0.1	0.1	1.9
	11/18/2011	1.3	6.6	19.4	144			
	12/21/2011	1.6	6.3	16.6	2	0.1	0.4	2.4
	2/3/2012	1.4	6.5	15.4	148			

Appendix E Continued

WCHS23 (7.8 mamsl)								
Depth (1.8 m)	Date Measured	Depth to Groundwater (m)	Hydraulic Head (mamsl)	Temperature (°C)	Specific Conductivity (uS/cm)	NH4-N (mg/L)	NO3-N (mg/L)	Cl (mg/L)
	2/25/2011	0.7	7.1	12.9	1	0.1	0.4	1
	3/25/2011	0.7	7.1	13.2	20			
	4/15/2011	0.8	7	16.6	48	0.1	0.1	3.7
	5/25/2011	1.1	6.7	20.2	28			
	6/13/2011	1.3	6.5	22.2	14	0.1	0.2	4
	7/13/2011	1.3	6.5	24.6	32			
	8/12/2011	1.5	6.3	25.1	107	5.1	0.7	0.8
	9/2/2011	0.5	7.2	25.1	13			
	10/28/2011	0.9	6.9	21.1	44	0.3	0.1	0.9
	11/18/2011	0.9	6.9	19.1	51			
	12/21/2011	1	6.8	16.5	44	0	0.8	1.8
	2/3/2012	1	6.8	14.4	45			

Appendix E Continued

WCHS24 (8.4 mamsl)								
Depth (2.4 m)	Date Measured	Depth to Groundwater (m)	Hydraulic Head (mamsl)	Temperature (°C)	Specific Conductivity (uS/cm)	NH4-N (mg/L)	NO3-N (mg/L)	Cl (mg/L)
	2/25/2011	1.5	6.9	12.7	194	0.4	6.1	2.8
	3/25/2011	1.5	6.9	13	92			
	4/15/2011	1.6	6.8	15	214	0.1	2.6	13
	5/25/2011							
	6/13/2011	2.2	6.2	20.5	629	0.4	21.4	57
	7/13/2011	2.1	6.2	22.4	623			
	8/12/2011	2.3	6	23.4	631	1.5	25.8	6.1
	9/2/2011	1.2	7.1	23.7	170			
	10/28/2011	2	6.4	21.2	278	1	0.2	20
	11/18/2011	1.8	6.6	19.5	256			
	12/21/2011	1.9	6.5	17.5	312	0.2	5.4	22.5
	2/3/2012	1.9	6.5	15	432			

Appendix E Continued

WCHSstream					
Date Measured	Temperature (°C)	Specific Conductivity (uS/cm)	NH4-N (mg/L)	NO3-N (mg/L)	Cl (mg/L)
2/25/2011	16.4	54	0	1.5	1
3/25/2011	14.7	68			
4/15/2011	21	156			
5/25/2011	24.1	24			
6/13/2011					
7/13/2011					
8/12/2011					
9/2/2011	23.7	70			
10/28/2011					
11/18/2011	13.7	149			
12/21/2011	15.6	214	0.1	1.1	7
2/3/2012	14.6	156			

Appendix F

Groundwater Recharge and Discharge Areas

Piezometer	Depth mbgs	Mean Water-table Depth mamsl	Recharge/Discharge Area
JWSES2	4.80	4.32	Recharge
JWSES3/GP2	5.82	4.48	
WCHS1s	1.95	1.29	Recharge
WCHS1d/GP4	3.61	1.38	
WCHS13s	2.50	2.00	Recharge
WCHS13d/GP5	3.60	2.03	
WCHS22s	1.95	1.43	Discharge
WCHS22d/GP6	3.56	1.42	

Appendix G

Hydraulic Conductivity Estimates

JWSES	
Piezometer	Hydraulic Conductivity (m/day)
2	1.19
4	0.74
5	0.11
6	0.02
7	0.05
8	0.05
9	0.16
10	2.15
11	0.01
12/GP3	0.10
13	0.01
14	0.10
15	0.07
16	0.95
17	0.14
19	0.19
20	2.62
21	0.55

Appendix G Continued

WCHS	
Piezometer	Hydraulic Conductivity (m/day)
1d/GP4	0.51
2	0.58
3	1.05
4	1.67
5	0.88
6	1.19
7	1.52
8	2.44
9	2.75
10	0.53
11	2.08
12	2.17
13d/GP5	0.54
14	0.90
15	1.07
16	1.41
17	1.00
18	0.83
19	0.18
20	0.78
21	1.79
23	0.33
24	1.11

Appendix H

Groundwater Quality

To evaluate nutrient transport at the sites, a combination of CEL lab nutrient data, field data collected with a calibrated YSI multimeter, and specific conductivity measurements were used. Laboratory DIN and Cl concentrations collected on June 13, October 28, and December 21, 2011 were used to create calibration curves to correct the YSI meter field measurements on the three sampling dates. Corrected measurements were used to better understand the DIN and Cl contributions to groundwater specific conductivity for a broader sampling area across the sites. Corrected DIN and Cl concentrations were compared to groundwater specific conductivity values at JWSES and WCHS site piezometers using linear regressions on the three sampling dates. Sample locations in the riparian area at JWSES were not included in the regressions because they were down gradient of the spring and geophysical survey area. Additionally, corrected DIN, Cl, and ECUCEL PO4 concentrations were evaluated to assess the fate and transport of wastewater constituents across the sites.

Throughout the study period, median (n = 6) YSI field DIN and Cl, and specific conductivity varied across the sites (Tables 5 and 6). At both sites, DIN and Cl concentrations, and specific conductivity were elevated in the drainfields relative to background locations. In the riparian area at JWSES, DIN and Cl decreased relative to the drainfield, but were elevated compared to background piezometers.

Piezometer	DIN (mg/L)	DIN Standard Deviation	Cl (mg/L)	Cl Standard Deviation	Specific Conductivity (µS/cm)
1/GP1	1.27	10.11	4.28	20.47	308
2s	1.09	1.28	7.22	3.09	87
3/GP2	0.86	1.74	6.75	3.46	110
4	14.92	114.95	55.00	90.84	413
5	8.05	32.03	99.10	52.84	500
6	25.79	89.23	66.49	50.96	647
7	8.16	9.29	114.36	79.70	1014
8	1.99	4.59	35.30	40.97	773
9	0.41	1.19	3.83	3.57	112
10	19.85	12.79	71.00	43.90	497
11	0.55	26.27	7.63	3.45	340
12/GP3	0.53	119.90	33.36	25.31	486
13	6.84	10.40	89.00	48.42	619
14	15.24	66.89	79.40	55.94	486
15	0.83	0.36	3.56	1.55	257
16	0.43	0.42	8.88	6.07	379
17	1.17	0.96	39.84	20.58	540
18	2.08	2.44	23.68	15.40	586
19	1.75	1.02	11.96	6.50	352
20	0.75	0.44	13.96	15.45	376
21	1.35	3.15	11.35	11.17	390
spring	3.59	2.79	29.08	17.58	448
spring/stream confluence	2.34	2.52	8.94	22.40	159
5 m upstream	0.75	0.51	4.13	5.42	144
5m downstream	1.09	0.70	6.76	3.47	149

Table 5. JWSES median (n = 6) YSI multimeter DIN and Cl concentrations with standard deviations and specific conductivity.

Piezometer	DIN (mg/L)	DIN Standard Deviation	Cl (mg/L)	Cl Standard Deviation	Specific Conductivity (μS/cm)
1s	0.18	0.89	18.94	5.31	79
1d/GP4	0.54	2.07	16.84	10.16	132
2	0.55	0.68	11.42	5.01	73
3	0.36	9.77	3.99	4.92	16
4	0.33	0.28	2.31	1.29	5
5s	0.16	0.17	3.68	3.56	30
5d	0.22	0.22	4.93	1.55	55
6	0.25	0.80	3.94	3.61	52
7	0.19	0.73	1.71	0.90	32
8	1.71	2.27	12.35	8.65	132
9	1.63	5.55	2.33	23.38	143
10	0.16	0.17	0.98	0.28	14
11	1.56	0.95	5.69	4.98	85
12	4.60	3.19	21.11	12.19	355
13s	38.35	58.51	37.23	45.41	671
13d/GP5	11.22	14.88	18.25	27.45	397
14	0.20	0.54	1.97	2.39	24
15	13.51	26.48	18.81	49.45	577
16	10.34	122.18	21.28	27.99	273
17	43.35	50.36	76.51	77.81	792
18	15.24	33.36	25.52	62.98	606
19	0.34	0.26	1.52	0.90	76
20	0.66	0.31	1.78	3.03	45
21	0.89	3.06	2.15	2.28	113
22s	1.19	0.75	1.60	1.05	39
22d/GP6	0.39	1.34	1.82	0.49	92
23	0.38	2.26	1.42	1.45	44
24	6.09	10.93	16.52	19.56	295
stream	0.01	0.71	4.01	4.26	156

Table 6. WCHS median (n = 6) YSI multimeter DIN and Cl concentrations with standard deviations and specific conductivity.

Best fit equations obtained from the calibration curves were multiplied by the DIN and Cl field measurements to obtain corrected values on the three sampling dates. The equations and R^2 values are included in Tables 7 and 8.

Sampling Date	DIN Best Fit Equation	R^2	Cl Best Fit Equation	R^2
June 13, 2011	DIN = 1.3498x + 1.1533	0.98	Cl = 0.7905x + 0.4551	0.95
October 28, 2011	DIN = 0.1625x + 3.2764	0.95	Cl = 0.4782x + 9.2233	0.96
December 21, 2011	DIN = 0.0533x + 4.6402	0.77	Cl = 0.167x + 12.284	0.74

Table 7. JWSES calibration curve best fit equations and R^2 values on June 13, October 28, and December 21, 2011.

Sampling Date	DIN Best Fit Equation	R^2	Cl Best Fit Equation	R^2
June 13, 2011	DIN = 1.3019x + 1.2053	0.98	Cl = 0.7199x + 5.1069	0.94
October 28, 2011	DIN = 10.977x – 6.0489	0.59	Cl = 1.6034x + 0.6924	0.45
December 21, 2011	DIN = 6.5664x - 3.2285	0.99	Cl = 1.3132x + 13.623	0.84

Table 8. WCHS calibration curve best fit equations and R^2 values on June 13, October 28, and December 21, 2011.

The median corrected DIN and Cl concentrations in the drainfields and at background piezometers are included in Tables 9 and 10.

Piezometer	DIN (mg/L)	Cl (mg/L)	Specific Conductivity (µS/cm)
1/GP1	4.96	12.78	176
2	3.82	10.48	99
3/GP2	4.07	13.53	86
4	28.07	52.63	587
5	11.56	36.22	559
6	42.73	35.99	641
7	7.84	66.95	1109
8	5.32	26.22	756
9	3.81	11.39	122
10	7.23	40.03	497
11	4.68	13.17	315
12/GP3	4.67	23.63	487
13	5.37	33.71	658
14	28.86	44.99	487
15	3.44	10.72	265
16	3.30	13.41	399
17	3.53	34.49	592
18	4.78	19.29	642
19	3.81	14.44	427
20	3.41	16.27	412
21	4.74	16.30	419
spring	4.84	20.77	431
spring/stream confluence	4.72	13.78	159
5 m upstream	3.30	11.29	155
5m downstream	3.32	12.48	149

Table 9. JWSES median (n = 3) corrected YSI multimeter DIN and Cl concentrations and specific conductivity.

Piezometer	DIN (mg/L)	Cl (mg/L)	Specific Conductivity (μS/cm)
1s	0	31.06	79
1d/GP4	2.05	19.50	123
2	1.47	21.94	142
3	1.58	17.52	16
4	1.53	7.27	6
5s	0	21.94	31
5d	0	8.71	65
6	0	13.03	63
7	0	7.27	20
8	3.17	9.91	110
9	10.09	16.68	188
10	0	2.74	33
11	7.41	4.49	116
12	7.45	25.98	371
13s	97.17	85.74	775
13d/GP5	53.80	54.78	764
14	0	10.15	22
15	84.46	75.66	777
16	78.39	25.26	319
17	131.58	108.05	785
18	108.33	90.78	902
19	0	7.27	67
20	1.76	11.59	51
21	2.92	10.15	102
22s	5.70	6.55	46
22d/GP6	0	6.55	78
23	1.47	7.99	44
24	29.64	43.18	312
stream	3.86	22.84	214

Table 10. WCHS median (n = 3) corrected YSI multimeter DIN and Cl concentrations and specific conductivity.

At JWSES, groundwater specific conductivity, and corrected DIN and Cl concentrations were elevated in the drainfields relative to background values across the three sampling dates. A

comparison of median corrected DIN and Cl concentrations to groundwater specific conductivity revealed $R^2 = 0.10$ and $R^2 = 0.73$ (Figure 25).

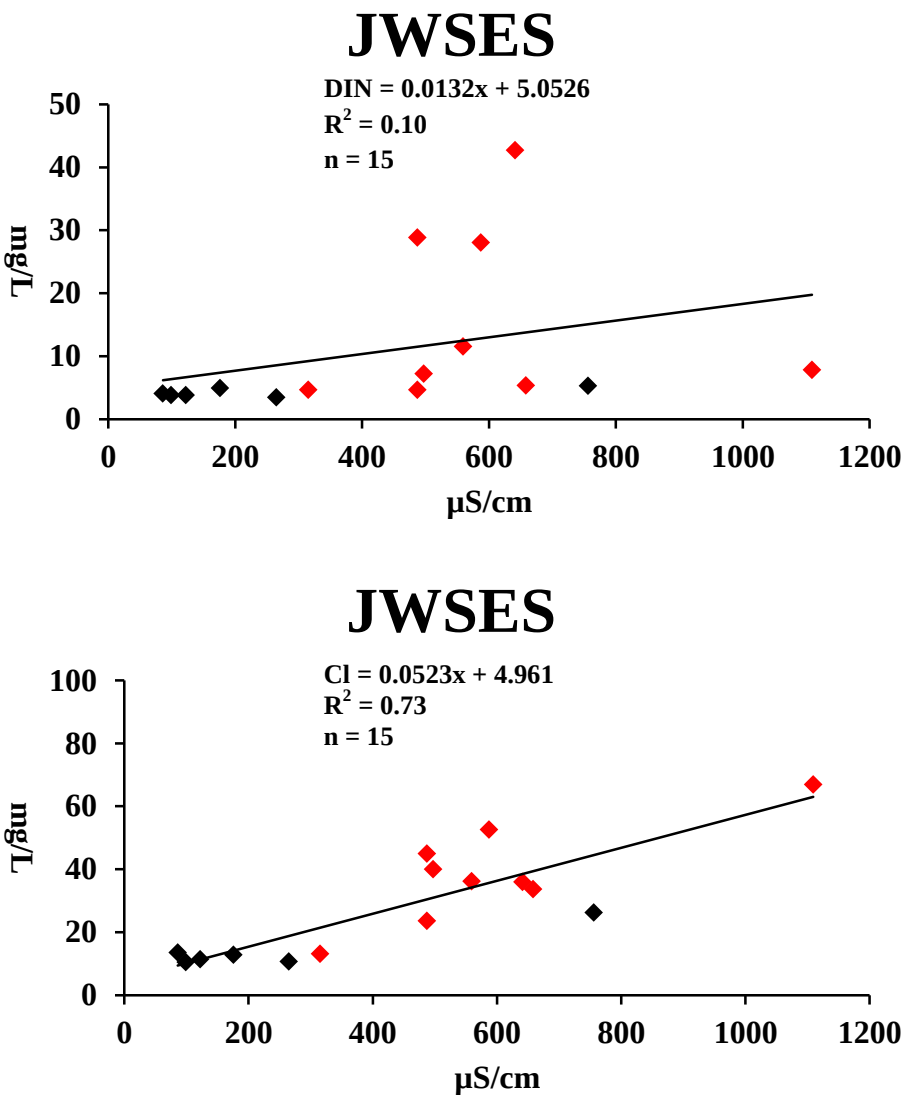

Figure 25. Corrected DIN and Cl concentrations compared to groundwater specific conductivity values at JWSES drainfield and background piezometers on June 13, October 28, and December 21, 2011. Drainfield piezometers are represented in red and background piezometers in black.

At WCHS, groundwater specific conductivity, DIN, and Cl concentrations were elevated in the drainfields relative to background values across the three sampling dates. A comparison of

DIN and Cl concentrations to groundwater specific conductivity revealed $R^2 = 0.82$ and $R^2 = 0.89$ (Figure 26).

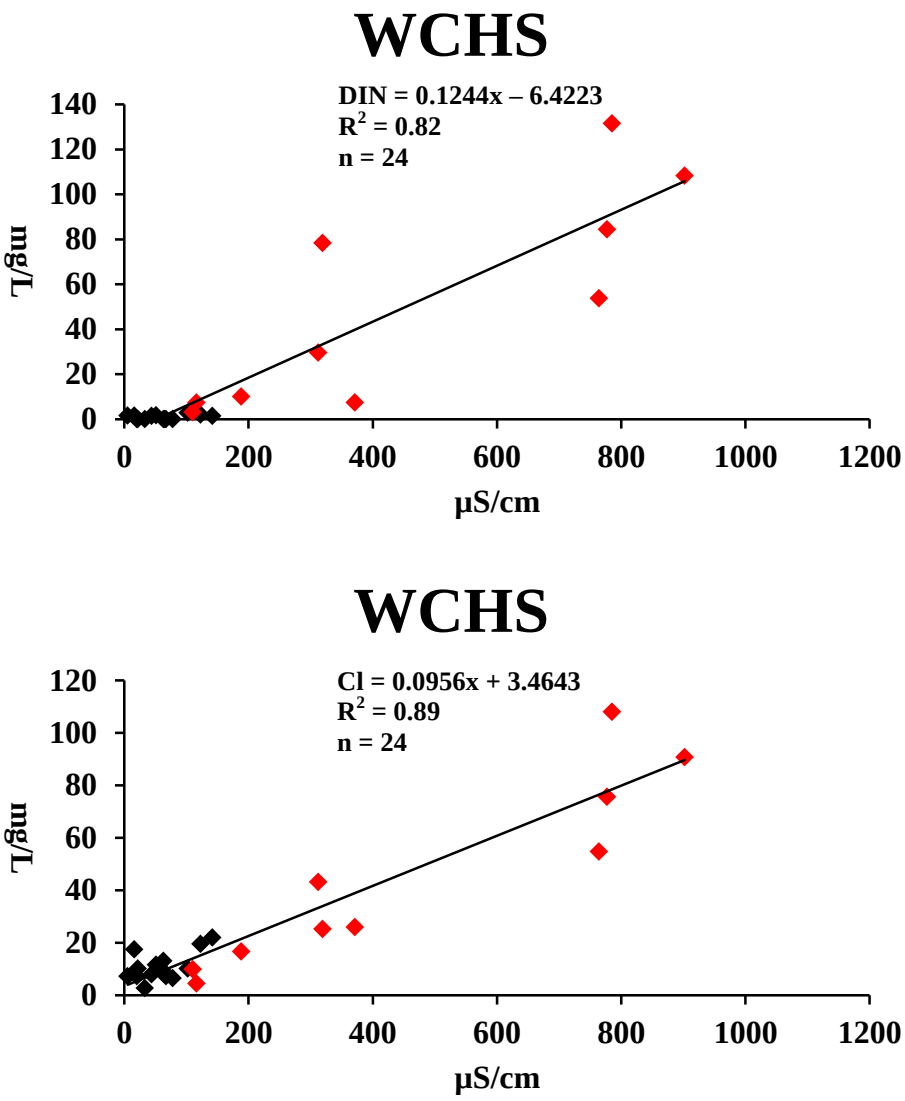

Figure 26. Corrected DIN and Cl concentrations compared to groundwater specific conductivity values at WCHS drainfield and background piezometers on June 13, October 28, and December 21, 2011. Drainfield piezometers are represented in red and background piezometers in black.

Comparisons of corrected DIN, Cl and ECUCEL PO4 concentrations across the three sampling dates at the southern wastewater distribution box at JWSES, in the drainfields, at

background piezometers, and the spring at JWSES revealed differences in nutrient and Cl concentrations across the sites (Figure 27). At WCHS, DIN concentrations above 100 mg/L were beyond the upper limit of calibration and were not included in the comparisons.

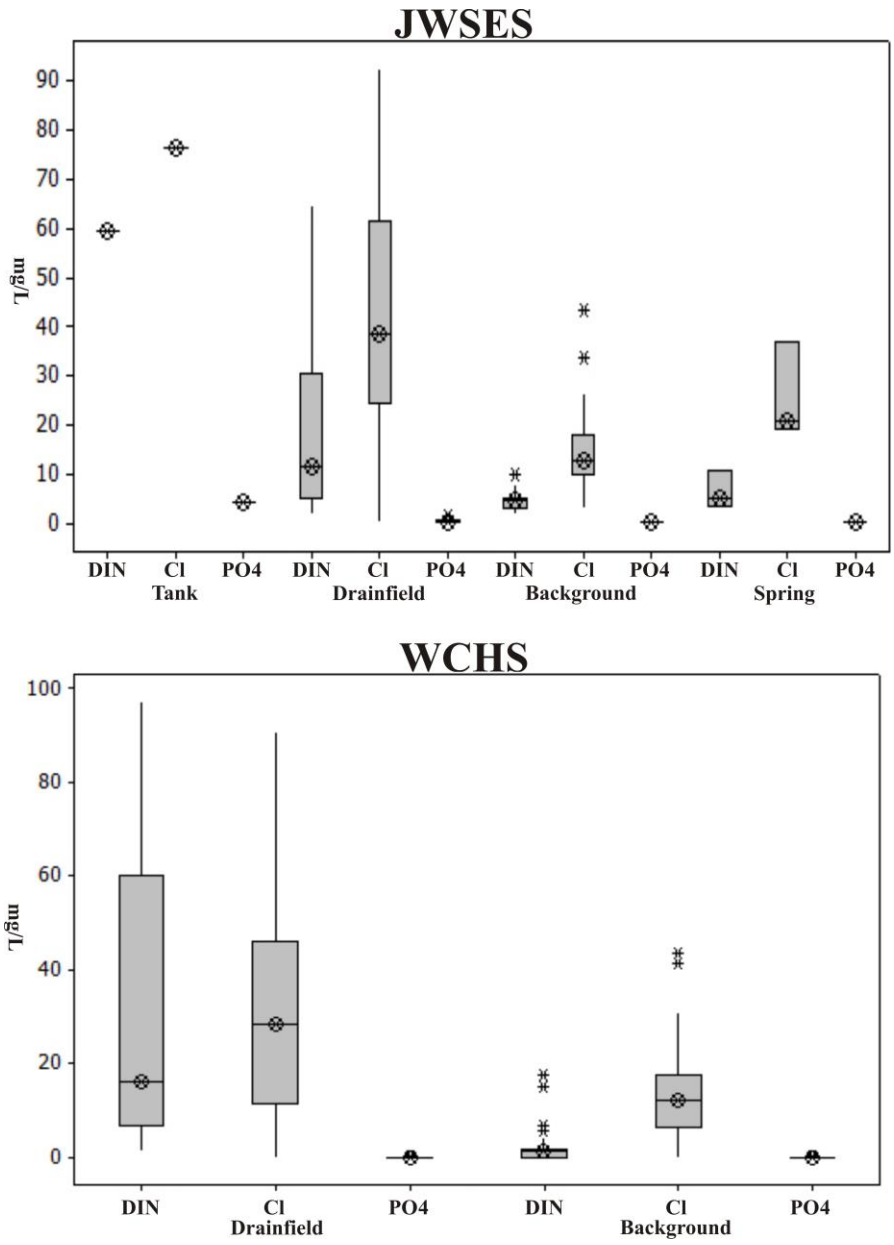

Figure 27. Boxplots of corrected DIN, Cl, and ECUCEL PO4 concentrations at the southern wastewater distribution box at JWSES, in the drainfields, at background piezometers, and the spring at JWSES on June 13, October 28, and December 21, 2011.

At the southern wastewater distribution box at JWSES on June 13, 2011, there was 59.33 mg/L of DIN, 76.34 mg/L of Cl, and 4.05 mg/L of PO4. Across the three sampling dates at drainfield piezometers, median DIN (n = 27) was 11.56 mg/L, median Cl (n = 27) was 38.53 mg/L, and median PO4 (n = 8) was 0.09 mg/L. On the same dates at background piezometers, median DIN (n = 18) was 4.37 mg/L, median Cl (n = 18) was 12.79 mg/L, and median PO4 (n = 5) was 0.12 mg/L. On the same dates at the spring, median (n = 3) DIN was 4.84 mg/L, median Cl was 20.77 mg/L, and median PO4 was 0.19 mg/L. The DIN and Cl concentrations decreased at the spring relative to the drainfield; although, the concentrations were elevated compared to background concentrations. On June 13, 2011, the DIN concentration at the spring was 10.6 mg/L, exceeding the North Carolina regulatory limit of 10 mg/L for surface waters.

At WCHS, across the three sampling dates at drainfield piezometers, median DIN (n = 26) was 20.43 mg/L, median Cl (n = 29) was 29.6 mg/L, and median PO4 (n = 10) was 0 mg/L. On the same dates at background piezometers, median DIN (n = 51) was 1.21 mg/L, median Cl (n = 51) was 12.31 mg/L, and median PO4 (n = 11) was 0 mg/L. Trace amounts of PO4 were measured across the site; however there was no discernable difference between drainfield and background concentrations.

Appendix I

As-built On-site Wastewater System Blueprints

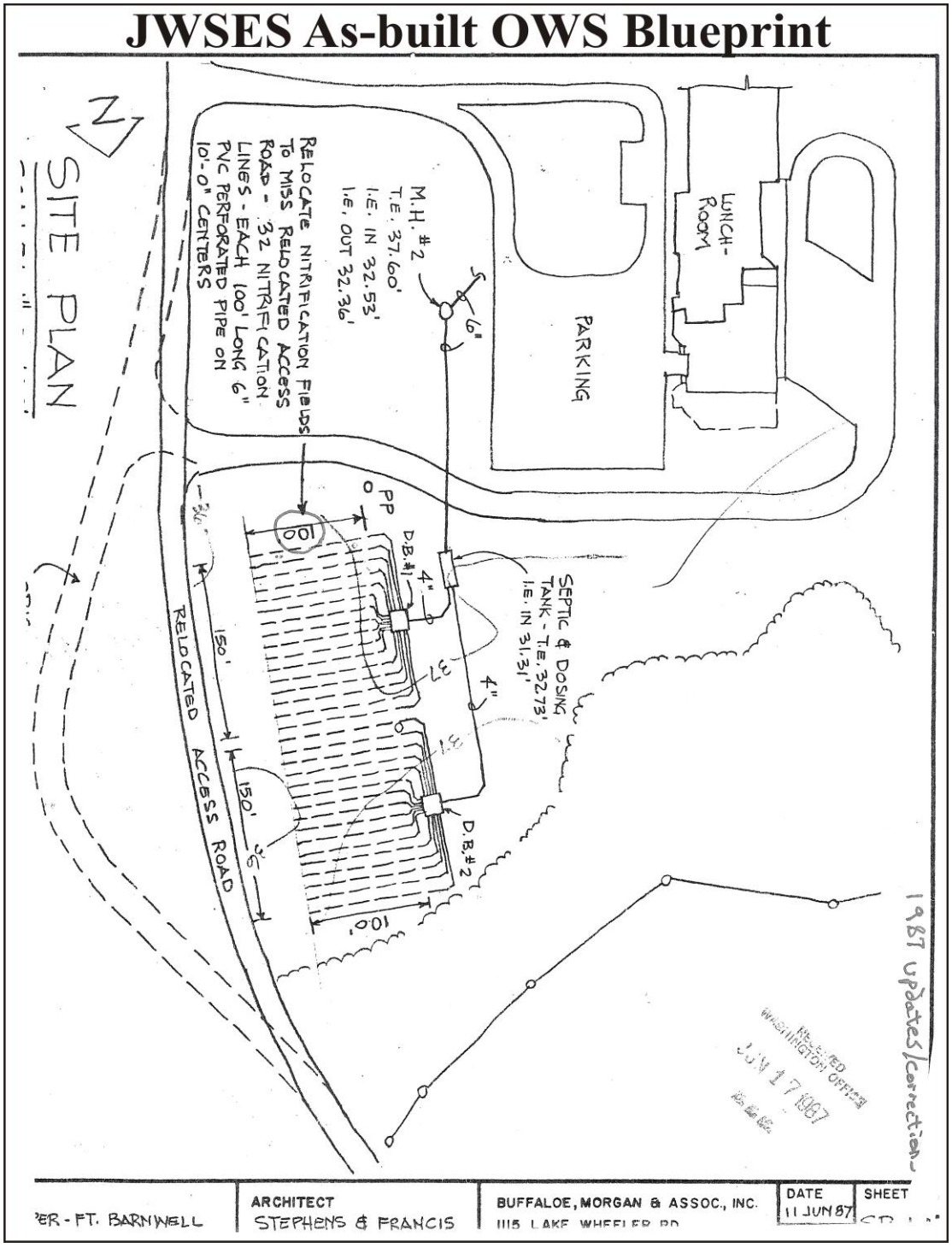

Appendix I Continued

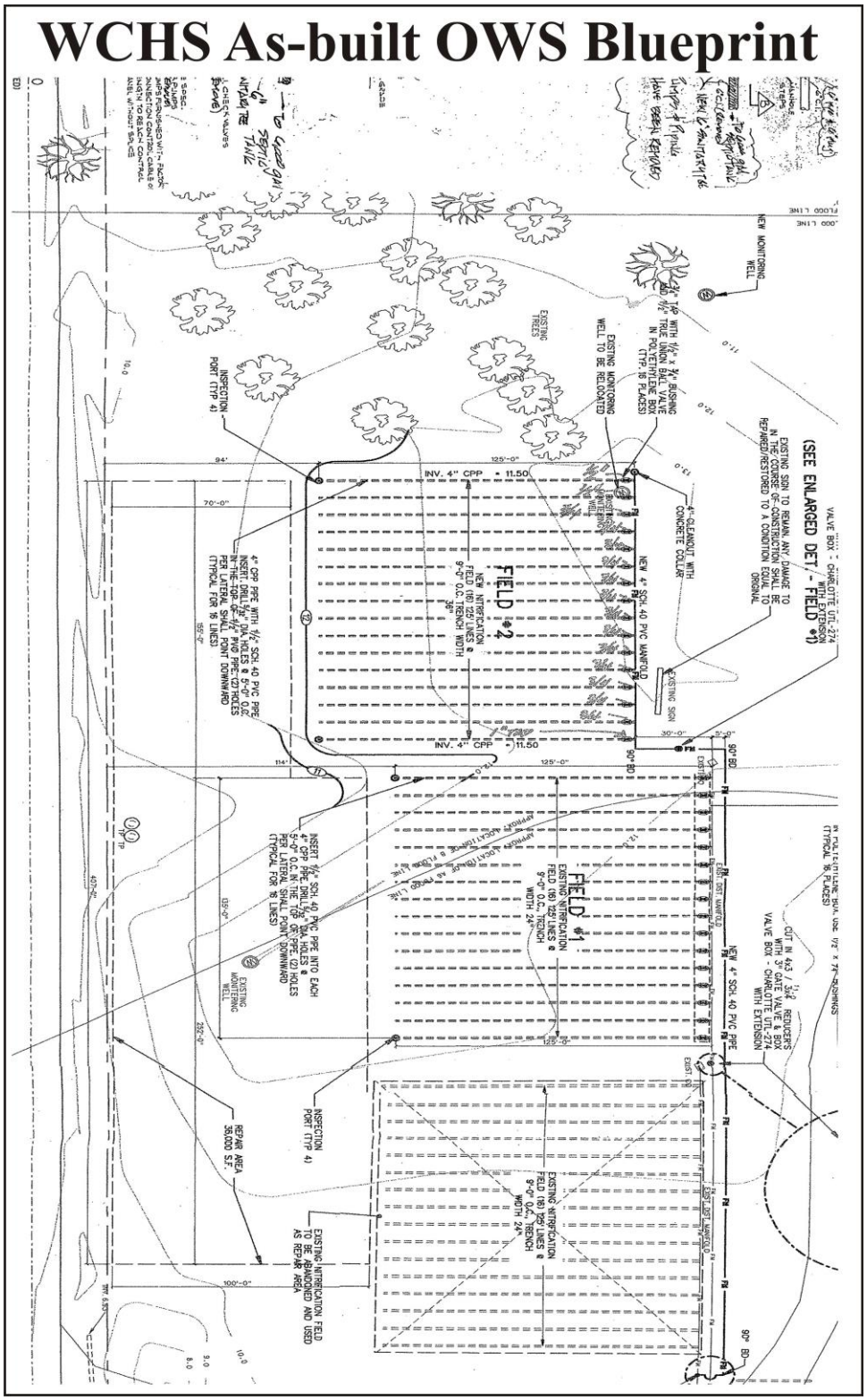

Appendix J

Bi-monthly Transect Resistivity Values

JWSES				
	May 25, 2011		July 13, 2011	
Piezometer X, Y Location (m)	Resistivity X, Y, Z Location (m)	Resistivity (Ω.m)	Resistivity X, Y, Z Location (m)	Resistivity (Ω.m)
1/GP1 (0, 0)	0, 0.07, -0.43	877	0, 2.04, -0.43	487
	0, 0.07, -1.28	1343	0, 2.04, -1.28	901
	0, 0.07, -2.18	1581	0, 2.04, -2.18	1823
	0, 0.07, -3.17	737	0, 2.04, -3.17	1707
	0, 2.57, -4.25	127	0, 4.54, -4.25	248
	0, 10.07, -5.45	492	0, 12.04, -5.45	810
	0, 15.07, -6.76	1117	0, 17.04, -6.76	1146
2 (0, 54)	0, 55.07, -0.43	1849	0, 54.54, -.043	851
	0, 55.07, -1.28	1796	0, 54.54, -1.28	1440
	0, 55.07, -2.18	1900	0, 54.54, -2.18	6938
	0, 55.07, -3.17	2040	0, 54.54, -3.17	39371
	0, 55.07, -4.25	1980	0, 54.54, -4.25	151445
	0, 55.07, -5.45	1776	0, 54.54, -5.45	169281
	0, 55.07, -6.76	1557	0, 54.54, -6.76	113464
3/GP2 (0, 59)	0, 60.07, -0.43	783	0, 59.54, -0.43	638
	0, 60.07, -1.28	817	0, 59.54, -1.28	313
	0, 60.07, -2.18	814	0, 59.54, -2.18	333
	0, 60.07, -3.17	630	0, 59.54, -3.17	955
	0, 60.07, -4.25	434	0, 59.54, -4.25	4935
	0, 60.07, -5.45	416	0, 59.54, -5.45	7663
	0, 60.07, -6.76	491	0, 59.54, -6.76	5211
4 (0, 95)	0, 95.07, -0.43	723	0, 94.54, -0.43	813
	0, 95.07, -1.28	416	0, 94.54, -1.28	888
	0, 95.07, -2.18	178	0, 94.54, -2.18	486
	0, 95.07, -3.17	85	0, 94.54, -3.17	205
	0, 95.07, -4.25	56	0, 94.54, -4.25	102
	0, 95.07, -5.45	62	0, 94.54, -5.45	186
	0, 95.07, -6.76	85	0, 94.54, -6.76	708

Appendix J Continued

JWSES				
	May 25, 2011		July 13, 2011	
Piezometer X, Y Location (m)	Resistivity X, Y, Z Location (m)	Resistivity (Ω.m)	Resistivity X, Y, Z Location (m)	Resistivity (Ω.m)
10 (0, 120)	0, 120.07, -0.43	267	0, 119.54, -0.43	310
	0, 120.07, -1.28	234	0, 119.54, -1.28	283
	0, 120.07, -2.18	131	0, 119.54, -2.18	197
	0, 120.07, -3.17	59	0, 119.54, -3.17	97
	0, 120.07, -4.25	27	0, 119.54, -4.25	36
	0, 120.07, -5.45	30	0, 119.54, -5.45	24
	0, 120.07, -6.76	59	0, 119.54, -6.76	25
13 (0, 137)	0, 137.57, -0.43	122	0, 137.04, -0.43	124
	0, 137.57, -1.28	114	0, 137.04, -1.28	184
	0, 137.57, -2.18	90	0, 137.04, -2.18	188
	0, 137.57, -3.17	60	0, 137.04, -3.17	116
	0, 137.57, -4.25	42	0, 137.04, -4.25	51
	0, 137.57, -5.45	46	0, 137.04, -5.45	33
	0, 137.57, -6.76	65	0, 137.04, -6.76	29
12/GP3 (0, 177)	0, 177.57, -0.43	218	0, 172.04, -0.43	272
	0, 177.57, -1.28	266	0, 177.04, -1.28	471
	0, 177.57, -2.18	432	0, 177.04, -2.18	958
	0, 177.57, -3.17	851	0, 177.04, -3.17	1283
	0, 177.57, -4.25	1991	0, 177.04, -4.25	917
	0, 177.57, -5.45	3460	0, 177.04, -5.45	565
	0, 177.57, -6.76	5038	0, 177.04, -6.76	411

Appendix J Continued

JWSES				
	September 2, 2011		November 18, 2011	
Piezometer X, Y Location (m)	Resistivity X, Y, Z Location (m)	Resistivity (Ω.m)	Resistivity X, Y, Z Location (m)	Resistivity (Ω.m)
1/GP1 (0, 0)	0, 0.43, -0.43	533	0, 0.12, -0.43	1062
	0, 0.43, -1.28	874	0, 0.12, -1.28	1330
	0, 0.43, -2.18	967	0, 0.12, -2.18	1529
	0, 0.43, -3.17	508	0, 0.12, -3.17	1394
	0, 2.93, -4.25	129	0, 5.12, -4.25	654
	0, 10.43, -5.45	447	0, 12.62, -5.45	997
	0, 15.43, -6.76	1630	0, 17.62, -6.76	1238
2 (0, 54)	0, 55.43, -0.43	980	0, 55.12, -0.43	1177
	0, 55.43, -1.28	761	0, 55.12, -1.28	1383
	0, 55.43, -2.18	960	0, 55.12, -2.18	1968
	0, 55.43, -3.17	1783	0, 55.12, -3.17	2200
	0, 55.43, -4.25	3517	0, 55.12, -4.25	1314
	0, 55.43, -5.45	4096	0, 55.12, -5.45	654
	0, 55.43, -6.76	3441	0, 55.12, -6.76	356
3/GP2 (0, 59)	0, 60.43, -0.43	302	0, 60.12, -0.43	690
	0, 60.43, -1.28	367	0, 60.12, -1.28	723
	0, 60.43, -2.18	503	0, 60.12, -2.18	870
	0, 60.43, -3.17	714	0, 60.12, -3.17	1066
	0, 60.43, -4.25	928	0, 60.12, -4.25	659
	0, 60.43, -5.45	986	0, 60.12, -5.45	212
	0, 60.43, -6.76	576	0, 60.12, -6.76	59
4 (0, 95)	0, 95.43, -0.43	1348	0, 95.12, -0.43	906
	0, 95.43, -1.28	2676	0, 95.12, -1.28	1088
	0, 95.43, -2.18	1586	0, 95.12, -2.18	994
	0, 95.43, -3.17	394	0, 95.12, -3.17	622
	0, 95.43, -4.25	65	0, 95.12, -4.25	238
	0, 95.43, -5.45	54	0, 95.12, -5.45	137
	0, 95.43, -6.76	150	0, 95.12, -6.76	117

Appendix J Continued

JWSES				
	September 2, 2011		November 18, 2011	
Piezometer X, Y Location (m)	Resistivity X, Y, Z Location (m)	Resistivity (Ω.m)	Resistivity X, Y, Z Location (m)	Resistivity (Ω.m)
10 (0, 120)	0, 120.43, -0.43	670	0, 120.12, -0.43	571
	0, 120.43, -1.28	526	0, 120.12, -1.28	375
	0, 120.43, -2.18	189	0, 120.12, -2.18	189
	0, 120.43, -3.17	70	0, 120.12, -3.17	102
	0, 120.43, -4.25	38	0, 120.12, -4.25	68
	0, 120.43, -5.45	34	0, 120.12, -5.45	65
	0, 120.43, -6.76	28	0, 120.12, -6.76	73
13 (0, 137)	0, 137.93, -0.43	176	0, 137.62, -0.43	237
	0, 137.93, -1.28	184	0, 137.62, -1.28	192
	0, 137.93, -2.18	151	0, 137.62, -2.18	153
	0, 137.93, -3.17	91	0, 137.62, -3.17	119
	0, 137.93, -4.25	45	0, 137.62, -4.25	104
	0, 137.93, -5.45	30	0, 137.62, -5.45	120
	0, 137.93, -6.76	22	0, 137.62, -6.76	164
12/GP3 (0, 177)	0, 172.93, -0.43	235	0, 177.62, -0.43	559
	0, 177.93, -1.28	346	0, 177.62, -1.28	681
	0, 177.93, -2.18	581	0, 177.62, -2.18	872
	0, 177.93, -3.17	826	0, 177.62, -3.17	5231
	0, 177.93, -4.25	1083	0, 177.62, -4.25	793
	0, 177.93, -5.45	1403	0, 177.62, -5.45	681
	0, 177.93, -6.76	1936	0, 177.62, -6.76	648

Appendix J Continued

JWSES		
	January 31, 2012	
Piezometer X, Y Location (m)	Resistivity X, Y, Z Location (m)	Resistivity (Ω.m)
1/GP1 (0, 0)	0, 2.45, -0.43	944
	0, 2.45, -1.28	1249
	0, 2.45, -2.18	1494
	0, 2.45, -3.17	1265
	0, 2.45, -4.25	514
	0, 9.95, -5.45	1152
	0, 14.95, -6.76	1768
2 (0, 54)	0, 54.95, -0.43	933
	0, 54.95, -1.28	812
	0, 54.95, -2.18	974
	0, 54.95, -3.17	1284
	0, 54.95, -4.25	1192
	0, 54.95, -5.45	654
	0, 54.95, -6.76	274
3/GP2 (0, 59)	0, 59.95, -0.45	1155
	0, 59.95, -1.28	1523
	0, 59.95, -2.18	2104
	0, 59.95, -3.45	2192
	0, 59.95, -4.25	1320
	0, 59.95, -5.45	652
	0, 59.95, -6.76	327
4 (0, 95)	0, 94.95, -0.43	1887
	0, 94.95, -1.28	1801
	0, 94.95, -2.18	1502
	0, 94.95, -3.17	799
	0, 94.95, -4.25	225
	0, 94.95, -5.45	83
	0, 94.95, -6.76	44

Appendix J Continued

JWSES		
	January 31, 2012	
Piezometer X, Y Location (m)	Resistivity X, Y, Z Location (m)	Resistivity (Ω.m)
10 (0, 120)	0, 119.95, -0.43	365
	0, 119.95, -1.28	317
	0, 119.95, -2.18	228
	0, 119.95, -3.17	161
	0, 119.95, -4.25	105
	0, 119.95, -5.45	74
	0, 119.95, -6.76	55
13 (0, 137)	0, 137.45, -0.43	190
	0, 137.45, -1.28	161
	0, 137.45, -2.18	133
	0, 137.45, -3.17	119
	0, 137.45, -4.25	113
	0, 137.45, -5.45	113
	0, 137.45, -6.76	112
12/GP3 (0, 177)	0, 177.45, -0.43	170
	0, 177.45, -1.28	226
	0, 177.45, -2.18	333
	0, 177.45, -3.17	460
	0, 177.45, -4.25	615
	0, 177.45, -5.45	756
	0, 177.45, -6.76	941

Appendix J Continued

WCHS				
	May 25, 2011		July 13, 2011	
Piezometer X, Y Location (m)	Resistivity X, Y, Z Location (m)	Resistivity (Ω.m)	Resistivity X, Y, Z Location (m)	Resistivity (Ω.m)
1d/GP4 (0, 0)	0, 0.55, -0.43	1013	0, 2.37, -0.43	1386
	0, 0.55, -1.28	907	0, 2.37, -1.28	1392
	0, 0.55, -2.18	627	0, 2.37, -2.18	999
	0, 0.55, -3.17	330	0, 2.37, -3.17	568
7 (0, 55)	0, 55.55, -0.43	7321	0, 54.87, -0.43	6173
	0, 55.55, -1.28	6040	0, 54.87, -1.28	6006
	0, 55.55, -2.18	1200	0, 54.87, -2.18	5017
	0, 55.55, -3.17	97	0, 54.87, -3.17	3016
8 (0, 84)	0, 85.55, -0.43	126	0, 84.87, -0.43	624
	0, 85.55, -1.28	96	0, 84.87, -1.28	156
	0, 85.55, -2.18	52	0, 84.87, -2.18	40
	0, 85.55, -3.17	29	0, 84.87, -3.17	30
12 (0, 100)	0, 100.55, -0.43	63	0, 99.87, -0.43	170
	0, 100.55, -1.28	51	0, 99.87, -1.28	230
	0, 100.55, -2.18	33	0, 99.87, -2.18	181
	0, 100.55, -3.17	43	0, 99.87, -3.17	136
13d/GP5 (0, 111)	0, 110.55, -0.43	86	0, 112.37, -0.43	84
	0, 110.55, -1.28	63	0, 112.37, -1.28	64
	0, 110.55, -2.18	41	0, 112.37, -2.18	49
	0, 110.55, -3.17	67	0, 112.37, -3.17	62
18 (0, 153)	0, 153.05, -0.43	76	0, 152.37, -0.43	59
	0, 153.05, -1.28	64	0, 152.37, -1.28	51
	0, 153.05, -2.18	65	0, 152.37, -2.18	39
	0, 153.05, -3.17	217	0, 152.37, -3.17	30
21 (0, 205)	0, 205.55, -0.43	764	0, 204.87, -0.43	372
	0, 205.55, -1.28	576	0, 204.87, -1.28	434
	0, 205.55, -2.18	289	0, 204.87, -2.18	555
	0, 205.55, -3.17	220	0, 204.87, -3.17	487
22d/GP6 (0, 255)	0, 255.55, -0.43	4669	0, 254.87, -0.43	5125
	0, 255.55, -1.28	2808	0, 254.87, -1.28	4731
	0, 255.55, -2.18	950	0, 254.87, -2.18	2725
	0, 255.55, -3.17	244	0, 254.87, -3.17	1037

Appendix J Continued

WCHS				
	May 25, 2011		July 13, 2011	
Piezometer X, Y Location (m)	Resistivity X, Y, Z Location (m)	Resistivity (Ω.m)	Resistivity X, Y, Z Location (m)	Resistivity (Ω.m)
23 (0, 310)	0, 310.55, -0.43	1584	0, 309.87, -0.43	1436
	0, 310.55, -1.28	1641	0, 309.87, -1.28	1267
	0, 310.55, -2.18	1569	0, 309.87, -2.18	993
	0, 295.55, -3.17	1157	0, 309.87, -3.17	738

Appendix J Continued

WCHS				
	September 2, 2011		November 18, 2011	
Piezometer X, Y Location (m)	Resistivity X, Y, Z Location (m)	Resistivity (Ω.m)	Resistivity X, Y, Z Location (m)	Resistivity (Ω.m)
1d/GP4 (0, 0)	0, 1.5, -0.43	1393	0, 1.11, -0.43	2301
	0, 1.5, -1.28	1388	0, 1.11, -1.28	1796
	0, 1.5, -2.18	1060	0, 1.11, -2.18	955
	0, 1.5, -3.17	625	0, 1.11, -3.17	476
7 (0, 55)	0, 54, -0.43	2356	0, 56.11, -0.43	3689
	0, 54, -1.28	2985	0, 56.11, -1.28	3032
	0, 54, -2.18	3950	0, 56.11, -2.18	2166
	0, 54, -3.17	3144	0, 56.11, -3.17	1323
8 (0, 84)	0, 84, -0.43	5102	0, 83.61, -0.43	454
	0, 84, -1.28	4482	0, 83.61, -1.28	150
	0, 84, -2.18	600	0, 83.61, -2.18	40
	0, 84, -3.17	49	0, 83.61, -3.17	33
12 (0, 100)	0, 99, -0.43	144	0, 101.11, -0.43	130
	0, 99, -1.28	191	0, 101.11, -1.28	84
	0, 99, -2.18	203	0, 101.11, -2.18	40
	0, 99, -3.17	192	0, 101.11, -3.17	18
13d/GP5 (0, 111)	0, 111.5, -0.43	62	0, 111.11, -0.43	155
	0, 111.5, -1.28	98	0, 111.11, -1.28	127
	0, 111.5, -2.18	193	0, 111.11, -2.18	85
	0, 111.5, -3.17	346	0, 111.11, -3.17	50
18 (0, 153)	0, 154, -0.43	51	0, 153.61, -0.43	119
	0, 154, -1.28	61	0, 153.61, -1.28	86
	0, 154, -2.18	47	0, 153.61, -2.18	38
	0, 154, -3.17	21	0, 153.61, -3.17	13
21 (0, 205)	0, 204, -0.43	4978	0, 206.11, -0.43	509
	0, 204, -1.28	3541	0, 206.11, -1.28	542
	0, 204, -2.18	1341	0, 206.11, -2.18	633
	0, 204, -3.17	677	0, 206.11, -3.17	499
22d/GP6 (0, 255)	0, 254, -0.43	1348	0, 256.11, -0.43	2502
	0, 254, -1.28	5373	0, 256.11, -1.28	2087
	0, 254, -2.18	6039	0, 256.11, -2.18	978
	0, 254, -3.17	1652	0, 256.11, -3.17	329

Appendix J Continued

WCHS				
	September 2, 2011		November 18, 2011	
Piezometer X, Y Location (m)	Resistivity X, Y, Z Location (m)	Resistivity (Ω.m)	Resistivity X, Y, Z Location (m)	Resistivity (Ω.m)
23 (0, 310)	0, 309, -0.43	1529	0, 311.11, -0.43	795
	0, 309, -1.28	1741	0, 311.11, -1.28	857
	0, 309, -2.18	1904	0, 311.11, -2.18	891
	0, 299, -3.17	1577	0, 311.11, -3.17	782

Appendix J Continued

WCHS		
	February 3, 2012	
Piezometer X, Y Location (m)	Resistivity X, Y, Z Location (m)	Resistivity (Ω.m)
1d/GP4 (0, 0)	0, 2.37, -0.43	952
	0, 2.37, -1.28	1089
	0, 2.37, -2.18	626
	0, 2.37, -3.17	227
7 (0, 55)	0, 54.87, -0.43	6824
	0, 54.87, -1.28	5261
	0, 54.87, -2.18	3500
	0, 54.87, -3.17	2648
8 (0, 84)	0, 84.87, -0.43	402
	0, 84.87, -1.28	224
	0, 84.87, -2.18	126
	0, 84.87, -3.17	113
12 (0, 100)	0, 99.87, -0.43	90
	0, 99.87, -1.28	123
	0, 99.87, -2.18	101
	0, 99.87, -3.17	50
13d/GP5 (0, 111)	0, 109.87, -0.43	157
	0, 109.87, -1.28	91
	0, 109.87, -2.18	49
	0, 109.87, -3.17	37
18 (0, 153)	0, 154.87, -0.43	42
	0, 154.87, -1.28	43
	0, 154.87, -2.18	52
	0, 154.87, -3.17	54
21 (0, 205)	0, 204.87, -0.43	431
	0, 204.87, -1.28	480
	0, 204.87, -2.18	475
	0, 204.87, -3.17	352
22d/GP6 (0, 255)	0, 254.87, -0.43	6442
	0, 254.87, -1.28	4407
	0, 254.87, -2.18	1738
	0, 254.87, -3.17	549

Appendix J Continued

WCHS		
	February 3, 2012	
Piezometer X, Y Location (m)	Resistivity X, Y, Z Location (m)	Resistivity (Ω.m)
23 (0, 310)	0, 309.87, -0.43	1019
	0, 309.87, -1.28	1061
	0, 309.87, -2.18	1115
	0, 297.37, -3.17	1102

Appendix K

Geophysical Survey Area and Transect Resistivity Values

JWSES		
	January 31, 2012	
Piezometer X, Y Location (m)	Resistivity X, Y, Z Location (m)	Resistivity (Ω.m)
1/GP1 (0, 0)	0, 9.95, -5.45	1152
2 (0, 54)	0, 54.95, -4.25	1192
3/GP2 (0, 59)	0, 59.95, -5.45	652
4 (0, 95)	0, 94.95, -4.25	225
5 (43, 2)	42, 2.23, -5.50	160
6 (18, 21)	18, 22.23, -5.50	49
7 (36, 32)	34, 32.23, -7.26	32
10 (0, 120)	0, 120, -4.25	105
12/GP3 (0, 177)	0, 177.45, -6.76	941
13 (0, 137)	0, 137.45, -5.45	113
14 (34, 48)	34, 47.23, -7.26	66

Appendix K Continued

WCHS		
	January 31, 2012	
Piezometer X, Y Location (m)	Resistivity X, Y, Z Location (m)	Resistivity (Ω.m)
1d/GP4 (0, 0)	0, 2.37, -3.17	227
7 (0, 55)	0, 54.87, -2.18	3500
8 (0, 84)	0, 84.87, -2.18	126
9 (29, 7)	30, 6.22, -2.64	3100
11 (28, 34)	30, 33.72, -2.64	1100
12 (0, 100)	0, 99.87, -2.18	101
13d/GP5 (0, 111)	0, 109.87, -3.17	37
16 (29, 52)	30, 51.22, -2.64	57
17 (26, 81)	26, 81.22, -2.64	55
18 (0, 153)	0, 154.87, -2.18	52
20 (34, 110)	34, 111, -2.64	1439
21 (0, 205)	0, 204.87, -2.18	475
22d/GP6 (0, 255)	0, 254.87, -3.17	549
23 (0, 310)	0, 309.87, -2.18	1115

Appendix L

Bi-monthly Transect Absolute Peak Amplitude Values

JWSES				
	July 13, 2011		September 2, 2011	
Piezometer X, Y Location (m)	Radar Signal Trace X, Y, Z Location (m)	APA	Radar Signal Trace X, Y, Z Location (m)	APA
1/GP1 (0, 0)	0, 0, -1.5	1243	0, 0, -1.5	1141
	0, 0, -2	322	0, 0, -2	555
	0, 0, -2.1	20	0, 0, -2.1	20
	0, 0, -2.5	690	0, 0, -2.5	863
	0, 0, -3.1	1704	0, 0, -3.1	1551
	0, 0, -3.5	45	0, 0, -3.5	378
	0, 0, -3.9	3363	0, 0, -3.9	4111
	0, 0, -4.1	967	0, 0, -4.1	2594
	0, 0, -4.9	1336	0, 0, -4.9	2015
	0, 0, -5.1	13410	0, 0, -5.1	4562
2 (0, 54)	0, 54, -4.5	6129	0, 54, -4.5	4193
3/GP2 (0, 59)	0, 59, -1.1	137	0, 59, -1.1	203
	0, 59, -1.9	1612	0, 59, -1.9	1551
	0, 59, -2.2	1243	0, 59, -2.2	1111
	0, 59, -2.9	1428	0, 59, -2.9	65
	0, 59, -3.3	1243	0, 59, -3.3	1151
	0, 59, -4.2	967	0, 59, -4.2	1051
	0, 59, -4.6	45	0, 59, -4.6	677
	0, 59, -5.4	3824	0, 59, -5.4	6405

Appendix L Continued

JWSES				
	July 13, 2011		September 2, 2011	
Piezometer X, Y Location (m)	Radar Signal Trace X, Y, Z Location (m)	APA	Radar Signal Trace X, Y, Z Location (m)	APA
4 (0, 95)	0, 95, -4.8	2073	0, 95, -4.8	4101
10 (0, 120)	0, 120, -4.5	2257	0, 120, -4.5	6866
13 (0, 137)	0, 137, -5.5	4377	0, 137, -5.5	8341
12/GP3 (0, 177)	0, 177, -1.7	229	0, 177, -1.7	45
	0, 177, -2.2	1059	0, 177, -2.2	1151
	0, 177, -3.1	598	0, 177, -3.1	1098
	0, 177, -3.4	782	0, 177, -3.4	888
	0, 177, -3.6	875	0, 177, -3.6	1150
	0, 177, -4.5	1059	0, 177, -4.5	888
	0, 177, -4.9	137	0, 177, -4.9	45
	0, 177, -5.6	598	0, 177, -5.6	45
	0, 177, -7.8	2073	0, 177, -7.8	4654

Appendix L Continued

JWSES				
	November 18, 2011		January 31, 2012	
Piezometer X, Y Location (m)	Radar Signal Trace X, Y, Z Location (m)	APA	Radar Signal Trace X, Y, Z Location (m)	APA
1/GP1 (0, 0)	0, 0, -1.5	45	0, 0, -1.5	782
	0, 0, -2	782	0, 0, -2	229
	0, 0, -2.1	45	0, 0, -2.1	45
	0, 0, -2.5	45	0, 0, -2.5	2165
	0, 0, -3.1	1704	0, 0, -3.1	3363
	0, 0, -3.5	3363	0, 0, -3.5	3087
	0, 0, -3.9	4930	0, 0, -3.9	5391
	0, 0, -4.1	2626	0, 0, -4.1	4469
	0, 0, -4.9	967	0, 0, -4.9	1796
	0, 0, -5.4	8064	0, 0, -5.4	4101
2 (0, 54)	0, 54, -4.5	4562	0, 54, -4.5	4562
3/GP2 (0, 59)	0, 59, -1.1	229	0, 59, -1.1	137
	0, 59, -1.9	322	0, 59, -1.9	322
	0, 59, -2.2	414	0, 59, -2.2	45
	0, 59, -2.9	45	0, 59, -2.9	782
	0, 59, -3.3	2073	0, 59, -3.3	1151
	0, 59, -4.2	1151	0, 59, -4.2	1612
	0, 59, -4.6	1151	0, 59, -4.6	1981
	0, 59, -5.4	7143	0, 59, -5.4	6866

Appendix L Continued

JWSES				
	November 18, 2011		January 31, 2012	
Piezometer X, Y Location (m)	Radar Signal Trace X, Y, Z Location (m)	APA	Radar Signal Trace X, Y, Z Location (m)	APA
4 (0, 95)	0, 95, -4.8	2257	0, 95, -4.8	2257
10 (0, 120)	0, 120, -4.5	2242	0, 120, -4.5	1796
13 (0, 137)	0, 137, -5.5	4746	0, 137, -5.5	2902
12/GP3 (0, 177)	0, 177, -1.7	45	0, 177, -1.7	414
	0, 177, -2.2	414	0, 177, -2.2	1151
	0, 177, -3.1	875	0, 177, -3.1	414
	0, 177, -3.4	45	0, 177, -3.4	322
	0, 177, -3.6	45	0, 177, -3.6	45
	0, 177, -4.5	229	0, 177, -4.5	598
	0, 177, -4.9	229	0, 177, -4.9	45
	0, 177, -5.6	137	0, 177, -5.6	45
	0, 177, -7.8	5668	0, 177, -7.8	3824

Appendix L Continued

WCHS				
	July 13, 2011		September 2, 2011	
Piezometer X, Y Location (m)	Radar Signal Trace X, Y, Z Location (m)	APA	Radar Signal Trace X, Y, Z Location (m)	APA
1d/GP4 (0, 0)	0, 0, -1.1	598	0, 0, -1.1	777
	0, 0, -1.6	3640	0, 0, -1.6	2594
	0, 0, -1.8	6958	0, 0, -1.8	45
	0, 0, -2.3	1243	0, 0, -2.3	829
	0, 0, -3	45	0, 0, -3	555
	0, 0, -3.5	3456	0, 0, -3.5	4838
	0, 0, -4.3	137	0, 0, -4.3	471
	0, 0, -4.7	782	0, 0, -4.7	1511
7 (0, 55)	0, 55, -2.2	13326	0, 55, -2.2	4377
8 (0, 84)	0, 84, -2.2	14240	0, 84, -2.2	1151
12 (0, 100)	0, 100, -2.3	4009	0, 100, -2.3	1151
13d/GP5 (0, 111)	0, 111, -0.7	506	0, 111, -0.7	1555
	0, 111, -1.1	45	0, 111, -1.1	929
	0, 111, -2.3	875	0, 111, -2.3	45
	0, 111, -3.2	414	0, 111, -3.2	45
	0, 111, -3.5	1612	0, 111, -3.5	1059
	0, 111, -4	45	0, 111, -4	370
	0, 111, -4.5	45	0, 111, -4.5	77
	0, 111, -4.8	875	0, 111, -4.8	509
18 (0, 153)	0, 153, -2.4	2257	0, 153, -2.4	1428
21 (0, 205)	0, 205, -2.2	10276	0, 205, -2.2	2626
22d/GP6 (0, 255)	0, 255, -1.1	2073	0, 255, -1.1	3851
	0, 255, -1.7	7143	0, 255, -1.7	8888
	0, 255, -2.2	967	0, 255, -2.2	501
	0, 255, -3.2	6036	0, 255, -3.2	3940
	0, 255, -3.5	14885	0, 255, -3.5	9816
	0, 255, -4.6	1428	0, 255, -4.6	708
23 (0, 310)	0, 305, -1.8	13226	0, 305, -1.8	9514

Appendix L Continued

WCHS				
	November 18, 2011		January 31, 2012	
Piezometer X, Y Location (m)	Radar Signal Trace X, Y, Z Location (m)	APA	Radar Signal Trace X, Y, Z Location (m)	APA
1d/GP4 (0, 0)	0, 0, -1.1	137	0, 0, -1.1	1612
	0, 0, -1.6	45	0, 0, -1.6	1981
	0, 0, -1.8	45	0, 0, -1.8	45
	0, 0, -2.3	322	0, 0, -2.3	967
	0, 0, -3	1059	0, 0, -3	137
	0, 0, -3.5	3456	0, 0, -3.5	3640
	0, 0, -4.3	598	0, 0, -4.3	1889
	0, 0, -4.7	1151	0, 0, -4.7	6221
7 (0, 55)	0, 55, -2.2	12581	0, 55, -2.2	4562
8 (0, 84)	0, 84, -2.2	1059	0, 84, -2.2	2534
12 (0, 100)	0, 100, -2.3	598	0, 100, -2.3	2073
13d/GP5 (0, 111)	0, 111, -0.7	45	0, 111, -0.7	5023
	0, 111, -1.1	229	0, 111, -1.1	1243
	0, 111, -2.3	45	0, 111, -2.3	598
	0, 111, -3.2	137	0, 111, -3.2	45
	0, 111, -3.5	782	0, 111, -3.5	782
	0, 111, -4	598	0, 111, -4	137
	0, 111, -4.5	137	0, 111, -4.5	322
	0, 111, -4.8	137	0, 111, -4.8	322
18 (0, 153)	0, 153, -2.4	322	0, 153, -2.4	875
21 (0, 205)	0, 205, -2.2	1336	0, 205, -2.2	3363
22d/GP6 (0, 255)	0, 255, -1.1	875	0, 255, -1.1	690
	0, 255, -1.7	414	0, 255, -1.7	1059
	0, 255, -2.2	322	0, 255, -2.2	2534
	0, 255, -3.2	1612	0, 255, -3.2	782
	0, 255, -3.5	4838	0, 255, -3.5	5944
	0, 255, -4.6	1336	0, 255, -4.6	229
23 (0, 310)	0, 305, -1.8	4009	0, 305, -1.8	7511

Appendix M

February 2011 – January 2012 Monthly Precipitation at the Craven County Airport

Month	Total (cm)
February	7.2
March	9.5
April	8.9
May	3.5
June	6.5
July	11.9
August	32.2
September	17.1
October	4.2
November	4.5
December	1.8
January	5.8